BACHELOR'S THESIS

NEUTRALINO-GLUINO COANNIHILATION IN THE MSSM

JORIN OVERWIENING

Institute of Theoretical Physics
Working Group Klasen

SUPERVISOR:
PD Dr. Karol Kovařík

21 September 2021

FIRST ASSESSOR:
PD Dr. Karol Kovařík

SECOND ASSESSOR:
Prof. Dr. Michael Klasen

DATE OF PRESENTATION
27/09/2021

LOCATION:
Münster

TIME FRAME:
01/07/2021 – 23/09/2021

Jorin Overwiening E-MAIL: overwiening@wwu.de

ABSTRACT

In this thesis, we introduced the phenomenological MSSM (pMSSM) as a model with the LSP neutralino $\tilde{\chi}_1^0$ as a WIMP dark matter candidate. We defined a pMSSM in which the neutralino thermal relic density $\Omega_{\tilde{\chi}_1^0} h^2 = 0.125$ is in accordance with the *Planck 2018* results [7] and showed that a mostly bino-wino like neutralino can be the (sole) dark matter particle. As the main part of this thesis, the coannihilation of neutralino with an NLSP gluino was calculated using four- and two-component spinor technique and it was shown that two-component calculations are more preferable in chiral theories such as SUSY. The results were then implemented in the programme `DM@NLO`, which integrates the differential cross-sections and – in combination with other dark matter software – calculates the mass parameters and $\Omega_{\tilde{\chi}_1^0}$ regarding the specified pMSSM. This thesis' process contributes with 0.2 % to $\Omega_{\tilde{\chi}_1^0}$. We have also shown that, in addition to the correct relic density, the chosen scenario – and thus, by extension, SUSY – is in agreement with recent experimental data from ATLAS and CMS.

KURZFASSUNG

In dieser Arbeit haben wir das phänomenologische MSSM (pMSSM) als ein Modell, mit dem LSP-Neutralino $\tilde{\chi}_1^0$ als WIMP-Kandidaten für dunkle Materie, eingeführt. Wir definierten ein pMSSM, in dem die thermische Reliktdichte des Neutralinos $\Omega_{\tilde{\chi}_1^0} h^2 = 0.125$ mit den *Planck 2018* Ergebnissen [7] übereinstimmt und zeigten, dass ein hauptsächlich Wino-Bino ähnliches Neutralino ein guter dunkle Materie Kandidat ist. Als Hauptteil dieser Arbeit berechneten wir die Koannihilation des Neutralinos mit einem NLSP-Gluino unter Verwendung der Vier- und Zweikomponenten-Spinor-Technik und zeigten die Vorteile von Zweikomponenten-Rechnungen in chiralen Theorien wie SUSY. Die Ergebnisse wurden dann in das Programm `DM@NLO` implementiert, welches die differentiellen Wirkungsquerschnitte integriert und – in Kombination mit anderen Programmen für dunkle Materie – die Massenparameter und $\Omega_{\tilde{\chi}_1^0}$ für das spezifizierte pMSSM berechnet. Der Prozess dieser Arbeit trägt mit $0,2\,\%$ zu $\Omega_{\tilde{\chi}_1^0}$ bei. Wir haben außerdem gezeigt, dass neben der richtigen Reliktdichte das gewählte Szenario – und damit im weiteren Sinne auch SUSY – in Übereinstimmung mit neuesten experimentellen Daten von ATLAS und CMS steht.

CONTENTS

1 INTRODUCTION 1

2 DARK MATTER 3
- 2.1 Evidence . . . 3
- 2.2 Candidates . . . 4
- 2.3 WIMPS . . . 4
  - 2.3.1 Relic Density . . . 5
  - 2.3.2 Detection . . . 7

3 SUPERSYMMETRY 8
- 3.1 Motivation . . . 8
  - 3.1.1 The fine-tuning Problem . . . 8
  - 3.1.2 Theoretical Considerations . . . 9
- 3.2 Framework . . . 10
  - 3.2.1 Algebra . . . 10
  - 3.2.2 Superfields . . . 10
  - 3.2.3 Lagrangians . . . 13
- 3.3 The MSSM . . . 14
  - 3.3.1 SUSY Breaking . . . 16
  - 3.3.2 Phenomenological Model . . . 17
  - 3.3.3 *R*-Parity . . . 18
  - 3.3.4 The Neutralino . . . 18

4 DIRAC CALCULATION 20
- 4.1 Cross-Section . . . 20
- 4.2 Feynman Diagrams . . . 21
  - 4.2.1 Fermion Number Violation . . . 22
  - 4.2.2 Invariant Amplitude . . . 24
- 4.3 Evaluation of Squared Amplitudes . . . 24
  - 4.3.1 T-Channel . . . 25
  - 4.3.2 U-Channel . . . 27
  - 4.3.3 Interference . . . 29

5 WEYL CALCULATION 34
- 5.1 Technique . . . 34
- 5.2 Feynman Diagrams . . . 35
- 5.3 Evaluation of Squared Amplitudes . . . 39
  - 5.3.1 T-Channel . . . 39
  - 5.3.2 U-Channel . . . 41
  - 5.3.3 Interference . . . 41
  - 5.3.4 Comparison to Four-Component . . . 43

6 NUMERICAL ANALYSIS 45
- 6.1 Implementation . . . 45
- 6.2 Cross-Sections . . . 46
  - 6.2.1 Chargino-Gluino Coannihilation . . . 47
- 6.3 Discussion . . . 48
  - 6.3.1 Neutralino Composition . . . 49
  - 6.3.2 Experimental Mass Bounds . . . 51

6.3.3 The "little" Hierarchy Problem . . . 52
7 CONCLUSION 54
7.1 Outlook . . . 55

A AUXILIARY CALCULATION 56
A.1 Dirac Calculation . . . 56
A.1.1 Hermitian Conjugate of Gauge Vertices . . . 56
A.1.2 Trace Calculation I . . . 56
A.1.3 Trace Calculation II . . . 57
A.1.4 Omitted Trace Calculations . . . 57
B DM@NLO 59
C FEYNMAN RULES 60
C.1 Four-Component . . . 60
C.1.1 Particle Lines . . . 60
C.1.2 Vertices . . . 60
C.1.3 Fermion Number Violation . . . 61
C.2 Two-Component . . . 62
D RELATIONS AND FORMULAE 63
D.1 Four-Component . . . 63
D.1.1 γ-Matrices . . . 63
D.1.2 Chirality Operator . . . 63
D.1.3 Completeness Relations . . . 63
D.1.4 Trace Theorems . . . 63
D.2 Two-Component . . . 63
D.2.1 σ-Matrices . . . 64
D.2.2 Spin and Helicity Sums . . . 64
D.2.3 Trace Theorems . . . 64
D.3 SU(N) . . . 64

BIBLIOGRAPHY 65

NOTATION AND CONVENTION

Following, applied conventions and notations will be introduced.

The metric tensor g of Minkowski space, as used here, is

$$g_{\mu\nu} = g^{\mu\nu} = \eta^{\mu\nu} I_4 = \mathrm{diag}(+1, -1, -1, -1),$$

where η is the Minkowski metric, I_N denotes the N-dimensional unit matrix and $\mu, \nu \in \{0, 1, 2, 3\}$ are the four-dimensional spacetime vector indices[1].

Contravariant four-vectors are denoted with raised indices and covariant four-vectors with lowered indices, like

$$x^\mu = (t; \vec{x}) \quad p^\mu = (E; \vec{p}) \quad \partial_\mu \equiv \frac{\partial}{\partial x^\mu} = (\partial/\partial t; \vec{\nabla}).$$

Through the complete thesis natural units will be used

$$\hbar = c = \varepsilon_0 = k_B = 1.$$

The totally antisymmetric pseudo-tensor is defined as

$$\varepsilon^{0123} = -\varepsilon_{0123} = +1.$$

Two useful abbreviation conventions are for four-component spinors

$$\bar{u} \equiv u^\dagger \gamma^0$$

and four four-momenta

$$\not{p} \equiv p_\mu \gamma^\mu.$$

Hermitian sigma matrices[2] $\sigma^\mu_{a\dot{b}}$ and $\bar{\sigma}^{\mu\dot{a}b}$, with $a, b \in \{1, 2\}$, as defined by [47, 49] are

$$\sigma^0 = \bar{\sigma}^0 = \begin{pmatrix} 1 & 0 \\ 0 & 1 \end{pmatrix} \qquad \sigma^1 = -\bar{\sigma}^1 = \begin{pmatrix} 0 & 1 \\ 1 & 0 \end{pmatrix}$$
$$\sigma^2 = -\bar{\sigma}^2 = \begin{pmatrix} 0 & -i \\ i & 0 \end{pmatrix} \qquad \sigma^3 = -\bar{\sigma}^3 = \begin{pmatrix} 1 & 0 \\ 0 & -1 \end{pmatrix},$$

or equivalently

$$\sigma^\mu = (I_2, \vec{\sigma}) \quad \text{and} \quad \bar{\sigma}^\mu = (I_2, -\vec{\sigma}),$$

where $\vec{\sigma}$ are the Pauli matrices. The sigma matrices, and all other four vectors, can be transformed between contra- and covariant vectors like usual

$$\sigma_\mu = g_{\mu\nu}\sigma^\nu = (I_2, -\vec{\sigma}) \quad \text{and} \quad \bar{\sigma}_\mu = g_{\mu\nu}\bar{\sigma}^\nu = (I_2, \vec{\sigma}).$$

1 *Greek indices* like μ, ν, ρ, σ run from 0 to 3 and *Roman indices* like i, j from 1 to 3, unless otherwise stated.
2 See van der Waerden notation below.

Generators of the $(\frac{1}{2},0)$ and $(0,\frac{1}{2})$ Lorentz group are

$$\sigma^{\mu\nu} \equiv \frac{i}{4}(\sigma^\mu\bar{\sigma}^\nu - \sigma^\nu\bar{\sigma}^\mu) \qquad \bar{\sigma}^{\mu\nu} \equiv \frac{i}{4}(\bar{\sigma}^\mu\sigma^\nu - \bar{\sigma}^\nu\sigma^\mu).$$

With the definition of the sigma matrices the Dirac or gamma matrices can be defined

$$\gamma^\mu = \begin{pmatrix} & \sigma^\mu \\ \bar{\sigma}^\mu & \end{pmatrix} \qquad \gamma^5 = i\gamma^0\gamma^1\gamma^2\gamma^3.$$

Last but not least we employ the convention to (mostly) dismiss the "$\cdot$" between vectors or matrices.

VAN DER WAERDEN NOTATION

We will now briefly introduce a notation that will be more convenient to use when one needs to distinguish between left and right chirality of spinors. Before, we only had four-component Dirac spinors

$$\vec{\Psi} = \begin{pmatrix} \psi \\ \chi \end{pmatrix}$$

in the $(\frac{1}{2},\frac{1}{2})$[3] representation of the Lorentz group $\mathrm{O}(1,3)$, where the ψ-part transforms according to the $(\frac{1}{2},0)$ representation (left chiral Weyl spinor) and χ according to the $(0,\frac{1}{2})$ representation (right chiral Weyl spinor)[4].

Since one has to distinguish and keep in mind their respective transformative representations, we will use the conventional notation of van der Waerden [47], which states that χ-like spinors have *lower, undotted indices*

$$\chi = \begin{pmatrix} \chi_1 \\ \chi_2 \end{pmatrix} \to \chi_a$$

and left-chiral, ψ-like spinors have *upper, dotted indices*

$$\psi = \begin{pmatrix} \psi^{\dot{1}} \\ \psi^{\dot{2}} \end{pmatrix} \to \psi^{\dot{a}},$$

in index notation and where $a \in \{1,2\}$.

Next to that we can, from now on closely following [8], define a χ-like, left chiral, spinor with *upper indices* via

$$\begin{pmatrix} \chi^1 \\ \chi^2 \end{pmatrix} \equiv i\sigma_2\chi = \begin{pmatrix} \chi_2 \\ -\chi_1 \end{pmatrix}.$$

This allows us, with a second left chiral spinor ξ, to create a Lorentz invariant via

$$(i\sigma_2\chi)^T\xi = \chi^a\xi_a$$

3 $(\frac{1}{2},\frac{1}{2}) = (\frac{1}{2},0)\otimes(0,\frac{1}{2})$

4 Both representations are irreducible. More background can be found in e.g. [31, 45].

and identify this with the *spin scalar-product* analogue to the dot-product $x_\mu y^\mu$ from special relativity. We can introduce a metric tensor, the *spinor metric* ϵ via [5]

$$\epsilon^{ab} \equiv i\sigma_2^{ab} = \begin{pmatrix} 0 & 1 \\ -1 & 0 \end{pmatrix} \quad \text{and} \quad \epsilon_{ab} \equiv -i\sigma_{2ab}0 \begin{pmatrix} 0 & -1 \\ 1 & 0 \end{pmatrix}.$$

It follows that

$$\chi^a = \epsilon^{ab}\chi_b \quad \text{and} \quad \chi_a = \epsilon_{ab}\chi^b.$$

Now we can do the same for ψ-like spinors and get, with the same definition of the spinor metric ϵ but with dotted indices, the same exact relations from above (but with dotted indices). Then, to be able to abbreviate e.g. a spinor product like $\psi_{\dot{a}}\xi^{\dot{a}}$ as $\psi\xi$ without loosing the information of their transforming representation, we define

$$\psi^{\dot{a}} \equiv \bar{\psi}^{\dot{a}}.$$

Here we will introduce the convention from [24] that only *descending* undotted indices and *ascending* dotted indices, like ${}^{a}{}_{a}$ and ${}_{\dot{a}}{}^{\dot{a}}$, may be suppressed.

From here on one can see that the complex conjugate of a left chiral spinor tranforms exactly like a right chiral spinor with lowered indices. With this and the abililty to raise lowered indices via ϵ, we can then define

$$\bar{\chi}_{\dot{a}} \equiv \chi_a^* \quad \text{and} \quad \psi^a \equiv \bar{\psi}^{\dot{a}*}.$$

As an enclosure we can write the Dirac spinor we started with in the new notation

$$\vec{\Psi} = \begin{pmatrix} \bar{\psi}^{\dot{a}} \\ \chi_a \end{pmatrix},$$

following the convention from [8].

χ-type Spinor Convention

We will follow the usual convention to (mostly) only use χ-type spinors to describe Dirac spinors. Therefore, we define *charge conjugation* at two-component level by

$$\chi^c \equiv i\sigma_2\chi^*, \quad \psi^c \equiv -i\sigma_2\psi^*$$

and can then write a general field of a particle p as

$$\vec{\Psi}^{(p)} = \begin{pmatrix} \chi_{\bar{p}}^c \\ \chi_p \end{pmatrix},$$

where $\bar{p}$ denotes the antiparticle of p. Particle fields can be named as $p_L = \chi_p$ and $\bar{p}_L^c = \chi_{\bar{p}}^c$.

5 Here the analogue would be the space time tensor $g^{\mu\nu}$, but with the important difference that ϵ is antisymmetric under interchange of the indices.

1 INTRODUCTION

The standard model (SM) is the most successful and most fundamental theory of particle physics to date. It yields great use by providing precise experimental predictions. Further confirmation lies in the observations of the top-quark [3, 4] in 1995, the tau-neutrino [33] in 2001 and the Higgs-boson [1] in 2012. Which were the remaining theorised, yet to be experimentally determined, elementary particles in the SM.

But the SM is not perfect. Despite the great achievements there are some flaws and concepts not understood. First of all, the SM inherits features that are added ad hoc. Two of them being the *hierarchy problem* and the *strong CP problem*. Further, the SM consists of 19 numerical parameters. But next to the need to experimentally measure their values, their origin and relations are unknown. There are experimental deviations that can not be explained by the SM as well. One prime example being the *muon g-2-experiment* measuring the anomalous magnetic dipole moment of the muon with a standard deviation σ of 4.2 [5] in comparison to the SM.

For the SM to be an inherently complete theory it needs to be extended. It fails to explain gravity, which is described by *general relativity*. It further delivers no explanation for the asymmetry of matter to antimatter (the *missing baryon problem*, solvable through the ad hoc added strong CP breaking). Next to that the SM yields little to no answers to what *dark matter* and *dark energy* are, but which, following cosmological observations from the recent years, should contribute with circa 26% and 69% to the total energy in the universe, respectively.

This thesis focuses on the last point made. We will introduce the *minimal supersymmetric standard model* (MSSM) as a *supersymmetry* (SUSY) extension to the SM.[1] This model proposes new particles next to the SM-ones with one being the neutralino. The neutralino, as a *weakly interactive massive particle* (WIMP), is a great candidate for dark matter. Main component of this thesis is the analytical calculation of the cross-section of the neutralino-gluino coannihilation (the gluino being another SUSY particle). This annihilation carries a missing contribution to the relic density of the neutralino in the programme `DM@NLO`[2], where the cross-section will be implemented and the relic density will be calculated numerically.

WE PROCEED AS FOLLOWS: In Chapter 2 we will start with a theoretical overview of dark matter. There, evidence for dark matter and possible candidates with an emphasis on WIMPs like the neutralino are listed. Further, we introduce the concept of relic density and derive its calculation. After that SUSY is introduced and motivated in Chapter 3. In this chapter, we will give an elementary but nonetheless technical introduction to SUSY. Main goal of the introduction to the SUSY framework will be to craft the SUSY Lagrangian. Last the MSSM and its most important aspects, such as the neutralino, with a focus on why it is a good candidate for dark matter, R-parity and soft SUSY breaking are described. After this theoretical introduction to the main concepts needed for this thesis, the actual calculations will be done. In Chapter 4 we compute the cross-section

1 The MSSM and more general SUSY allows for a lot of applications in theories beyond the SM. Some of them will be shortly stated next to the introduction and motivation of SUSY.

2 See Appendix B.

for the neutralino-gluino coannihilation in the usual four-component or Dirac spinor presentation. The next chapter, Chapter 5, features the same calculation but with a two-component spinor technique, which is introduced there as well. The last part of this thesis is the numerical analysis of the found results for the cross-section in the last two chapters. This and the calculation of the relic density – via integration of the Boltzmann equation – for the neutralino will be done in Chapter 6, where we implement the process in `DM@NLO`. There we will get information about the relevance of this specific annihilation process and discuss scenarios inside of the MSSM.

The programme `DM@NLO` and the software chain including other dark matter software is described in Appendix B. In Appendix C we summarize – for the sake of clarity – the Feynman rules and in Appendix D the relations useful for the cross-section calculations from Chapter 4 and Chapter 5.

2 DARK MATTER

In this first chapter, we will briefly introduce the idea behind dark matter, why we need it and state answers to what exactly dark matter could be. For this chapter is mainly meant to be a short primer with the main concepts and, therefore, will often direct to sources going into more detail.

We already introduced dark matter with the fact that baryonic matter only accounts for a very small amount of total energy in the Universe. The *Planck 2018* results [7] from the *Planck collaboration* yield

$$\Omega_{DM}h^2 = 0.120 \pm 0.001 \quad \text{and} \quad \Omega_{BM}h^2 = 0.0224 \pm 0.0001 \tag{2.1}$$

for the density of dark matter and baryonic matter in the Universe today, respectively. h is the Hubble parameter. This lets us conclude that most of matter in the Universe is dark matter. The astonishing fact is, we can not see or interact with it directly. Therefore, trying to answer the question of what dark matter is, is a very theoretical one. Experiments only provide lower bounds which must be adhered to by theories wanting to solve the dark matter problem. In the next Chapter 3 we will introduce the MSSM, which is one possible theoretical framework with a possible candidate.

2.1 EVIDENCE

The first examination of gravitational anomaly can be contributed to Fritz Zwicky in 1933. While examining the Coma galaxy cluster he calculated the gravitational attraction from the observed rotational velocities from said cluster. By calculating the attraction again, but with luminous matter only, he obtained an around 400 times smaller value and, thus, concluded there has to be some kind of *dark* matter. [50]

In the following century, much more pieces of evidence were to come. On galactic-scale, it was and is done by the observation of rotation curves of galaxies, one example work being [15]. On galaxy-cluster-scale it is done by calculating the real mass of clusters via for example the virial theorem and comparing it to its "luminous mass", following the procedure from Zwicky. One more recent example for this procedure is [13]. The last scale, the cosmological scale, which promises to deliver not only local densities but the total amount of dark matter in the Universe, can be examined by analysing the Cosmic Microwave Background (CMB). One often recited data set is delivered by the WMAP [6]. For a richer and more detailed summary of evidential approaches consult Chapter 2 in [17].

The Planck collaboration – mentioned above – took the most promising results from all these different approaches, most recently 2018, and combined them to get the distribution with confidence limits stated in (2.1). What should be clear by now is that the evidence for dark matter is compelling and astonishingly mostly coherent between all astrophysical scales.

2.2 CANDIDATES

With clear proof of matter missing in the Universe, the next step is to find candidates that can be the dark matter particle. There are many theories of many different candidates. For we cannot list all of them, we will introduce only two candidates and refer once more to [17], the *particle dark matter report* from Gianfranco Bertone et al., for a more complete enumeration.

One of the first and most promising candidates was the SM neutrino. The neutrino only interacts via the weak-interaction and via gravity. Therefore, it is a *dark* particle – as it should be for a dark matter candidate. A strong argument in favour of the neutrino was the fact that its existence is known compared to many hypothetical candidates. But recent updates to the neutrino's mass via CMB and geometrical analysis yield $\sum m_\nu < 0.2\,\mathrm{eV}$ as an upper bound (see e.g. [17]). A simple calculation from [51]

$$\Omega_\nu h^2 = \frac{\sum m_\nu}{93.14\,\mathrm{eV}} \lesssim 0.002, \tag{2.2}$$

derived by taking the relative contribution of neutrino density ρ_ν to the critical density ρ_c – needed to halt the Universe's expansion, shows that neutralinos are simply not abundant enough to be the main contribution to dark matter. As a result, we need to find other particles to fully explain dark matter.

Today the most studied dark matter candidates are WIMPs. The next section will be fully devoted to their description.

2.3 WIMPS

Weakly Interactive Massive Particles (WIMPs) are hypothetical particles that only interact via the weak force and via gravity – like the neutrino – but are supposed to have masses in the range of tenth GeV to several TeV. Most WIMPs can, in their theoretical model, be adjusted to exactly the right constant density, the so-called *relic density*, to be dark matter. Further, they can be detected in many ways and deliver doable calculations of their relic density.

WIMPs are categorized as *cold matter* and are so-called *thermal relics*. They are assumed to have been in local thermodynamic equilibrium at the early stages of the Universe. The *equilibrium abundance* of a WIMP depends on the ratio of its mass to temperature relative to some density. This relative density is often chosen to be the entropy density $s \propto T^3$. Therefore, we can define a new variable, the *comoving number density*

$$Y \equiv \frac{n_X}{s}, \tag{2.3}$$

where n_X corresponds to the number density of the WIMP with mass m_X. A particle in the early Universe will follow its equilibrium abundance if its interaction rate is sufficiently high to keep it in thermodynamic equilibrium. Roughly one can say that the interaction rate needs to be greater than the expansion rate of the Universe H. If not, the particle can not stay in equilibrium and it *decouples*, Y will be constant from thereon. This process is called *freeze-out*. An illustration of this process can be seen in Figure 2.1.

One most promising candidate for a WIMP is the SUSY particle neutralino. We will come back to the neutralino in the next chapter, where we will introduce SUSY in general.

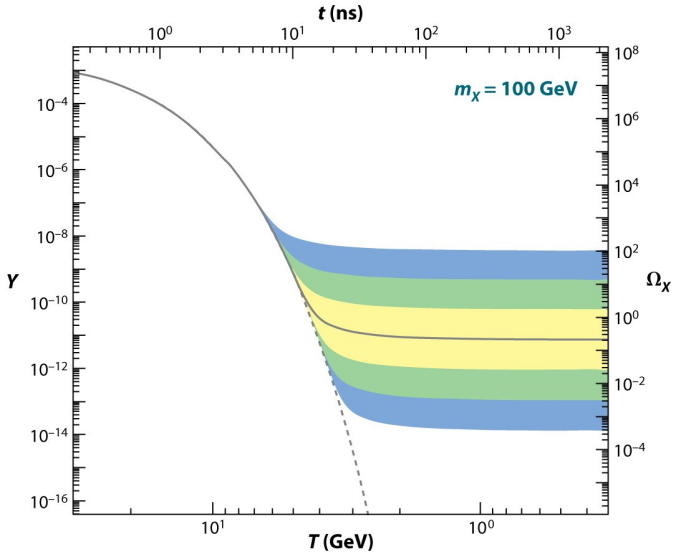

Figure 2.1: The comoving number density Y (left) and resulting thermal relic density Ω_X (right) of a 100 GeV, P-wave annihilating dark matter particle as a function of temperature T (bottom) and time t (top). The solid contour is for an annihilation cross-section that yields the correct relic density, and the shaded regions are for cross-sections that differ by 10, 102, and 103 from this value. The dashed contour is the number density of a particle that remains in thermal equilibrium. [27]

2.3.1 Relic Density

The thermal relic density Ω_X of the WIMP X, as seen in Figure 2.1, is the value one needs to find for a particle X to be able to make a statement whether X is dark matter or if X is at least carrying a substantial contribution to (2.1). Therefore, in this section, we will shortly state a rough analysis and derivation of Ω_X.

We start with the Boltzmann equation and manipulate it to be an equation for the number density n of a particle [1]

$$\frac{dn}{dt} = -3Hn - \langle \sigma_A v \rangle \left(n^2 - n_{eq}^2 \right), \tag{2.4}$$

where σ_A is the total annihilation cross-section, v is the velocity and the brackets $\langle \cdots \rangle$ denote the thermal averaged value of some quantity. n_{eq} is the number density at thermal equilibrium, which under the assumption of a heavy particle yields in the Maxwell-Boltzmann approximation

$$n_{eq} \sim \left(\frac{m_X T}{2\pi} \right)^{3/2} e^{-m_X/T}. \tag{2.5}$$

Usually one calculates (2.4) numerically. We will in the following introduce some approximations so that we get analytical solvable expressions.

Now we can make use of the comoving number density Y as defined in (2.3) and exploit the conservation of entropy per comoving volume sR^3 to get [2]

$$s\dot{Y} = \dot{n} + 3Hn. \tag{2.6}$$

1 Consult [34] for a detailed derivation. From here on we will for convenience neglect the X in n_X.

2 This equivalence can be easily checked by remembering that $H = \dot{R}/R$ and the fact that $n \propto 1/R^3$, with R the *scale factor* of the Universe. See e.g. [34].

With that and substituting (2.3) in (2.4) we get

$$s\dot{Y} = -\langle\sigma_A v\rangle s^2 \left(Y^2 - Y_{eq}^2\right), \tag{2.7}$$

where $Y_{eq} = n_{eq}/s$. From here on we will only sketch the remaining procedure as described in [34]. The idea is to expand $\langle\sigma_A v\rangle$ in terms of v^2 and introduce a new variable $\Delta = Y - Y_{eq}$. Then (2.7) can be solved analytically in the two extreme regions where $T \ll T_f$ and $T \gg T_f$, with T_f being the freeze-out temperature of the specific particle. Integrating the latter one of these equations from T_f to T_0, the temperatur today, gives a result for the comoving number density for today, namely Y_0. Then we can use Y_0 to calculate the density of particle X via

$$\rho_X = m_X n_0 = m_X s_0 Y_0, \tag{2.8}$$

where s_0 is the entropy density for $T = T_0$. Using the definition of Ω and inserting ρ_X then yields

$$\Omega_X h^2 = \frac{\rho_X}{\rho_c} \sim \frac{1}{\langle\sigma_A v\rangle}, \tag{2.9}$$

where in the last step we made an order-of-magnitude estimate using an approximation from [32]. And note that the thermal relic density is inversely proportional to the annihilation cross-section. If m_X is the only mass scale then we can write the cross-section as $\sigma_A v \propto m_X^{-2}$, see [27], and can construct the graph shown in Figure 2.1 for $m_X = 100\,\text{GeV}$.

Last it is needed to state that till now we only considered annihilation but no coannihilation processes for the WIMP. As it was shown in [28] the calculation of the relic abundance fails for other particles having masses close to m_X. Then coannihilation of X with that particle can contribute substantially to the relic density. The main difference is now that we need to include all possible coannihilations and (2.4) changes to

$$\frac{dn}{dt} = -3Hn - \sum_{i,j=1}^{N} \langle\sigma_{ij} v_{ij}\rangle (n_i n_j - n_i^{eq} n_j^{eq}) \tag{2.10}$$

for $i, j = \{1, \cdots, N\}$ particles. Following that, one needs to do different approximations or numerical computations that will not be discussed here, but can be looked up in e.g. [17]. Nevertheless, one can achieve an expression dependant on the cross-section, like shown prior to (2.9). Nowadays all numerical codes, such as `MicrOMEGAs` [16], include coannihilations.

Concluding we can say that the goal will be to calculate the cross-sections of annihilation and coannihilation processes of WIMP X (with some partner particle P for the coannihilations). The effective cross-section – given by [14] – is

$$\begin{aligned}\sigma_{\text{eff}} = \frac{g_X^2}{g_{\text{eff}}^2}\Big[&\sigma_{XX} + 2\sigma_{XP}\frac{g_P}{g_X}(1+\Delta)^{3/2}e^{-x\Delta} \\ &+ \sigma_{PP}\frac{g_P^2}{g_X^2}(1+\Delta)^3 e^{-2x\Delta}\Big],\end{aligned} \tag{2.11}$$

where $x = m_X/T$ and $\Delta = (m_P - m_X)/m_X$ denotes the mass splitting between the masses of WIMP and coannihilation partner. g_X and g_P are the numbers of degrees of freedom of X and P, respectively. The effective coupling is given by

$$g_{\text{eff}} = g_X + g_P(1+\Delta)^{3/2}\exp(-x\Delta). \tag{2.12}$$

By assuming that X and P are in chemical equilibrium the problem reduces to solving a single Boltzmann equation via the effective cross-section (2.11).

2.3.2 Detection

Last we will very briefly talk about the detection of WIMPs. As mentioned above, it is highly recommended to consult [17], alternatively Section 2.3 in [25] gives a good overview too.

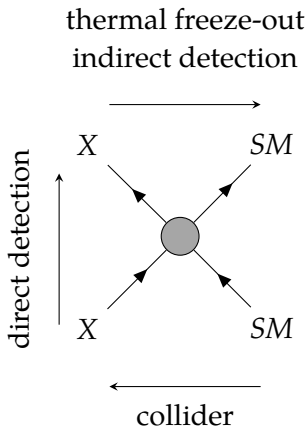

Figure 2.2: The different ways to search for WIMP dark matter candidates demonstrated by a scattering of WIMP X with SM particles.

There are three different channels for the detection of dark matter, as listed in Figure 2.2. We will focus on WIMPs that interact not only gravitational with SM particles:

- **Direct detection** tries to measure the interactions between the WIMP candidate X and a SM nucleus. Two prime examples being XENON [10] and EDELWEISS [11].
- **Indirect detection** searches for SM final states of $X, X \to SM, SM$ annihilations and coannihilations mostly from massive stellar areas such as centres of galaxies. This is the process that happened at the freeze-out, as mentioned above. IceCube [2] and Super-Kamiokande [48] detect neutralinos in hindsight to them being viable end-products from dark matter annihilations.
- **Collider** rely on scattering two SM particles and measuring anomalies like missing energy, which lead to conclude there are X final states not detected.

This thesis' process is one possible freeze-out (or indirect detection) coannihilation of the neutralino as the WIMP with another theoretical particle, the so-called gluino. The next chapter is devoted to the theoretical introduction of the neutralino (and gluino) in SUSY. After that, in Chapter 6 we will come back to the discussion about the relic density, where we actually calculate the cross-section and discuss the process and the neutralino as a dark matter candidate.

3 SUPERSYMMETRY

The framework in which we will be working is *supersymmetry* (SUSY). As we will see, SUSY (with some regulations) yields a very promising candidate for a WIMP and dark matter, the neutralino. In this chapter, SUSY is introduced, and a phenomenological framework with neutralino dark matter is crafted.

3.1 MOTIVATION

We start by giving hints on the motivation of SUSY. For this was done many times we restrict this section to two brief examples. But we refer to [38] for a theoretical and more complete overview.

The most important motivation for SUSY in our case is the possibility for a great dark matter candidate. We will come back to this discussion at the end of this chapter when we have introduced a special SUSY theory, the MSSM, in which the neutralino actually fulfils the requirements of being a WIMP.

Next to the two following points, there are several more quantitative indications, such as the SM being unable to restrict the Higgs mass, the possibility of SUSY extensions allowing for unification of the three coupling constants and, therefore, hoping for a *grand unified theory* (GUT) and SUSY being able to explain *electroweak symmetry breaking* (EWSB).

3.1.1 The fine-tuning Problem

The Higgs self-interaction potential is

$$V = -\mu^2 \phi^\dagger \phi + \frac{\lambda}{4}(\phi^\dagger \phi)^2, \tag{3.1}$$

with $\phi = (\phi^+, \phi^0)$ the SU(2) doublet "Higgs" field and $\mu^2 > 0, \lambda > 0$ the interaction strengths. μ is

$$\mu^2 = \mu^2_{\text{tree}} - \lambda\Lambda^2 \tag{3.2}$$

a combination of a tree-level value μ_{tree} and a one-loop correction term that is dependant on the energy cut-off Λ, which depicts the upper loop-integration bound. Λ can theoretically go up to infinity because of the SM being renormizable. But then we encounter a problem: the *vacuum expectation value* of the neutral Higgs field VEV $= \langle 0|\phi^0|0\rangle$ is in the order of hundreds of GeV and the mass of the Higgs boson is proportional to μ (and, therefore, all masses in the SM are). If now Λ grows to very large GeV scales, we can only save physics by *fine-tuning*. This means we need an equally huge value for μ_{tree} so that in (3.2) they cancel nearly completely but to a rest, which is physically acceptable.

This is in fact no "natural" behaviour. This problem can be solved by SUSY in the way that we will get new particles and, hence, new loop-interactions for the Higgs particle that can help with cancelling the divergence given by Λ. In Figure 3.1 this is depicted with two new scalars S and S' that couple to the Higgs boson.

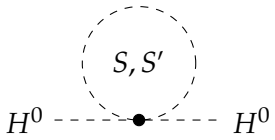

Figure 3.1: Self-energy Higgs graph contribution with SUSY-scalars S, S'.

Here it has to be stated that this motivation for SUSY is becoming less and less important. Because of new searches not finding evidence for SUSY particles the masses of the possible interaction superpartners are gaining lower bounds in the range of several hundred GeV to one thousand GeV (see PDG [51]). By masses going higher than the VEV value the correction of SUSY grows smaller. Up to a point, at which one again needs to have fine-tuning of significant scale.

3.1.2 Theoretical Considerations

We will state a consideration, following Section 1.3 in [8], that SUSY is the most general extension of the Poincaré group underlying the SM and, hence, of great theoretical relevance.[1]

All SM symmetry charges Q, such as the electromagnetic or the isospin charge, are Lorentz scalars. Therefore, they do not alter a state's spin j

$$Q|j\rangle = |j\rangle. \tag{3.3}$$

But we know that the generators of the Poincaré group, the momentum operator P_μ that generates translations and the generator of rotations and boosts $M_{\mu\nu}$, behave like space-time displacements. So are there any spin altering (non Lorentz scalar), conserved operators? The *Coleman-Mandula-Theorem* states – very roughly – that there are no allowed non-trivial [2] conserved quantities, apart from the generators of the Poincaré group. Luckily it turns out that charges which transform spinor-like under Lorentz transformation are not actually excluded. By defining such a charge as Q_a with spinor component a one can see that it will change the spin

$$Q_a|j\rangle = |j \pm \tfrac{1}{2}\rangle. \tag{3.4}$$

So the newfound operator can be used to transform between bosonic and fermionic particles.[3]

The important next step is to now create a new *super*-algebra describing our system. Q_a, as a conserved quantity, has to commute with the Hamilton operator

$$[Q_a, H] = 0 \quad \text{and} \quad [\{Q_a, Q_b\}, H] = 0. \tag{3.5}$$

Furthermore, the anticommutator $\{Q_a, Q_b\}$ has to be conserved too. By seeing that said commutator inherits 3 degrees of freedom we can say that it transforms like a spin-1

1 It is highly recommended to consult Part II of [45] for a good, comprehensive introduction to the Lorentz and Poincaré group and, in later chapters, for an introduction of *quantum field theory* (QFT) and the SM building upon these.

2 Not Lorentz scalar.

3 Far more groundbreaking than this is the fact that (3.4) predicts new *superpartners* to the known SM particles with the same characteristics but with different spin! This means, if SUSY in any form turns out to be physically true, we only know half of the particles in the universe. Furthermore, the new *superparticles* can be useful as we will see with the neutralino as a dark matter candidate. This discussion of superpartner particles will be continued in the MSSM in Section 3.3.

object. Following the Coleman-Mandula-Theorem, the only conserved four-vector that can describe this new symmetric object is P_μ. Therefore,

$$\{Q_a, Q_b\} \sim P_\mu, \tag{3.6}$$

where the "$\sim$" states constants and proper matrices for contracting the "$_\mu$" are missing.

(3.6) now tells us that we have a connection and interaction between space-time symmetry and internal symmetries.[4] We have successfully extended the Poincaré algebra and – more strikingly – space-time itself by now being able to take the square root of derivatives in the form of Q_a. In Section 3.2.2 we will extend space-time by the newfound fermionic degrees of freedom in terms of the so called *superspace*.

3.2 FRAMEWORK

We will now start to build the framework for SUSY, the main goal being the construction of the SUSY Lagrangian $\mathcal{L}_{\text{SUSY}}$. For a more sophisticated review of SUSY see e.g. the lecture notes by Quevedo [37].

3.2.1 Algebra

The super-algebra we partially derived in Section 3.1.2 can be completed to be [5]

$$[P_\mu, Q_a] = 0 \tag{3.7}$$
$$[P_\mu, \bar{Q}^{\dot{b}}] = 0 \tag{3.8}$$
$$[M_{\mu\nu}, Q_a] = -(\sigma_{\mu\nu})_a{}^b Q_b \tag{3.9}$$
$$[M_{\mu\nu}, \bar{Q}^{\dot{a}}] = i(\bar{\sigma}_{\mu\nu})^{\dot{a}}{}_{\dot{b}} \bar{Q}^{\dot{b}} \tag{3.10}$$

and

$$\{Q_a, \bar{Q}_{\dot{b}}\} = (\sigma_{\mu\nu})_{a\dot{b}} P_\mu \tag{3.11}$$

with the generators of $(\frac{1}{2}, 0)$ and $(0, \frac{1}{2})$ Lorentz groups $\sigma_{\mu\nu}$ being the missing matrix from (3.6).

One important consequence originates from (3.7) and (3.8), namely that Q_a commutes with P^2. This means physically that all particles within one irreducible representation of the superalgebra, a *supermultiplet*, have to have the same mass. This, however, can not be true for the supersymmetric partners with the same mass as the SM particles should have been already experimentally discovered by now. This is a hint at the need for symmetry-breaking of SUSY. This, in hindsight on its need to adjust $\mathcal{L}_{\text{SUSY}}$, will be discussed in Section 3.3.1.

3.2.2 Superfields

To be able to build $\mathcal{L}_{\text{SUSY}}$ we need all possible field interactions for our supermultiplets. These, so called *superfields*, which not only are dependant on x^μ but also on new fermionic

4 See the *Haag-Łopuszański-Sohnius-Theorem* for more detail.

5 Taken from [18]. The algebra was originally derived following the Haag-Łopuszański-Sohnius-Theorem.

degrees, will be constructed in the *superspace-formalism*, which will now be introduced as a first step.

Remember the well-known unitary space-time translation operator $U(x) = \exp(-ixP)$ with generator P^μ. Analogue to P^μ we should think of Q as generating shifts in the spinor argument. Like xP we can define the new fermionic degrees of freedom by θQ and $\theta^* Q^\dagger$, namely θ and θ^*. This will now allow us to build a (unitary) SUSY transformation

$$U(x,\theta,\theta^*) \equiv \mathrm{e}^{ixP}\mathrm{e}^{i\theta Q}\mathrm{e}^{i\bar{\theta}\bar{Q}}, \tag{3.12}$$

which achieves space-time **and** spinorial translations. If a field $\phi(0)$ transforms under (3.12) we can define it as a superfield Φ that obeys

$$\Phi(x,\theta,\theta^*) = U(x,\theta,\theta^*)\Phi(0)U^{-1}(x,\theta,\theta^*). \tag{3.13}$$

Consider now

$$U(y,\xi,\xi^*)U(x,\theta,\theta^*), \tag{3.14}$$

which should induce transformations in space-time as well as in θ,θ^*, just like $U(y)U(x)$ induces the shift $x \to y$ in only x^μ. (3.14) can be evaluated using the famous *Baker-Campbell-Hausdorff-Identity* (see [8]) and we can identify the induced transformations as

$$0 \to \theta \to \theta^* + \xi^* \tag{3.15}$$
$$0 \to \theta^* \to \theta^* + \xi^* \tag{3.16}$$
$$0 \to x^\mu \to x^\mu + y^\mu - i\theta^a(\sigma^\mu)_{ab}\bar{\xi}^{\dot{b}}, \tag{3.17}$$

where in the last equation we see the, already phenomenological mentioned, fact of interaction between internal (spinorial) symmetries and space-time.

We can write Q in superspace representation via

$$Q_a = -i\frac{\partial}{\partial\theta_a} - \sigma^\mu_{a\dot{b}}\bar{\theta}^{\dot{b}}\partial_\mu \tag{3.18}$$
$$\bar{Q}_{\dot{a}} = i\frac{\partial}{\partial\bar{\theta}^{\dot{a}}} + \theta^b\sigma^\mu_{b\dot{a}}\partial_\mu, \tag{3.19}$$

which can be achieved by considering infinitesimal displacements.[6] As a small sanity check one can insert the new Q's into (3.7)-(3.11) and see that it indeed does satisfy the superalgebra.

Let us now consider a superfield F. In general F can be highly reducible. But to identify the supermultiplets we need irreducible representations. Therefore, we need to constrain F. This can be done by defining – very similiar to Q – new covariant chiral derivatives

$$\mathcal{D}_a \equiv \frac{\partial}{\partial\theta_a} + i\sigma^\mu_{a\dot{b}}\bar{\theta}^{\dot{b}}\partial_\mu \tag{3.20}$$
$$\bar{\mathcal{D}}_{\dot{a}} \equiv -\frac{\partial}{\partial\bar{\theta}^{\dot{a}}} + i\theta^b\sigma^\mu_{b\dot{a}}\partial_\mu, \tag{3.21}$$

which do satisfy the SUSY algebra (3.7)-(3.11) and are, hence, valid SUSY transformations. Then, possible constraints on F can be choosen to be

$$\bar{\mathcal{D}}_{\dot{a}}F = 0 \tag{3.22}$$
$$\mathcal{D}_a F^\dagger = 0 \tag{3.23}$$
$$F = F^\dagger, \tag{3.24}$$

6 See for derivation Section 6.2 in [8]. Recall the analogue procedure for e.g. the angular momentum operator.

where, if F obeys them, F is a supermultiplet.

(3.22)-(3.24) now tell us that we should have three different behaving superfields. A superfield transforming like (3.22) is called a *left chiral superfield* $\Phi(x,\theta)$ and a superfield transforming like (3.23) is called a *right chiral superfield* $\Phi^\dagger(x,\theta^*)$. Because of the fields only depending on either θ or θ^* they contain only χ or ψ-like spinors, respectively, and, therefore, we are right to call them *left* or *right* fields. The most general left and right chiral superfields can, in terms of their expansion in θ or θ^*, be written as [7]

$$\Phi(x,\theta) = \phi(x) + \theta\chi(x) + \frac{1}{2}\theta\theta F(x) \tag{3.25}$$

$$\Phi^\dagger(x,\theta^*) = \phi^*(x) + \theta^*\psi(x) + \frac{1}{2}\overline{\theta\theta}F^*(x), \tag{3.26}$$

where we have included three component fields, namely a complex scalar $\phi(x)$ transforming in the $(0,0)$ representation, a complex (left or right) two-spinor $\chi(x)$ or $\psi(x)$ transforming in the $(\frac{1}{2},0)$ or $(0,\frac{1}{2})$ representation and again a complex scalar, the *auxiliary field* $F(x)$. This choice is mandatory to ensure Φ transforms like a Lorentz scalar and we, thus, have a superfield consisting of fermionic and bosonic fields.[8]

The SUSY transformation of these component fields, exemplary for the left chiral field, can be evaluated to be [9]

$$\delta_\epsilon\phi \sim \epsilon\chi \tag{3.27}$$

$$\delta_\epsilon\psi \sim i\partial_\mu\phi\sigma^\mu\epsilon^* - F\epsilon \tag{3.28}$$

$$\delta_\epsilon F \sim i\partial_\mu\psi\sigma^\mu\epsilon^* \tag{3.29}$$

and we, as a result, have a transformation between fermionic and bosonic components. One more thing to notice is that (3.29) states F transforms like a total derivative and is, hence, Lorentz invariant. The F containing, so called *F-term*, of Φ is, therefore, the part we later need for constructing the (Lorentz invariant) Lagrangians.

Before we start to construct the SUSY Lagrangian the last possible superfield as defined by (3.24) has to be discussed. These *vector superfields* are dependant on θ **and** θ^*. Similiar to Φ a general vector superfield V can be found (see e.g. [38]). V has double the terms of the chiral superfields. We can, however, by postulating gauge invariance and taking a suited supergauge, reduce the free component fields to three again. One possible choice is the *Wess-Zumino gauge*. Then, the general vector field V can be found to be

$$V_{\mathrm{WZ}}(x,\theta,\theta^*) = \theta\sigma^\mu\theta^*A_\mu(x) + \theta\theta\theta^*\lambda^*(x) + \frac{1}{4}\theta\theta\overline{\theta\theta}D(x), \tag{3.30}$$

with the real vectorfield $A_\mu(x)$, its fermionic superpartner $\lambda(x)$ and an auxiliary scalar field $D(x)$. Via the transformation behaviour of D

$$\delta_\epsilon D \sim i\partial_\mu(\lambda\sigma^\mu\epsilon^* + \lambda^*\bar{\sigma}^\mu\epsilon) \tag{3.31}$$

we can again see that the auxiliary field D is Lorentz invariant and, therefore, the *D-term* of V is the important part to build Lagrangians.

---

7 There can not be higher orders of θ, because of their fermionic nature, which states that $\theta_a^2 = 0$. The factor of $1/2$ is convention.

8 In other words, we already have the description of an SM particle and its superpartner in the form of superfields, where they are described by the ϕ and χ fields.

9 The "$\sim$" denotes the lack of conventional prefactors.

3.2.3 Lagrangians

To now build the SUSY Lagrangian, we need to consider interactions of all superfields. We begin with only chiral superfields and will then adapt the chiral Lagrangian to include vector superfields in non-abelian supermultiplets.

Before we start counting all Φ interactions we can reduce this number by a large margin. This can be done by remembering that the Lagrangian has to have dimension of $D = 4$. Because the dimensions of the component fields ϕ, χ and F are set by (3.25), we only have four possibilities to combine Φ superfields while remaining four-dimensional (See [37]). The first possibility, with only showing the significant F-term, is [10]

$$\Phi_i \Phi_j \big|_F = \phi_i F_j + \phi_j F_i - \chi_i \chi_j, \tag{3.32}$$

the product of two left chiral superfields, where i and j denote different types of superfields. The second one is the three-product, namely

$$\Phi_i \Phi_j \Phi_k \big|_F = \sum_{i,j,k}^{\text{cyclic}} \phi_i \phi_j F_k - \sum_{i,j,k}^{\text{cyclic}} \chi_i \chi_j \phi_k. \tag{3.33}$$

With the last missing chiral product being the trivial single Φ_i, we can now define the so called *superpotential*

$$\mathcal{W} \equiv h_i \Phi_i + \frac{1}{2} M_{ij} \Phi_i \Phi_j + \frac{1}{6} y_{ijk} \Phi_i \Phi_j \Phi_k, \tag{3.34}$$

which consists of all chiral superfield interactions mentioned before plus some coupling constants to supress the indices.

The last possibility is the product of χ and ψ-type superfields

$$\Phi^\dagger \Phi \big|_D = F F^* - \phi \partial_\mu \partial^\mu \phi^* - i \psi \sigma_\mu \partial^\mu \chi, \tag{3.35}$$

which behaves like a vector superfield and we, therefore, have to consider only the D-term.

With the superpotential (3.34) and (3.35) we can then write a first SUSY invariant Lagrangian describing chiral interactions

$$\mathcal{L}_{\text{chiral}} = \Phi_i^\dagger \Phi_i \big|_D + \left[\mathcal{W} + \text{h.c.} \right]_F \tag{3.36}$$

$$= \frac{i}{2} \partial_\mu \phi_i^* \partial^\mu \phi_i + \bar{\chi}_i i \bar{\sigma}^\mu \partial_\mu \chi_i + F_i^* F_i + \frac{\partial \mathcal{W}}{\partial \phi_i} F_i - \frac{1}{2} \frac{\partial^2 \mathcal{W}}{\partial \phi_i \partial \phi_j} \chi_i \chi_j + \text{h.c.}, \tag{3.37}$$

where the second equation is just the Lagrangian written out in component fields. There we can, in the first two terms, identify the *Klein-Gordon equation* and the *Weyl equation*, describing massless scalars and spinors. Furthermore, $F(x)$ can – via the equations of motion – be expressed in terms of $\phi(x)$, so that we have a supermultiplet only consisting of bosonic degrees of freedom given by ϕ and fermionic degrees of freedom given by χ.

We now have to include missing vector superfields, that is we need to consider gauge interactions. For this part, we will follow a shortened procedure taken from [38] for non-abelian gauge supermultiplets.[11]

10 From now on omitting "(x)" from component fields.

11 Non-abelian means that the generators of the gauge group do not commute. We can afterwards re-establish the abelian case by letting the generators commute again.

A possible general gauge transformation acting on a left and right chiral superfield is

$$\Phi_i{}' \equiv \exp(-i\hat{\Lambda}_{ij})\Phi_j \tag{3.38}$$
$$\Phi_i^{\dagger\prime} \equiv \Phi_j \exp(-i\hat{\Lambda}_{ji}^{\dagger}), \tag{3.39}$$

with $\hat{\Lambda}_{ij} = 2g(\Lambda^a(x,\theta)T_a)_{ij}$ and i, j now indexing superfield (particle) type and gauge group. The gauge group generator T and the chiral superfield Λ have to obey

$$\bar{\mathcal{D}}^{\dot{a}}\hat{\Lambda} = 0 \tag{3.40}$$
$$\mathcal{D}_a\hat{\Lambda}^{\dagger} = 0 \tag{3.41}$$

so that the chirality does not change under the gauge transformation. The gauge group transformation for a vector superfield V is

$$\mathrm{e}^{V'} = \mathrm{e}^{-i\Lambda^{\dagger}}\mathrm{e}^{V}\mathrm{e}^{i\Lambda} \tag{3.42}$$
$$\mathrm{e}^{-V'} = \mathrm{e}^{-i\Lambda}\mathrm{e}^{V}\mathrm{e}^{i\Lambda^{\dagger}}. \tag{3.43}$$

Further, we need to include the supersymmetric analogue to the field strength tensor $F^{\mu\nu}$ and, therefore, an analogue to the Maxwell-term from *quantum electro dynamics* (QED). This can be achieved by defining the *supersymmetric field strength* as

$$W_a = -\frac{1}{4}\overline{\mathcal{D}\mathcal{D}}\mathrm{e}^{-V}\mathcal{D}_a\mathrm{e}^{V} \tag{3.44}$$
$$\bar{W}^{\dot{a}} = -\frac{1}{4}\mathcal{D}\mathcal{D}\mathrm{e}^{V}\bar{\mathcal{D}}^{\dot{a}}\mathrm{e}^{-V}. \tag{3.45}$$

So that the Maxwell-term analogue would be $1/16(W^aW_a + \bar{W}_{\dot{a}}\bar{W}^{\dot{a}})$, which transforms as left- and right-handed superfields and we, thus, need to consider only the F-term for the Lagrangian.

With that and the considerations from before we can finally write down a SUSY Lagrangian including chiral and gauge supermultiplets

$$\mathcal{L}'_{\mathrm{SUSY}} = \Phi_i^{\dagger}\mathrm{e}^{V_{ij}}\Phi_j\big|_D + \frac{1}{16}\Big[W^aW_a + \bar{W}_{\dot{a}}\bar{W}^{\dot{a}}\Big]_F + \Big[\mathcal{W} + \mathrm{h.c.}\Big]_F. \tag{3.46}$$

However, $\mathcal{L}'_{\mathrm{SUSY}}$ is not complete in the sense that it includes unphysical degrees of freedom originating in certain gauges from the gauge superfields. This can be solved by including additional terms into the Lagrangian, via so called *ghost-fields*, which add "negative" degrees of freedom to compensate for the unphysical degrees.[12]

With all that in mind we can construct the full SUSY Lagrangian as

$$\mathcal{L}_{\mathrm{SUSY}} = \mathcal{L}'_{\mathrm{SUSY}} + \mathcal{L}_{\mathrm{ghosts}}. \tag{3.47}$$

We will not state $\mathcal{L}_{\mathrm{ghosts}}$ here explicitly, but refer to e.g. [38]. It will be sufficient for future discussion to know that no relevant parameters describing the model occur in $\mathcal{L}_{\mathrm{ghosts}}$.

3.3 THE MSSM

The *minimal supersymmetric standard model* (MSSM) is the minimal field-containing, $N = 1$ and R-parity conserving (more on that in Section 3.3.3) SUSY extension to the SM. To

12 This idea comes from Faddeev and Popov [26] and holds for general gauge quantum field theories.

build this minimal extension we can construct a supermultiplet per SM particle. The SM fermions, corresponding to their chirality, are either embedded into the chiral superfield (3.25) or (3.26) in form of the left and right chiral spinors χ or ψ.[13] The scalar superfield ϕ then is the bosonic superpartner of each fermionic SM particle. These *scalar particles*[14] (sparticles) only differ in spin and are listed in the second column in the first two rows of Table 3.1. All SUSY partner particles will be denoted by a tilde. The χ parts of SM

PARTICLES		SPIN 0	SPIN 1/2	$SU(3)_c, SU(2)_L, SU(1)_y$
squarks, quarks	Q	$(\tilde{u}_L, \tilde{d}_L)$	(u_L, d_L)	$\mathbf{3}, \mathbf{2}, 1/3$
(×3 generations)	$\bar{u}$	$\tilde{\bar{u}}_L = \tilde{u}_R^\dagger$	$\bar{u}_L = u_R^c$	$\bar{\mathbf{3}}, \mathbf{1}, -4/3$
	$\bar{d}$	$\tilde{\bar{d}}_L = \tilde{d}_R^\dagger$	$\bar{d}_L = d_R^c$	$\bar{\mathbf{3}}, \mathbf{1}, 2/3$
sleptons, leptons	L	$(\tilde{\nu}_{eL}, \tilde{e}_L)$	(ν_{eL}, e_L)	$\mathbf{1}, \mathbf{2}, -1$
(×3 generations)	$\bar{e}$	$\tilde{\bar{e}}_L = \tilde{e}_R^\dagger$	$\bar{e}_L = e_R^c$	$\bar{\mathbf{1}}, \mathbf{1}, 2$
Higgs, Higgsinos	H_u	(H_u^+, H_u^0)	$(\tilde{H}_u^+, \tilde{H}_u^0)$	$\mathbf{1}, \mathbf{2}, 1$
	H_d	(H_d^0, H_d^-)	$(\tilde{H}_d^0, \tilde{H}_d^-)$	$\mathbf{1}, \mathbf{2}, -1$

Table 3.1: Chiral supermultiplet fields in the MSSM. [8]

fermions are $SU(2)_L$ doublets, whereas the ψ parts are $SU(2)_L$ singlets. Furthermore, we remember our convention to write everything in terms of (antiparticle) left chiral spinors, by charge conjugation of the right chiral ones, as it is depicted in the third column for fermions. The sparticles carry the index L or R just for being able to differentiate them (corresponding to the superpartners chirality).[15]

Next, in the third row of Table 3.1, the two Higgs supermultiplets are listed, with weak hypercharge $y = \pm 1$. We need two (chiral) supermultiplets because the superpotential can only depend on ϕ but not on $\phi^\dagger$ to uphold SUSY invariance (see Chapter 5 in [8]). That is we can not, like in the SM, use the Higgs doublet and its charge conjugate (related to $\phi^\dagger$), but we instead are forced to implement two Higgs doublets. This yields a new parameter $\tan\beta$, which is the ratio of VEVs of the two Higgs.[16] The superpartners are the so called *Higgsinos*.[17] In contrast to the SM fermions here we have a boson (ϕ in Φ) in the SM but get a fermionic superpartner (χ in Φ).

In Table 3.2, one can find the SM vector bosons with their corresponding superpartners, the *gauginos*. They have to reside in vector supermultiplets, defined in (3.30). There one can see that the superpartners, related to λ, are fermions. Like in the SM, after EWSB, the gauginos $\tilde{W}^0$ and $\tilde{B}^0$ mix to give mass eigenstates for the respective superpartners of Z-boson and photon, the *zino* ($\tilde{Z}^0$) and the *photino* ($\tilde{\gamma}$).

Now it is only left to specify an MSSM superpotential with the new supermultiplets from Table 3.1. It is by choice[18]

$$W_{\text{MSSM}} = y_u^{ij} \bar{u}_i Q_j H_u - y_d^{ij} \bar{d}_i Q_j H_d - y_e^{ij} \bar{e}_i L_j H_d + \mu H_u H_d, \tag{3.48}$$

13 They can not be members of the vector supermultiplet because their left and right chirality parts transform differently under the gauge group.

14 Nomenclature is to prepend an "s~" for scalar SUSY particles, so *squarks*, *sleptons* etc.

15 As a notation we write as the spinor name the particle abbreviation, e.g. $\bar{u}_L$ instead of $\chi_{\bar{u}}$.

16 This will not add a new parameter since we can use $\tan\beta$ instead of the VEV of the Higgs like in the SM.

17 The general nomenclature will be to append an "~ino" for the superpartners with spin 1/2.

18 In fact most other choices for the superpotential are forbidden by R-parity, which will be discussed in Section 3.3.3.

NAMES	SPIN 1/2	SPIN 1	$SU(3)_c, SU(2)_L, SU(1)_y$
gluinos, gluons	$\tilde{g}$	g	$\mathbf{8}, \mathbf{1}, 0$
winos, W boson	$\tilde{W}^{\pm}, \tilde{W}^0$	$W^{\pm}, W^0$	$\mathbf{1}, \mathbf{3}, 0$
bino, B boson	$\tilde{B}$	B	$\mathbf{1}, \mathbf{1}, 0$

Table 3.2: Gauge supermultiplet fields in the MSSM. [8]

where y are the SM Yukawa couplings, and μ is the SUSY mass term of the Higgs doublets. This is surprisingly nice as we only get one new parameter, namely μ, in comparison to the SM.

To build the MSSM Lagrangian we, next to W_{MSSM}, should consider how the gauge superfield V is specified and how it interacts with the left and right chiral superfields. This will not be done here, for it is merely technical.

Last but not least we shortly introduce one of the reasons why the MSSM is so attractive. The three scale-dependant (*running*) gauge couplings $SU(3)_c \times SU(2)_L \times SU(1)_y$ of the SM do not converge or unify. But if one believes in a *grand unified theory* (GUT), one (mostly) needs these to unify to a more fundamental single force describing all forces.[19] However, in the MSSM as we have defined it, this unification is fulfilled (see Figure 3.2).

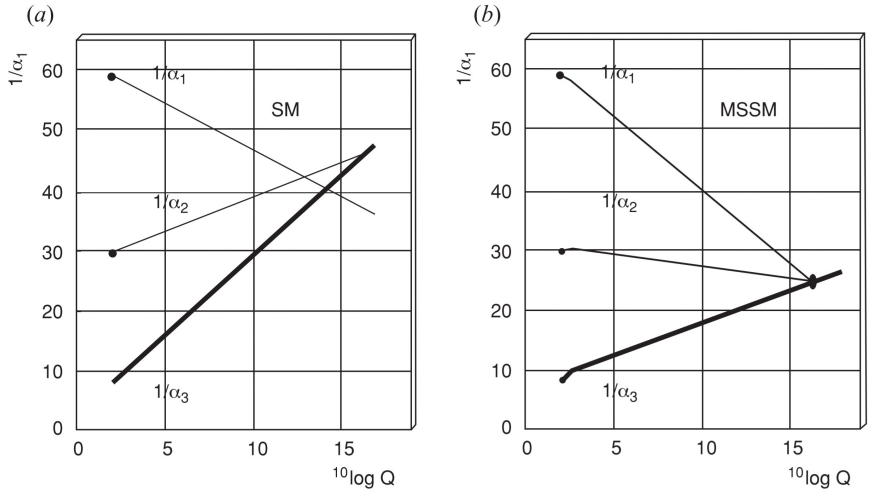

Figure 3.2: (a) Failure of the SM couplings to unify. (b) Gauge coupling unification in the MSSM. The blob represents model-dependant threshold corrections at the GUT scale.[8]

3.3.1 SUSY Breaking

As stated above, SUSY can be broken, and in fact, it should be. This is due to the fact that till now no supersymmetric particles (like stated in Table 3.1) have been found in experiment. If SUSY would not be broken all particle masses inside a supermultiplet would be equal,[20] suggesting that the superpartners should be found in collider experiments.[21] For that not being the case, we need to assume the superpartners are heavier than the SM particles, and, therefore, need to *break* the (mass-) symmetry.

19 Often it is believed that the three running couplings from above were unified shortly after the Big Bang.
20 Recall (3.7) and (3.8).
21 E.g. the *selectron* would have the same 511 keV mass as the electron.

One way to do this is *spontaneous breaking*, like the Higgs mechanism for the electroweak symmetry.[22] The other way is to add a symmetry-breaking term to the Lagrangian. This is the far more general approach and, till we do not know how exactly SUSY is broken, the more suitable one.

More precisely we will introduce SUSY *soft*-breaking. This means the Lagrangian should have only positive mass dimension terms, like "$M\chi\chi$". Terms like these are needed because they do not create new divergencies and, therefore, do not spoil the solving of the mass fine-tuning problem. The Lagrangian soft-breaking term, which will result in superpartners having different masses than their SM counterparts, can be found to be [23]

$$\mathcal{L}^{\text{soft}}_{\text{MSSM}} \sim -M_3\tilde{g}^a - M_2\tilde{W}^a\tilde{W}^a - M_1\tilde{B}\tilde{B} \tag{3.49}$$

$$- m^2_{\tilde{q}ij}\tilde{Q}^\dagger_i\tilde{Q}_j - m^2_{\tilde{u}ij}\tilde{u}^\dagger_{Li}\tilde{u}_{Lj} - m^2_{\tilde{d}ij}\tilde{d}^\dagger_{Li}\tilde{d}_{Lj} \tag{3.50}$$

$$- m^2_{\tilde{L}ij}\tilde{L}^\dagger_i\tilde{L}_j - m^2_{\tilde{e}ij}\tilde{e}^\dagger_{Li}\tilde{e}_{Lj} \tag{3.51}$$

$$- m^2_{H_u}H^\dagger_u H_u - m^2_{H_d}H^\dagger_d H_d - \mu H_u H_d \tag{3.52}$$

$$- A^{ij}_u\tilde{u}_{Li}\tilde{Q}_j H_u + A^{ij}_d\tilde{d}_{Li}\tilde{Q}_j H_d + A^{ij}_e\tilde{e}_{Li}\tilde{L}_j H_d. \tag{3.53}$$

Each of the four first rows is responsible for the masses of all the MSSM particles in the order: gauginos (3.49) (M_i are the gaugino masses), squarks (3.50), sleptons (3.51) and Higgs' (3.52). The last row (3.53) is the *scalar mixing term* with the *triple scalar couplings* A. With that, we finally have found an extension of SUSY that could be physically true. However, two new problems occur. First, we now have not only one new parameter in comparison to the standard model (μ from the superpotential Higgs interaction term) but 105 new ones that fully stem from (3.49)-(3.53). Although not practically a problem, so many degrees of freedom make it unpredictable for it is nearly impossible to know all parameters in detail. The second problem originates from the huge impact of higher order corrections in $\mathcal{L}^{\text{soft}}_{\text{MSSM}}$ to observables in the SM. To solve these, we will in the next section introduce a phenomenological model of the MSSM.

3.3.2 Phenomenological Model

The *phenomenological minimal supersymmetric standard model* (pMSSM) tries to be in agreement with phenomenological constraints by introducing three assumptions in the known MSSM:

- No new sources of CP-violation.
  (soft breaking parameters ⇒real)
- No flavour changing neutral currents.
  (mass matrices and trilinear couplings ⇒diagonal)
- First and second generation universality.
  (soft breaking sfermion-mass ⇒universal between first two generations)

After implementing these assumptions the pMSSM is again, even in higher orders, in agreement with the SM and reduces the parameter space to only 19, which are depicted in Table 3.3. These are (with one exception) exactly the same parameters we will need

22 This is done by giving the Higgs a non-vanishing VEV.

23 Taken from [8]. Surprisingly the construction is quite limited by needing to be SUSY invariant and the demand to be soft (see above). The "~" denotes missing factors and h.c.-terms.

PARAMETER	DESCRIPTION
$\tan\beta$	Ratio of the Higgs VEVs
M_{H^3}	Pseudoscalar Higgs boson mass
μ	Higgs-higgsino mass parameter
M_1, M_2, M_3	Bino, wino and gluino masses
$m_{\tilde{e}_L}, m_{\tilde{e}_R}, m_{\tilde{q}_{L1}}, m_{\tilde{u}_R}, m_{\tilde{d}_R}$	1st and 2nd generation L_L, e_R, Q_L, u_R and d_R masses
$m_{\tilde{\tau}_L}, m_{\tilde{\tau}_L}, m_{\tilde{q}_{L3}}, m_{\tilde{t}_R}, m_{\tilde{b}_R}$	3rd generation L_L, e_R, Q_L, u_R and d_R masses
A_t, A_b, A_τ	Trilinear couplings for t-, b- and τ-quark

Table 3.3: The 19 free parameters of the pMSSM.

to implement for the model of MSSM in which the numerical calculation of the relic density will take place (Chapter 6).

3.3.3 R-Parity

We already said that the MSSM is R-parity conserving. This is due to the fact that the proton will not decay into SUSY particles if R-parity is conserved, and the proton is stable – as it should be. Hence, this new parity is defined as

$$R \equiv (-1)^{3B+L+2S}, \tag{3.54}$$

where B and L are the baryon and lepton number, respectively. R from (3.54), therefore, has to be conserved for all SUSY-SM particle interactions. This, however, yields new phenomenological implications:

- The lightest supersymmetric particle (LSP) is absolutely stable.
- All sparticles decay into products containing an odd number of LSP's.
- Sparticles can only be produced in pairs.

In addition to a new parity, one needs to conserve when building SM and SUSY interactions, we get the most important fact that the LSP – if it is electrically neutral – is a very promising candidate for a WIMP and dark matter. The LSP is in fact the neutralino, and so we finally have made the connection from dark matter to SUSY.

3.3.4 The Neutralino

After finding that the neutralino is a great candidate for dark matter we will, in this last section to SUSY, introduce the neutralino.

The masses of the wino $\tilde{W}^0$ and bino $\tilde{B}$ are just given by (3.49) and do not mix. However, with non-vanishing Higgs VEV they do mix with $\tilde{H}_u$ and $\tilde{H}_d$.[24] Therefore, we can write the corresponding gauge eigenstate basis as

$$\tilde{G}^0 \hat{=} \begin{pmatrix} \tilde{B} \\ \tilde{W}^0 \\ \tilde{H}_d^0 \\ \tilde{H}_u^0 \end{pmatrix}. \tag{3.55}$$

The mass term in the MSSM Lagrangian involving the fields in $\tilde{G}^0$ then reads as

$$\mathcal{L}_{\text{MSSM}|_{\tilde{G}^0}} = -\frac{1}{2}\tilde{G}^{0T} M_{\tilde{G}^0} \tilde{G}^0 + \text{h.c.}, \tag{3.56}$$

where

$$M_{\tilde{G}^0} = \begin{pmatrix} M_1 & 0 & -\cos\beta \sin\theta_W m_Z & \sin\beta \sin\theta_W m_Z \\ 0 & M_2 & \cos\beta \cos\theta_W m_Z & -\sin\beta \cos\theta_W m_Z \\ -\cos\beta \sin\theta_W m_Z & \cos\beta \cos\theta_W m Z & 0 & -\mu \\ \sin\beta \sin\theta_W m_Z & -\sin\beta \cos\theta_W m_Z & -\mu & 0 \end{pmatrix}. \tag{3.57}$$

Now, to get the mass eigenstates (the physical particles), we can diagonalize $M_{\tilde{G}^0}$ and we get

$$m_{\chi_i^0} = \left(M^D_{\tilde{G}^0}\right)_{ii} \tag{3.58}$$

the masses from the four gaugino and higgsino mixed states, the neutralinos χ_i^0. Where $i = 1$ denotes the lightest one and all heavier ones decay into it.

Likewise to this procedure, one can get all new masses from the superpartners we introduced via the soft SUSY breaking.

TO SUMMARIZE: We have extended the Poincaré group (in the most general way possible) and got a new symmetry connecting fermions and bosons. The new fundamental degrees of freedom allowed us to build new superfields, which, if irreducible, are supermultiplets. We built the new Lagrangian for SUSY and introduced a physical minimal SUSY extension of the SM, the MSSM. In the phenomenological version of the MSSM we then concluded that SM particles have to lie in supermultiplets with their corresponding superpartners. Finally, we constructed the neutralino as the LSP as a mixed state of gauginos and higgsinos.

In the next chapters, we will calculate the annihilation (more precise the invariant amplitude, but more on that in the next chapter) of neutralino with gluino, the supermultiplet partner of the gluon.

24 This can be seen in the $\Phi^\dagger e^V \Phi$ term, which we did not state, see instead Section 7.3 in [8].

4 DIRAC CALCULATION

We will now, in this and the following chapter, calculate the neutralino-gluino coannihilation analytically on *tree-level* [1]. The gluino has, in most pMSSM spectra, a very similar mass compared to the neutralino. As we already stated in Section 2.3.1, the coannihilation of the WIMP with other equal-mass particles can contribute to the relic density (see (2.11)). Therefore, this specific process should be considered. For this is to this point no process included in the programme `DM@NLO` (see Appendix B) our task will be to calculate the corresponding invariant amplitude analytically and then, in Chapter 6, implement it in `DM@NLO`, in which the total cross-section will be calculated and further used in connected software to calculate the neutralino relic density.

In the current chapter, we will follow the standard technique for computing scattering processes and their cross-sections, namely squaring the scattering-matrix (S-matrix) amplitude, summing over all possible states, such as spin and colour, and then calculating the traces of γ-matrix products. Here we will use the four-component spinor formalism from Dirac [2].

In comparison to that, in Chapter 5, we will make use of a technique created by Dreiner, Haber and Martin which uses two-component (or Weyl-) spinors, that works with helicity amplitudes. The benefits and motivation for this different approach will be described in that chapter as well.

4.1 CROSS-SECTION

To be able to analyse a scattering process one needs to compute the cross-section of that process. The differential cross-section of a general two-particle collision can be constructed via the S-matrix elements $\langle f|S|i\rangle$, where $|i\rangle$ is the two-particle initial state, $\langle f|$ is the n-particle final state and S is the time evolution operator and describes the particle's transitions. Following [44] the differential cross-section can be found to be

$$d\sigma = \frac{1}{(2E_1)(2E_2)|\vec{v}_1 - \vec{v}_2|}|M|^2 d\Pi_{LIPS}, \tag{4.1}$$

where $E_{1,2}$ and $\vec{v}_{1,2}$ are the energies and velocities of the two initial particles, respectively, M is the nontrivial part of the S-matrix called **invariant amplitude** and

$$d\Pi_{LIPS} \equiv (2\pi)^4 \delta^4(\Sigma p) \times \prod_{\text{final states } j} \frac{d^3 p_j}{(2\pi)^3} \frac{1}{2E_{p_j}} \tag{4.2}$$

is called the Lorentz-invariant phase space or LIPS, where the Dirac delta distribution ensures conservation of momenta.

One can define the denominator in (4.1) as the *incident flux*

$$F \equiv (2E_1)(2E_2)|\vec{v}_1 - \vec{v}_2| = 4((p_1 p_2)^2 - m_1^2 m_2^2)^{\frac{1}{2}}, \tag{4.3}$$

1 This means that no loops in the Feynman diagrams (no higher perturbation order) will be included.
2 Consult e.g. [46].

where the second equality holds for a collinear collision between particles 1 and 2.[3] $p_{1,2}$ and $m_{1,2}$ are the particle's momentum and mass, respectively.

In the centre-of-mass frame and for a $2 \to 2$ scattering, the cross-section simplifies to

$$\left(\frac{d\sigma}{d\Omega}\right)_{CM} = \frac{1}{64\pi^2 E_{CM}^2}\frac{p_f}{p_i}|M|^2\theta(E_{CM} - m_1' - m_2'), \tag{4.4}$$

with the solid angle element $d\Omega$, the centre-of-mass energy E_{CM}, the momentum of final and initial state particles $p_{f,i}$ and the final state particle masses $m_{1,2}'$. This expression just needs to be integrated over $d\Omega$ to get the total cross-section.

In (4.4) the momenta and the centre-of-mass energy can be measured, such that the whole physics takes place in the invariant amplitude M and, thence, M will be the main focus of the following calculations. Furthermore, the actual cross-section calculation will be done inside `DM@NLO`, in which we (mostly) only implement the invariant amplitude.

4.2 FEYNMAN DIAGRAMS

Our goal now is to compute the invariant amplitude M. To achieve this, we will follow the Feynman-diagram approach[4]. This means we need to find all possible paths from the initial particles that contribute to the total amplitude M, construct their associated Feynman diagrams and compute their amplitudes and then, as the last step, combine them for the total amplitude of the process.

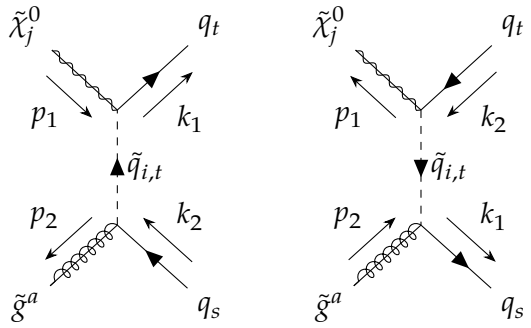

(a) t-channel **(b)** u-channel

Figure 4.1: Feynman diagrams for neutralino-gluino coannihilation. Initial state particles are neutralino $\tilde{\chi}_j^0(p_1)$, with $j \in \{0,1,2,3\}$ the composition state, and gluino $\tilde{g}^a(p_2)$, with a the colour charge. Propagator is the squark $\tilde{q}_{i,t}(q = p_1 - p_3)$ with i the squark generation index and t the color charge. Final state particles are quark $q_t(k_1)$, with the same color charge t like the propagator, and antiquark $q_s(k_2)$, with, because of the gluino strong coupling, from the propagator different color charge s. The arrows on the particle lines mark the direction of fermion number flow and the floating arrows represent the chosen fermion flow [5].

We start by setting both our initial states, neutralino and gluino, as the incoming particles with momenta p_1 and p_2, respectively. First, one notices that neutralino and

3 For a derivation see [29].

4 The more general technique would be to craft the interaction Lagrangians for the coupling of the individual particles. This is way more time-consuming but just equally physically true, because of the Feynman rules originating from the Lagrangians. In Appendix C, however, the respective Lagrangians for the particle interactions are listed for the sake of completeness (but not derived).

5 Listed preemptively for completeness, for an explanation see Section 4.2.1.

gluino do not couple to each other and, therefore, we only have to consider processes with a propagator in between them, namely t and u-channel amplitudes. The gluino interacts via the strong force and, thereby, couples to quarks and their respective supersymmetric analogues, the squarks. Due to R-parity conservation (see Section 3.3.3) and the need to get a standard model particle as the final state, the only possibility is the gluino-squark to quark interaction, where the colour of the quark and squark needs to differ, through the gluino interaction.

The neutralino can interact via either its gaugino part and, hence, the weak interaction or via the higgsino part (Yukawa coupling). Combining this with the propagating squark we need from the gluino vertex, the only possible standard model final state from the neutralino-squark coupling is a quark whose colour is equal to the squark's.

Last, one needs to consider the fermion number flow, which has to be continuous. This means we need to set one final state particle as antiquark and henceforth the other one as a quark, propagating forward in time.

All these result in the Feynman diagrams sketched in Figure 4.1. As we said, we do not have an s-channel diagram and the t and u-channel diagrams only differ in the final state positions, or more precisely in their respective momenta.

4.2.1 Fermion Number Violation

Till now we did not take into account the fact that we are dealing with Majorana [6] type particles, the neutralino and gluino. Their self-conjugacy results in different contractions which, through the anticommutativity of fermionic operators, get different signs. This results in a change of the relative sign of interfering Feynman graphs. One can, using e.g. Wick's theorem, do some extra work to determine the relative sign, but this is cumbersome and does not relate to the simplicity one gets from Feynman diagrams. Therefore, we will follow an approach by Denner et. al. [21] that presents simple Feynman rules for fermion-number-violating interactions and introduce it here briefly.

The main difference is the replacement of the usual fermion number flow in Feynman graphs with a continuous fermion flow. The difference is that one then needs to consider two expressions for each vertex, the fermion flow parallel and antiparallel to the flow of fermion number. From this, one gets multiple amplitudes from each graph for every fermion flow possibility. If the achieved amplitudes differ in their relative sign one needs to consider them separately.

Following [21], from the Majorana-Dirac Lagrangian, one gets multiple new expressions, with the two for our process relevant ones being

$$\Gamma' = C\Gamma^T C^{-1} = \eta\Gamma \quad \text{with } \eta = \begin{cases} +1 \text{ for } \Gamma \in \{1, i\gamma^5, \gamma_\mu\gamma^5\} \\ -1 \text{ for } \Gamma \in \{\gamma_\mu, \sigma_{\mu\nu}\} \end{cases}, \tag{4.5}$$

where Γ is a general fermionic interaction term with γ matrices and the corresponding coupling constant [7] and

$$v(p,s) = C\bar{u}(p,s)^T, \tag{4.6}$$

with u and v the usual Dirac spinors. C is the charge-conjugation matrix that fulfils

$$C^{-1} = C^T = -C. \tag{4.7}$$

6 Majorana particles fulfil $\Psi_M = (\psi, \psi^c)$ and are, therefore, their own antiparticles.

7 Here already, from the second equation, one can identify the equivalence for vertices if the vertex-term only contains e.g. γ^5-matrices. For a pure Majorana coupling $\Gamma' = \Gamma$ holds.

From these Denner et. al. derived a whole new set of Feynman rules. Most of them are not relevant for our process, so – for the sake of clarity – are not stated here explicitly. The three relevant ones can be found in Section C.1.3. With these, we can now compute the different amplitudes we get for all fermion flow permutations.

We begin the application of this new ruleset by first realising that our propagator is scalar and, therefore, does not need to be changed. Secondly, we identify that we have two permutations for each vertex and can now calculate these separately.

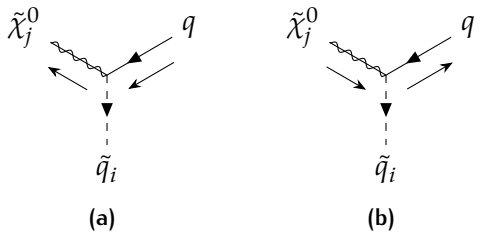

Figure 4.2: The two possible fermion flow permutations (floating arrows) for one specific fermion number flow direction (arrows on lines).

The neutralino-quark-squark vertex has two fermion flow permutations for each fermion number flow. Examplary this is shown in Figure 4.2 for the u-channel upper vertex. We can now construct, following the rules from Section C.1.3, the invariant amplitude for Figure 4.2a (parallel fermion flow)

$$iM = i\bar{u}_{\tilde{\chi}}\Gamma v_q \tag{4.8}$$

and Figure 4.2b (antiparallel fermion flow)

$$iM' = (-1)i\bar{u}_q\Gamma' v_{\tilde{\chi}}, \tag{4.9}$$

where the minus-sign originates from the inverted permutation order $\tilde{\chi} \to q$ in comparison to the arbitrary reference order set by the first graph $q \to \tilde{\chi}$. To get the relative sign for these two amplitudes we can follow steps similar to Example 3.1 from [21].[8] First we need to convert (4.6) to

$$\bar{u}(p,s) = v(p,s)^T C, \tag{4.10}$$

via taking the transpose, using the property $C^T = C^{-1}$ from (4.7) and multiplying by C from the left. Then we can substitute this and the original expression for the spinors $\bar{u}_q$ and $v_{\tilde{\chi}}$ into (4.8) and get

$$\begin{aligned} iM' &= -iv_q^T C\Gamma' C\bar{u}_{\tilde{\chi}}^T && (4.11)\\ &= iv_q^T \Gamma^T \bar{u}_{\tilde{\chi}}^T && (4.12)\\ &= i\bar{u}_{\tilde{\chi}}\Gamma v_q, && (4.13) \end{aligned}$$

where in (4.12) we made use of the relation $-C = C^{-1}$ from (4.7) and (4.5). This finally shows us that the graphs with different fermion flow from Figure 4.2 have the same relative sign and are, therefore, equivalent.

Because we did not specify Γ and can identify the spinors freely with every fermionic particle, we can conclude that the derivation of $iM' = iM$ holds for all interactions of a

8 This was the exact reason why the explicit setup from Figure 4.2 was chosen, to get an easy comparison.

Majorana fermion with a Dirac fermion and a scalar boson, regardless of the fermion number flow. As a very important bottom line, we get the fact that we do not need to think about the relative sign in our Feynman graphs and can choose the fermion flow freely because all permutations are the same.

As a result, the definition of choice of spinors u or v depends on the direction of fermion flow we choose and not – anymore – on the fermion number flow like usual.[9] As a result, we can choose the fermion flows in Figure 4.1 free of any restrictions and for convenience took the same direction as the fermion number flow. Furthermore, we only need to consider one permutation and, thence, only one Feynman diagram. One last thing to state is that the fermion number flow still determines the interaction Lagrangian, so the choice of fermion flow really only changes u and v and one has to take the same couplings for every permutation.

4.2.2 Invariant Amplitude

From Figure 4.1 we can see that we can deconstruct the total invariant amplitude M in two part-amplitudes belonging to the t- and u-channel diagrams, respectively. In order to get the cross-section from (4.4), we need the magnitude square of M, so we have to include their amount squares and we get the real part of the interference term from multiplying out the square

$$|M|^2 = |M_t|^2 + |M_u|^2 + 2\,\mathrm{Re}\, M_t M_u^\dagger. \tag{4.14}$$

Till now we did not include e.g. spin or colour and, therefore, we only computed the *unpolarized* cross-section. To allow the scattering to be in all possible spin and colour configurations, we need to make the replacement

$$|M|^2 \longrightarrow \overline{|M|}^2 = \frac{1}{2s_i+1}\frac{1}{N^2-1}\sum_{\text{spin,colour}} |M|^2, \tag{4.15}$$

where we have to average over the initial state particle spins s_i and colours in $\mathrm{SU}(N)$ and sum over the spins and colours of the final state particles, the invariant amplitude M.

Combining (4.14) and (4.15) we get

$$\overline{|M|}^2 = \overline{|M_t|}^2 + \overline{|M_u|}^2 + 2\,\mathrm{Re}\,\overline{M_t M_u^\dagger}. \tag{4.16}$$

From here on the task will be to calculate the three averaged amplitudes $\overline{|M_t|}^2$, $\overline{|M_u|}^2$ and $\mathrm{Re}\,\overline{M_t M_u^\dagger}$, where we can, following the Feynman rules listed in Appendix C, build the underlying amplitudes M_t and M_u from the Feynman diagrams in Figure 4.1.

4.3 EVALUATION OF SQUARED AMPLITUDES

9 This yields some interesting consequences we will make use of later on.

4.3.1 T-Channel

We begin by calculating the t-channel amplitude $\overline{|M_t|}^2$ in (4.16). From the corresponding Feynman diagram Figure 4.1a we can, using the Feynman rules from Appendix C, construct the invariant amplitude

$$\begin{aligned} iM_t &= \bar{u}(k_1)\Big(-i(b_{ij}^{\tilde{q}}P_L + a_{ij}^{\tilde{q}}P_R)\Big)u(p_1)\left(\frac{i}{t-m_{\tilde{q}_i}^2}\right) \\ &\quad \times \bar{v}(p_2)\Big(\sqrt{2}ig_s T_{st}^a(R_{i2}P_R - R_{i1}P_L)\Big)v(k_2) \qquad (4.17) \\ &= \frac{i\sqrt{2}g_s}{t-m_{\tilde{q}_i}^2}T_{st}^a\Big[\bar{u}(k_1)(b_{ij}^{\tilde{q}}P_L + a_{ij}^{\tilde{q}}P_R)u(p_1)\Big]\Big[\bar{v}(p_2)(R_{i2}P_R - R_{i1}P_L)v(k_2)\Big], \qquad (4.18) \end{aligned}$$

where in the last step we exploited the fact that we can drag the coupling constants, the propagator term and the matrix element T_{st}^a in front of the four-vector spinor terms. To get $|M_t|^2$ we then need to form the transpose conjugate of (4.18) [10]

$$-iM_t^\dagger = \frac{-i\sqrt{2}g_s}{t-m_{\tilde{q}_{i'}}^2}T_{st}^{a*}\Big[\bar{u}(p_1)(b_{i'j}^{\tilde{q}*}P_R + a_{i'j}^{\tilde{q}*}P_L)u(k_1)\Big]\Big[\bar{v}(k_2)(R_{i'2}P_L - R_{i'1}P_R)v(p_2)\Big]. \qquad (4.19)$$

The calculation to get the Hermitian transpose of the terms in square brackets is to be found in Section A.1.1. The rest consists of constants or matrix elements only and, therefore, just has to be complex conjugated. Now we can construct the spin and colour averaged magnitude-square of iM_t and get

$$\overline{|M_t|}^2 = \sum_{i,i'}\frac{2g_s^2}{(t-m_{\tilde{q}_i})(t-m_{\tilde{q}_{i'}})}M_{t,c}\,M_{t,s}, \qquad (4.20)$$

where $M_{t,c}$ and $M_{t,s}$ are the amplitude parts with colour and spin dependencies, respectively. Furthermore, it is needed to take the sum of all possible propagating squark generations, i and i'.

The colour-dependant part consists of the sum over the colour indices a, s, t of the T_{st}^a matrix elements from the gluino vertices and the colour-averaging factor in colour-SU(N)

$$M_{t,c} = \frac{1}{N^2-1}\sum_{a,s,t}T_{st}^a T_{ts}^a = \frac{1}{N^2-1}C_F\delta_a^a = \frac{1}{2}, \qquad (4.21)$$

where we used $T_{st}^{a*} = T_{ts}^a$ in the first equation and the SU(N) relations from Section D.3 and the fact that $\delta_a^a = N$ in the last two steps. As a result, the N's cancel and we get a constant prefactor of $1/2$.

The following calculation of the spin-dependant amplitude $M_{t,s}$ requires a little more work. First of all, it consists of an averaging factor of $1/4$ for the two spin $1/2$ initial particles. Next, we have the sum over all external particle spins s_1, s_2, s_3 and s_4 (of

10 Here it is needed to set a new variable for the squark generation index, namely i', to include the fact that we are dealing with two different processes (the other one being (4.18)) and, thus, two different possibilities for the generation of the propagating squark (The external particles are the ones to be measured and have, thereby, set generations).

neutralino, gluino, quark and antiquark in that exact order), where we need to sum the external spinors u and v. The calculation of the spin-amplitude evaluates to

$$\begin{aligned} M_{t,s} = \frac{1}{4} \sum_{\substack{s_1,s_2 \\ s_3,s_4}} & \left[\bar{u}(k_1)_\alpha^{(s_3)} (b_{ij}^{\tilde{q}} P_L + a_{ij}^{\tilde{q}} P_R)_{\alpha\beta} u(p_1)_\beta^{(s_1)}\right] \\ & \times \left[\bar{v}(p_2)_\gamma^{(s_2)} (R_{i2} P_R - R_{i1} P_L)_{\gamma\delta} v(k_2)_\delta^{(s_4)}\right] \\ & \times \left[\bar{u}(p_1)_\xi^{(s_1)} (b_{i'j}^{\tilde{q}*} P_R + a_{i'j}^{\tilde{q}*} P_L)_{\xi\eta} u(k_1)_\eta^{(s_3)}\right] \\ & \times \left[\bar{v}(k_2)_\kappa^{(s_4)} (R_{i'2} P_L - R_{i'1} P_R)_{\kappa\gamma} v(p_2)_\gamma^{(s_2)}\right] \end{aligned} \tag{4.22}$$

$$\begin{aligned} = \frac{1}{4} & \left[(\not{k}_1 + m_1')_{\eta\alpha} (b_{ij}^{\tilde{q}} P_L + a_{ij}^{\tilde{q}} P_R)_{\alpha\beta} (\not{p}_1 + m_1)_{\beta\xi} (b_{i'j}^{\tilde{q}*} P_R + a_{i'j}^{\tilde{q}*} P_L)_{\xi\eta}\right] \\ & \times \left[(\not{p}_2 - m_2)_{\lambda\gamma} (R_{i2} P_R - R_{i1} P_L)_{\gamma\delta} (\not{k}_2 - m_2')_{\delta\kappa} (R_{i'2} P_L - R_{i'1} P_R)_{\kappa\lambda}\right] \end{aligned} \tag{4.23}$$

$$= \frac{1}{4} L_{\eta\eta}^{\tilde{\chi}} L_{\lambda\lambda}^{\tilde{g}}. \tag{4.24}$$

To get (4.23) we can separate the square-bracket terms in two sums, one over s_1 and s_3 and the other over s_2 and s_4, and then use the completeness relations, see Section D.1.3. We can identify the resulting expressions in square brackets in (4.23) as two traces [11] $L_{\eta\eta}^{\tilde{\chi}}$ and $L_{\lambda\lambda}^{\tilde{g}}$ corresponding to the two neutralino and gluino vertices and can then, as a next step, calculate them separately.

Calculation of the first trace for the neutralino vertex coupling yields

$$L_{\eta\eta}^{\tilde{\chi}} = \mathrm{Tr}\left[(\not{k}_1 + m_1')(b_{ij}^{\tilde{q}} P_L + a_{ij}^{\tilde{q}} P_R)(\not{p}_1 + m_1)(b_{i'j}^{\tilde{q}*} P_R + a_{i'j}^{\tilde{q}*} P_L)\right] \tag{4.25}$$

$$\begin{aligned} = m_1 m_1' & \,\mathrm{Tr}\left[(b_{ij}^{\tilde{q}} P_L + a_{ij}^{\tilde{q}} P_R)(b_{i'j}^{\tilde{q}*} P_R + a_{i'j}^{\tilde{q}*} P_L)\right] \\ & + \mathrm{Tr}\left[\not{k}_1 (b_{ij}^{\tilde{q}} P_L + a_{ij}^{\tilde{q}} P_R) \not{p}_1 (b_{i'j}^{\tilde{q}*} P_R + a_{i'j}^{\tilde{q}*} P_L)\right] \end{aligned} \tag{4.26}$$

$$= 2p_1k_1 (b_{ij}^{\tilde{q}} b_{i'j}^{\tilde{q}*} + a_{ij}^{\tilde{q}} a_{i'j}^{\tilde{q}*}) + 2m_1 m_1' (b_{ij}^{\tilde{q}} a_{i'j}^{\tilde{q}*} + b_{i'j}^{\tilde{q}*} a_{ij}^{\tilde{q}}), \tag{4.27}$$

where in (4.25) we multiplied out and used the commutating properties of the chirality operator [12]. The two resulting traces in (4.27) can then be calculated via the trace-calculations I (see Section A.1.2) and II (see Section A.1.3), respectively.

To calculate the second trace $L_{\lambda\lambda}^{\tilde{g}}$ the procedure is very similar and, again using I and II, yields as a result (4.30)

$$L_{\lambda\lambda}^{\tilde{g}} = \mathrm{Tr}\left[(\not{p}_2 - m_2)(R_{i2} P_R - R_{i1} P_L)(\not{k}_2 + m_2')(R_{i'2} P_L - R_{i'1} P_R)\right] \tag{4.28}$$

$$\begin{aligned} = m_2 m_2' & \,\mathrm{Tr}\left[(R_{i2} P_R - R_{i1} P_L)(R_{i'2} P_L - R_{i'1} P_R)\right] \\ & + \mathrm{Tr}\left[\not{p}_2 (R_{i2} P_R - R_{i1} P_L) \not{k}_2 (R_{i'2} P_L - R_{i'1} P_R)\right] \end{aligned} \tag{4.29}$$

$$= 2p_2k_2 (R_{i2} R_{i'2} + R_{i1} R_{i'1}) - 2m_2 m_2' (R_{i2} R_{i'1} + R_{i'2} R_{i1}). \tag{4.30}$$

This together with the other trace (4.27) can then be used to get the spin-amplitude $M_{t,s}$ of (4.24). Next to that we take the result from the colour-dependant amplitude

11 To clarify: with Einstein's summation convention, we calculate the diagonal entries of two matrices corresponding to the summation over each of η and λ in (4.23).

12 See Section D.1.2.

(4.21) and substituting both in (4.20) will then yield the final result for the t-channel amplitude

$$\overline{|M_t|}^2 = g_s^2 \sum_{i,i'} \frac{1}{(t - m_{\tilde{q}_i})(t - m_{\tilde{q}_{i'}})} \Big[p_1 k_1 (b_{ij}^{\tilde{q}} b_{i'j}^{\tilde{q}*} + a_{ij}^{\tilde{q}} a_{i'j}^{\tilde{q}*}) + m_1 m_1' (b_{ij}^{\tilde{q}} a_{i'j}^{\tilde{q}*} + b_{i'j}^{\tilde{q}*} a_{ij}^{\tilde{q}}) \Big] \times \Big[p_2 k_2 (R_{i2} R_{i'2} + R_{i1} R_{i'1}) - m_2 m_2' (R_{i2} R_{i'1} + R_{i'2} R_{i1}) \Big]. \tag{4.31}$$

4.3.2 U-Channel

The second amplitude part we need – in order to get the complete invariant amplitude for the scattering process – can be constructed in a very similar way compared to the preceding t-channel amplitude. Again, using the Feynman rules listed in Appendix C and applying them to the u-channel Feynman diagram Figure 4.1b, the invariant amplitude of the u-channel can be found and simplified as follows [13]

$$iM_u = \bar{v}(p_1)\Big(- i(b_{ij}^{\tilde{q}} P_R + a_{ij}^{\tilde{q}} P_L)\Big) v(k_2) \Big(\frac{i}{u - m_{\tilde{q}_i}^2} \Big) \times \bar{u}(k_1)\Big(\sqrt{2} i g_s T_{st}^a (R_{i2} P_L - R_{i1} P_R) \Big) u(p_2) \tag{4.32}$$

$$= \frac{i\sqrt{2} g_s}{u - m_{\tilde{q}_i}^2} T_{st}^a \Big[\bar{v}(p_1)(b_{ij}^{\tilde{q}} P_R + a_{ij}^{\tilde{q}} P_L) v(k_2) \Big] \Big[\bar{u}(k_1)(R_{i2} P_L - R_{i1} P_R) u(p_2) \Big]. \tag{4.33}$$

The associated Hermitian transpose of (4.33) is

$$-iM_u^\dagger = \frac{-i\sqrt{2} g_s}{u - m_{\tilde{q}_{i'}}^2} T_{st}^{a*} \Big[\bar{v}(k_2)(b_{i'j}^{\tilde{q}*} P_L + a_{i'j}^{\tilde{q}*} P_R) v(p_1) \Big] \Big[\bar{u}(p_2)(R_{i'2} P_R - R_{i'1} P_L) u(k_1) \Big], \tag{4.34}$$

where again, the calculation from Section A.1.1 for the transpose conjugation of the terms in square brackets and the complex conjugate of the remaining constants has been used. Then, with these results, we can construct the amplitude-square of M_u

$$\overline{|M_u|}^2 = \sum_{i,i'} \frac{2 g_s^2}{(u - m_{\tilde{q}_i})(u - m_{\tilde{q}_{i'}})} M_{u,c} M_{u,s} \tag{4.35}$$

and again identify and define new amplitudes with only spin ($M_{u,s}$) or colour dependency ($M_{u,c}$) to calculate them separately.

The colour amplitude is equivalent to the t-channel analogue (4.21) and results in

$$M_{u,c} = \frac{1}{N^2 - 1} \sum_{a,s,t} T_{st}^a T_{ts}^a = \frac{1}{2}. \tag{4.36}$$

13 Again, just dragging the constants and matrix elements in front of the spinor expressions, like in (4.18).

Next we need to calculate the spin-dependant part

$$
\begin{aligned}
M_{u,s} = \frac{1}{4} \sum_{\substack{s_1,s_2\\ s_3,s_4}} & \left[\bar{v}(p_1)_\alpha^{(s_1)} (b_{ij}^{\tilde{q}} P_R + a_{ij}^{\tilde{q}} P_L)_{\alpha\beta} v(k_2)_\beta^{(s_4)}\right] \\
& \times \left[\bar{u}(k_1)_\gamma^{(s_3)} (R_{i2} P_L - R_{i1} P_R)_{\gamma\delta} u(p_2)_\delta^{(s_2)}\right] \\
& \times \left[\bar{v}(k_2)_\xi^{(s_4)} (b_{i'j}^{\tilde{q}*} P_L + a_{i'j}^{\tilde{q}*} P_R)_{\xi\eta} v(p_1)_\eta^{(s_1)}\right] \\
& \times \left[\bar{u}(p_2)_\kappa^{(s_2)} (R_{i'2} P_R - R_{i'1} P_L)_{\kappa\gamma} u(k_1)_\gamma^{(s_3)}\right] \qquad (4.37)
\end{aligned}
$$

$$
\begin{aligned}
= \frac{1}{4} \Big[& (\not{p}_1 - m_1)_{\eta\alpha} (b_{ij}^{\tilde{q}} P_R + a_{ij}^{\tilde{q}} P_L)_{\alpha\beta} (\not{k}_2 - m_2')_{\beta\xi} (b_{i'j}^{\tilde{q}*} P_L + a_{i'j}^{\tilde{q}*} P_R)_{\xi\eta} \Big] \\
& \times \left[(\not{k}_1 + m_1')_{\lambda\gamma} (R_{i2} P_L - R_{i1} P_R)_{\gamma\delta} (\not{p}_2 + m_2)_{\delta\kappa} (R_{i'2} P_R - R_{i'1} P_L)_{\kappa\lambda} \right] \qquad (4.38) \\
= \frac{1}{4} & L_{\eta\eta}^{\tilde{\chi}} L_{\lambda\lambda}^{\tilde{g}}, \qquad (4.39)
\end{aligned}
$$

where we again needed to sum over the external particle spins s and used the completeness relations from Section D.1.3 in (4.37). We can then identify two traces, belonging to the two vertices for the neutralino- and gluino-quark-squark coupling and denote them $L_{\eta\eta}^{\tilde{\chi}}$ and $L_{\lambda\lambda}^{\tilde{g}}$ in the last step in (4.39).

We begin by calculating the trace corresponding to the neutralino vertex. Here it can be exploited that this and the following gluino trace are, under exchange of constants, equal to the traces (4.27) and (4.30) from the t-channel. As a result, the already calculated traces can be used under the exchange of certain constants, e.g. as listed in (4.41). The first trace then yields

$$
\begin{aligned}
L_{\eta\eta}^{\tilde{\chi},u} &= \mathrm{Tr}\left[(\not{p}_1 - m_1)(b_{ij}^{\tilde{q}} P_R + a_{ij}^{\tilde{q}} P_L)(\not{k}_2 - m_2')(b_{i'j}^{\tilde{q}*} P_L + a_{i'j}^{\tilde{q}*} P_R)\right] && (4.40) \\
&\hat{=} L_{\eta\eta}^{\tilde{\chi},t} \quad \text{with} \begin{cases} \not{k}_1 \to \not{p}_1,\ m_1' \to -m_1,\ b_{ij}^{\tilde{q}} \to a_{ij}^{\tilde{q}},\ a_{ij}^{\tilde{q}} \to b_{ij}^{\tilde{q}}, \\ \not{p}_1 \to \not{k}_2,\ m_1 \to -m_2',\ b_{i'j}^{\tilde{q}*} \to a_{i'j}^{\tilde{q}*},\ a_{i'j}^{\tilde{q}*} \to b_{i'j}^{\tilde{q}*} \end{cases} && (4.41) \\
&= 2p_1k_1(b_{ij}^{\tilde{q}} b_{i'j}^{\tilde{q}*} + a_{ij}^{\tilde{q}} a_{i'j}^{\tilde{q}*}) + 2m_1m_1'(b_{ij}^{\tilde{q}} a_{i'j}^{\tilde{q}*} + b_{i'j}^{\tilde{q}*} a_{ij}^{\tilde{q}}). && (4.42)
\end{aligned}
$$

And equally for the gluino vertex trace

$$
\begin{aligned}
L_{\lambda\lambda}^{\tilde{g},u} &= \mathrm{Tr}\left[(\not{k}_1 + m_1')(R_{i2} P_L - R_{i1} P_R)(\not{p}_2 + m_2)(R_{i'2} P_R - R_{i'1} P_L)\right] && (4.43) \\
&\hat{=} L_{\lambda\lambda}^{\tilde{\chi},t} \quad \text{with} \begin{cases} \not{p}_1 \to \not{p}_2,\ m_1 \to m_2,\ b_{ij}^{\tilde{q}} \to R_{i2}, \\ a_{ij}^{\tilde{q}} \to -R_{i1},\ b_{i'j}^{\tilde{q}*} \to R_{i'2},\ a_{i'j}^{\tilde{q}*} \to -R_{i'1} \end{cases} && (4.44) \\
&= 2p_2k_1(R_{i2}R_{i'1} + R_{i1}R_{i'1}) - 2m_2m_1'(R_{i2}R_{i'1} + R_{i'2}R_{i1}), && (4.45)
\end{aligned}
$$

with the change of constants as in (4.41).

As a result we can substitute the calculated traces in (4.38) and get, together with the colour amplitude (4.36) and the prefactors listed in (4.35), the final result for the u-channel amplitude

$$
\begin{aligned}
\overline{|M_u|}^2 = g_s^2 \sum_{i,i'} & \frac{1}{(u - m_{\tilde{q}_i})(u - m_{\tilde{q}_{i'}})} \left[p_1k_2(b_{ij}^{\tilde{q}} b_{i'j}^{\tilde{q}*} + a_{ij}^{\tilde{q}} a_{i'j}^{\tilde{q}*}) + m_1m_2'(b_{ij}^{\tilde{q}} a_{i'j}^{\tilde{q}*} + b_{i'j}^{\tilde{q}*} a_{ij}^{\tilde{q}})\right] \\
& \times \left[p_2k_1(R_{i2}R_{i'2} + R_{i1}R_{i'1}) - m_1'm_2(R_{i2}R_{i'1} + R_{i'2}R_{i1})\right]. \qquad (4.46)
\end{aligned}
$$

4.3.3 Interference

The last part from (4.16) we need to calculate – in order to get the total amplitude – is the mixterm, or interference, $\mathrm{Re}\,\overline{M_t M_u^\dagger}$ of the t- and u-channel diagrams from Figure 4.1. Usually one only needs to take the already calculated amplitudes M_t from (4.18) and the hermitian conjugate of M_u from (4.34) and compute their multiplication. But, if we take this approach with the mixed amplitudes, we will get a problem that prevents us from going any further. In the step where one usually can use the completeness relations to solve the spin-dependant amplitude, like in (4.22) for the t-channel or in (4.37) for the u-channel, the spinors for the same particle from the different diagrams have opposite fermion flow. As a result, they connote different spinors u and v and it is then not possible to use the completeness relation [14]. To address this problem we need

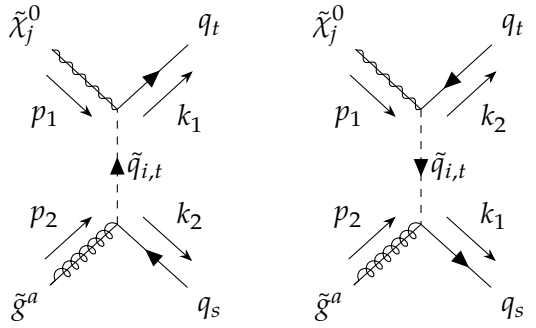

(a) t-channel **(b)** u-channel

Figure 4.3: Feynman diagrams for the computation of the interference-term of t- and u-channel, where only the fermion flow has changed, so one can use the completeness relations. The rest, like particles and generations, is the same as before in Figure 4.1.

to use the result from our evaluation of Feynman rules for fermion number violating interactions in Section 4.2.1. As a reminder, we got that for our Feynman graphs all fermion flow directions are equal and we, therefore, only need to compute one specific fermion flow permutation and can choose the fermion flow freely. This second fact can now be exploited by us to achieve a configuration of spinors that will allow us to use the completeness relation again. This specific set of fermion flow directions is shown in Figure 4.3. At this point, we will just set the fermion flow arbitrary like shown because nothing prevents us from doing so.

After the adjustment of the fermion flow, and, hence, the Feynman diagrams, we can build the corresponding invariant amplitudes following Appendix C as usual.[15] The resulting amplitudes for the interference of the last missing third term of the total amplitude in (4.16) are then found to be

$$iM_t = \frac{i\sqrt{2}g_s}{t - m^2_{\tilde{q}_i}} T^a_{st}\Big[\bar{u}(k_1)(b^{\tilde{q}}_{ij}P_L + a^{\tilde{q}}_{ij}P_R)u(p_1)\Big]\Big[\bar{u}(k_2)(R_{i2}P_R - R_{i1}P_L)u(p_2)\Big] \quad (4.47)$$

14 Both spinors need to be either u- or v-like, see Section D.1.3.

15 Remember that the fermion flow only tells us wether to take u or v but we have to take the same couplings and propagator terms.

for the t-channel and

$$iM_u = \frac{i\sqrt{2}g_s}{u - m^2_{\tilde{q}_{i'}}} T^a_{st}\Big[\bar{u}(k_2)(a^{\tilde{q}}_{i'j}P_L + b^{\tilde{q}}_{i'j}P_R)u(p_1)\Big]\Big[\bar{u}(k_1)(R_{i'1}P_L - R_{i'2}P_R)u(p_2)\Big] \tag{4.48}$$

for the u-channel diagram from Figure 4.3. These vary only in the direction of the coupling vertices and in the interchange of the u- and v-spinors, compared to their analogues (4.18) and (4.33).

To form the squared magnitude we then need the Hermitian conjugate of any one of these too. Let us choose M_u and we will get

$$-iM^\dagger_u = \frac{-i\sqrt{2}g_s}{u - m^2_{\tilde{q}_{i'}}} T^{\dagger a}_{st}\Big[\bar{v}(k_2)(a^{\tilde{q}*}_{i'j}P_L + b^{\tilde{q}*}_{i'j}P_R)v(p_1)\Big]\Big[\bar{u}(p_2)(R_{i'1}P_R - R_{i'2}P_L)u(k_1)\Big], \tag{4.49}$$

where again, the matrix element T^a_{st} and the constants just need to be complex conjugated and Section A.1.1 was used to get the conjugate transpose of the spinor terms. The combination of these results yields

$$\overline{|M_t M^\dagger_u|} = \sum_{i,i'} \frac{2g_s^2}{(t - m^2_{\tilde{q}_i})(u - m^2_{\tilde{q}_{i'}})} M_{int,c}\, M_{int,s}, \tag{4.50}$$

whereby, as it is already known from before, we can identify parts only dependant on spin or colour, respectively.

The colour-amplitude gives

$$M_{int,c} = \frac{1}{N^2 - 1}\sum_{a,s,t} T^a_{st}T^a_{ts} = \frac{1}{2}, \tag{4.51}$$

as above, only a factor.

The spin amplitude differs from previous calculations in that the spinor terms can no longer be divided into two spin sums and we, therefore, get a single large expression that must be summed over all external spins. To simplify the following calculations we will introduce two short forms for the significant parts of the vertex coupling terms of

$$\text{neutralino: } V^{\tilde{\chi}}_{ij} \equiv b^{\tilde{q}}_{ij}P_L + a^{\tilde{q}}_{ij}P_R \quad \text{and} \quad \text{gluino: } V^{\tilde{g}}_i \equiv R_{i2}P_R - R_{i1}P_L. \tag{4.52}$$

With that, the spin-dependant amplitude follows as

$$M_{int,s} = \frac{1}{4}\sum_{s_1,s_2,s_3,s_4}\left[\bar{u}(k_1)^{(s_3)}_{\alpha}\left(V^{\tilde{\chi}}_{ij}\right)_{\alpha\beta}u(p_1)^{(s_1)}_{\beta}\right]\left[\bar{u}(k_2)^{(s_4)}_{\gamma}\left(V^{\tilde{g}}_{i}\right)_{\gamma\delta}u(p_2)^{(s_2)}_{\delta}\right]$$
$$\times\left[\bar{u}(p_1)^{(s_1)}_{\xi}\left(V^{\tilde{\chi}}_{i'j}\right)_{\xi\eta}u(k_2)^{(s_4)}_{\eta}\right]\left[\bar{u}(p_2)^{(s_2)}_{\kappa}\left(V^{\tilde{g}}_{i'}\right)_{\kappa\lambda}u(k_1)^{s_3}_{\lambda}\right] \tag{4.53}$$

$$= \frac{1}{4}\Big[(\not{k}_1 + m'_1)_{\lambda\alpha}\left(V^{\tilde{\chi}}_{ij}\right)_{\alpha\beta}(\not{p}_1 + m_1)_{\beta\xi}\left(V^{\tilde{\chi}}_{i'j}\right)_{\xi\eta}$$
$$(\not{k}_2 + m'_2)_{\eta\gamma}\left(V^{\tilde{g}}_{i}\right)_{\gamma\delta}(\not{p}_2 + m_2)_{\delta\kappa}\left(V^{\tilde{g}}_{i'}\right)_{\kappa\lambda}\Big] \tag{4.54}$$

$$= \frac{1}{4}\Big\{\operatorname{Tr}\left[\not{k}_1 V^{\tilde{\chi}}_{ij}\not{p}_1 V^{\tilde{\chi}}_{i'j}\not{k}_2 V^{\tilde{g}}_{i}\not{p}_2 V^{\tilde{g}}_{i'}\right] + m_1 m'_1\operatorname{Tr}\left[V^{\tilde{\chi}}_{ij}V^{\tilde{\chi}}_{i'j}\not{k}_2 V^{\tilde{g}}_{i}\not{p}_2 V^{\tilde{g}}_{i'}\right]$$
$$+ m'_1 m'_2\operatorname{Tr}\left[V^{\tilde{\chi}}_{ij}\not{p}_1 V^{\tilde{\chi}}_{i'j}V^{\tilde{g}}_{i}\not{p}_2 V^{\tilde{g}}_{i'}\right] + m_2 m'_1\operatorname{Tr}\left[V^{\tilde{\chi}}_{ij}\not{p}_1 V^{\tilde{\chi}}_{i'j}\not{k}_2 V^{\tilde{g}}_{i}V^{\tilde{g}}_{i'}\right]$$
$$+ m_1 m'_2\operatorname{Tr}\left[\not{k}_1 V^{\tilde{\chi}}_{ij}V^{\tilde{\chi}}_{i'j}V^{\tilde{g}}_{i}\not{p}_2 V^{\tilde{g}}_{i'}\right] + m_1 m_2\operatorname{Tr}\left[\not{k}_1 V^{\tilde{\chi}}_{ij}V^{\tilde{\chi}}_{i'j}\not{k}_2 V^{\tilde{g}}_{i}V^{\tilde{g}}_{i'}\right]$$
$$+ m_2 m'_2\operatorname{Tr}\left[\not{k}_1 V^{\tilde{\chi}}_{ij}\not{p}_1 V^{\tilde{\chi}}_{i'j}V^{\tilde{g}}_{i}V^{\tilde{g}}_{i'}\right] + m_1 m_2 m'_1 m'_2\operatorname{Tr}\left[V^{\tilde{\chi}}_{ij}V^{\tilde{\chi}}_{i'j}V^{\tilde{g}}_{i}V^{\tilde{g}}_{i'}\right]\Big\}. \tag{4.55}$$

Here we can see that our random choice of the fermion flow was not so random at all and we can, like wanted, use the completeness relations from Section D.1.3 in (4.53) to solve the spin sum. In (4.54) we could then identify a trace and as the last step in (4.55) break that trace in eight smaller ones by multiplying out the momentum-and-mass terms like $(\not{k}_1 + m'_1)$. There we already simplified by applying the trace theorem that an odd number of γ-matrices (or in our case slashed momenta) will vanish.[16] And so the only traces left have either zero, two or four slashed momenta.

In the following, the task is to separately calculate the traces obtained. The first one, with all four slashed momenta, yields

$$\operatorname{Tr}\left[\not{k}_1 V^{\tilde{\chi}}_{ij}\not{p}_1 V^{\tilde{\chi}}_{i'j}\not{k}_2 V^{\tilde{g}}_{i}\not{p}_2 V^{\tilde{g}}_{i'}\right] \tag{4.56}$$
$$= \operatorname{Tr}\left[\not{k}_1\not{p}_1\not{k}_2\not{p}_2(b^{\tilde{q}}_{ij}P_R + a^{\tilde{q}}_{ij}P_L)(a^{\tilde{q}*}_{i'j}P_R + b^{\tilde{q}*}_{i'j}P_L)(R_{i2}P_L - R_{i1}P_R)(R_{i'1}P_L - R_{i'2}P_R)\right] \tag{4.57}$$

$$= \frac{1}{2}(b^{\tilde{q}}_{ij}a^{\tilde{q}*}_{i'j}R_{i1}R_{i'2} + a^{\tilde{q}}_{ij}b^{\tilde{q}*}_{i'j}R_{i2}R_{i'1})\operatorname{Tr}\left[\not{k}_1\not{p}_1\not{k}_2\not{p}_2\right]$$
$$+ \frac{1}{2}(b^{\tilde{q}}_{ij}a^{\tilde{q}*}_{i'j}R_{i1}R_{i'2} - a^{\tilde{q}}_{ij}b^{\tilde{q}*}_{i'j}R_{i2}R_{i'1})\operatorname{Tr}\left[\not{k}_1\not{p}_1\not{k}_2\not{p}_2\gamma^5\right] \tag{4.58}$$
$$= 2(b^{\tilde{q}}_{ij}a^{\tilde{q}*}_{i'j}R_{i1}R_{i'2} + a^{\tilde{q}}_{ij}b^{\tilde{q}*}_{i'j}R_{i2}R_{i'1})[k_1p_1k_2p_2 - k_1k_2p_1p_2 + k_1p_2p_1k_2]$$
$$+ 2(b^{\tilde{q}}_{ij}a^{\tilde{q}*}_{i'j}R_{i1}R_{i'2} - a^{\tilde{q}}_{ij}b^{\tilde{q}*}_{i'j}R_{i2}R_{i'1})i\varepsilon^{k_1k_2p_1p_2}, \tag{4.59}$$

where to get (4.58), we dragged the momenta in front of the rest and used the commutation relations of the chirality operators (see Section D.1.1) and are then left with two traces with and without one γ^5-matrix. In the last step we then made use of the two trace theorems (D.13) and (D.15) to be able to solve the two traces from before and as a result, get (4.59).

The, now following, six traces with two slashed momenta from (4.55) are very similar[17] to each other and, hence, for the sake of clarity – only the first one is stated here explicitly.

16 See trace theorems in Section D.1.4.

17 They only vary in momenta and their position inside the trace and, thence, by shifting the momenta in front and using the commutation relations, only have different momenta and left or right handed chirality operators.

See Section A.1.4 for the other calculations and results. The trace with momenta $\not{k}_1$ and $\not{p}_1$ yields

$$\begin{aligned}
&\mathrm{Tr}\left[\not{k}_1 V_{ij}^{\tilde{\chi}} \not{p}_1 V_{i'j}^{\tilde{\chi}} V_i^{\tilde{g}} V_{i'}^{\tilde{g}}\right] && (4.60)\\
&\quad = \mathrm{Tr}\left[\not{k}_1 \not{p}_1 (b_{ij}^{\tilde{q}} P_R + a_{ij}^{\tilde{q}} P_L)(a_{i'j}^{\tilde{q}*} P_R + b_{i'j}^{\tilde{q}*} P_L)(R_{i2} P_R - R_{i1} P_L)(R_{i'1} P_L - R_{i'2} P_R)\right] && (4.61)\\
&\quad = -\frac{1}{2}(b_{ij}^{\tilde{q}} b_{i'j}^{\tilde{q}*} R_{i2} R_{i'1} + a_{ij}^{\tilde{q}} a_{i'j}^{\tilde{q}*} R_{i1} R_{i'2}) \,\mathrm{Tr}\left[\not{k}_1 \not{p}_1\right] && (4.62)\\
&\quad = -2(b_{ij}^{\tilde{q}} b_{i'j}^{\tilde{q}*} R_{i2} R_{i'1} + a_{ij}^{\tilde{q}} a_{i'j}^{\tilde{q}*} R_{i1} R_{i'2}) k_1 p_1, && (4.63)
\end{aligned}$$

where in the first step we dragged $\not{p}_1$ to the left of $V_{ij}^{\tilde{\chi}}$ and, therefore, needed to switch the chirality operators from left to right and vice versa. Then, in (4.61), we can make use of the fact that, after multiplying out, all terms with an odd number of γ^5-matrices will vanish. After that we can pull the constants out of the trace and get the trace of the two slashed momenta, which can be calculated via the trace theorem (D.12). As a result we get (4.63).

Last but not least, it remains to calculate the trace without momenta

$$\begin{aligned}
&\mathrm{Tr}\left[V_{ij}^{\tilde{\chi}} V_{i'j}^{\tilde{\chi}} V_i^{\tilde{g}} V_{i'}^{\tilde{g}}\right] && (4.64)\\
&\quad = -2(b_{ij}^{\tilde{q}} b_{i'j}^{\tilde{q}*} R_{i'1} R_2 + a_{i'j}^{\tilde{q}*} a_{ij}^{\tilde{q}} R_{i2} R_{i'2}), && (4.65)
\end{aligned}$$

whereby we had to substitute the definitions of (4.52), to use the chirality operator commutation relations and to multiply out and neglect all traces with an odd number of γ^5's.[18]

Finally we can, with the results from the colour dependant amplitude (4.51) and the eight calculated traces that, together, form the spin-amplitude, construct the total amplitude of the interference of t- and u-channel

$$\begin{aligned}
\mathrm{Re}\,\overline{M_t M_u^\dagger} = \frac{g_s^2}{2} \sum_{i,i'} \frac{1}{(t - m_{\tilde{q}_i}^2)(u - m_{\tilde{q}_{i'}}^2)} \Big\{ &\\
&(b_{ij}^{\tilde{q}} a_{i'j}^{\tilde{q}*} R_{i1} R_{i'2} + a_{ij}^{\tilde{q}} b_{i'j}^{\tilde{q}*} R_{i2} R_{i'1})[k_1 p_1 k_2 p_2 - k_1 k_2 p_1 p_2 + k_1 p_2 p_1 k_2]\\
&+ m_1 m_1' k_2 p_2 (b_{ij}^{\tilde{q}} b_{i'j}^{\tilde{q}*} R_{i2} R_{i'1} + a_{i'j}^{\tilde{q}*} a_{ij}^{\tilde{q}} R_{i1} R_{i'2}) + m_1' m_2' p_1 p_2 (b_{ij}^{\tilde{q}} a_{i'j}^{\tilde{q}*} R_{i2} R_{i'1} + a_{ij}^{\tilde{q}} b_{i'j}^{\tilde{q}*} R_{i1} R_{i'2})\\
&- m_2 m_1' k_2 p_1 (b_{ij}^{\tilde{q}} a_{i'j}^{\tilde{q}*} R_{i'1} R_{i1} + a_{ij}^{\tilde{q}} b_{i'j}^{\tilde{q}*} R_{i2} R_{i'2}) + m_1 m_2' k_1 p_2 (b_{ij}^{\tilde{q}} b_{i'j}^{\tilde{q}*} R_{i1} R_{i'2} + a_{i'j}^{\tilde{q}*} a_{ij}^{\tilde{q}} R_{i2} R_{i'1})\\
&- m_1 m_2 k_1 k_2 (b_{ij}^{\tilde{q}} b_{i'j}^{\tilde{q}*} R_{i2} R_{i'2} + a_{i'j}^{\tilde{q}*} a_{ij}^{\tilde{q}} R_{i'1} R_{i1}) - m_2 m_2' k_1 p_1 (b_{ij}^{\tilde{q}} a_{i'j}^{\tilde{q}*} R_{i2} R_{i'2} + a_{ij}^{\tilde{q}} b_{i'j}^{\tilde{q}*} R_{i'1} R_{i1})\\
&- m_1 m_1' m_2 m_2' (b_{ij}^{\tilde{q}} b_{i'j}^{\tilde{q}*} R_{i'1} R_{i1} + a_{i'j}^{\tilde{q}*} a_{ij}^{\tilde{q}} R_{i2} R_{i'2}) \Big\}. \qquad (4.66)
\end{aligned}$$

TO CONCLUDE: By analyzing (4.31) and (4.46) one can see that these are per forma equal, and only the momenta are either in t or u configuration. For we do not expect the masses to differ very much and can already theorize that the cross-sections too should be very similar.

The invariant amplitudes were additionally checked via the programme `FeynCalc` [39], which is integrated as a package in `Mathematica`. For this we implemented the "starting amplitudes" for t-channel (4.18), u-channel (4.33) and for the interference term (4.47) and (4.48) into `FeynCalc`. `FeynCalc` then, after running the same computation steps

18 See Equation D.14 for the corresponding trace theorem and Section D.1.1 for the commutation relations of the chirality operator and γ-matrices.

we did, delivers the same results for the averaged and amplitude squared invariant amplitudes (4.31), (4.46) and (4.66).

After the two-component spinor calculation in the next chapter, we will in Chapter 6 implement these into `DM@NLO`, where we can discuss the three amplitudes and analyze the then computed cross-sections further.

5 WEYL CALCULATION

In Chapter 4, we calculated the invariant amplitude in the usual four-component spinor technique. As stated, in this chapter we will follow a different approach that will make use of calculations with two-component spinors.

We will begin by giving some background and motivation. First, one can notice that Weyl spinors are more elementary in that sense, that they transform like irreducible representations, whereas Dirac spinors do not. In SUSY, Weyl spinors are included naturally through the symmetry generators of supersymmetric field theories. Supplementary, the chirality in the SM plays a crucial role in the form of fermionic quantum numbers and interactions. Because left and right chiral spinors are combined in the four-component notation, one needs to extract the information about their respective chiral transformation cumbersome with the help from the chirality operators P_L and P_R.[1] Although the last point is neglectable if one is working in *quantum electro dynamics* (QED) or *quantum chromo dynamics* (QCD), because of them being parity conserving, at the point of EWSB it will be more natural to work with Weyl spinors.

All this, and the consideration that the couplings we deal with only have Parity operator dependencies,[2] let us conclude that the two-component fermion ansatz should be of interest for the neutralino-gluino coannihilation.

Therefore, in the next step, the said technique will be introduced and shortly illustrated. After that, we will compute the cross-section using the two-component formalism and check whether we get the same result as in the four-component Dirac calculation.

5.1 TECHNIQUE

The used two-component spinor formalism only differs from the "usual" technique in the actual computation step. The general procedure, such as squaring the amplitude, averaging over states followed by computing traces of matrices, remains the same and takes place in four-component notation. Only the fact if either two or four component spinors, and, thence, traces of either γ- or σ-matrices, are being calculated is different in said step. One gets new relations for solving the spin (helicity) and colour sums and for computing the traces, yet the overall technique stays similar and is comparable. But applying only the formalism to change the spinors from four to two components without further adjustment, will yield calculations that become impractical very fast because of the drastic increase in the number of diagrams one needs to compute.

Therefore, in [24], Dreiner et. al. introduced the idea to use the *helicity amplitude technique*[3] alongside the two-component formalism for spinors. The amplitudes are then decomposed into simpler helicity-eigenstate graphs, which then can be calculated. Because of their calculations being in terms of Lorentz scalar invariants, it is more convenient and one usually needs only a set of the same schematics for solving all amplitudes. Resulting, all amplitudes can be simply put together.

1 See Section D.1.2.
2 With the rest being constants and matrix elements, see the coupling terms in Appendix C.
3 For an overview consult e.g. [22].

Furthermore, instead of using four-component spinor wave functions that are distinguished by particle or antiparticle status, here the two-component spinors are discerned by their respective Lorentz group transformation properties. This explains the advantage in handling theories with Majorana particles and theories, where left chiral fermions transform differently than right chiral fermions.

TO SHORTLY STATE THE FINAL PROCEDURE: (Following [24]) One starts analogue to the machinery used in four-component formalism. This is to construct the corresponding Feynman graphs but with helicity flow instead of the usual fermion number flow. Here one has to include the fact that there are multiple permutations and, therefore, multiple Feynman diagrams for each left or right chiral interaction. Thereby, one can take the same amplitudes as in four-component and just needs to include the correct transforming part of the vertex coupling terms regarding either a χ- or ψ-like interaction. This is accompanied by changing the four-spinor wave functions u and v with the two-spinor ones, namely x and y for left or right chiral spinor, respectively. The then following part, where one has to sum over all particle states such as spin and colour, can be solved via the new trace theorems and relations for helicity sums for two-component fermions. As a last step the amplitudes just have to be added together and, as a result, one will get the same presentation of the final amplitude.

In our process, we will make use of a computing aid. The squark will be given a chirality handling. This of course will not change anything physically, but it will ease differentation and naming of the 16 amplitudes we will get. Furthermore, it will be of great help to examine which components of the Lagrangians will couple later on. The squark's chirality will be denoted by $\tilde{q}_L$ or $\tilde{q}_R$, respectively.

5.2 FEYNMAN DIAGRAMS

We will now begin by constructing the helicity amplitudes and their corresponding Feynman diagrams which, summed together, will yield the total invariant amplitude of the neutralino-gluino coannihilation. Here the main difference is that we will have, as stated before, way more amplitudes compared to the four-component formalism. As a second difference, we do not need to calculate traces with more than two σ-matrices. This is because the couplings from the vertices between neutralino-quark-squark and gluino-quark-squark only depend on the chirality operator that vanishes in two-component notation. Nevertheless, we, therefore, need to consider which part of the couplings transform χ- or ψ-like. As a result, we get not only four but eight vertices and need to include their permutations as well. So we get not two diagrams but four.[4]

In addition to that, we now need to discern whether the squark couples to gaugino or higgsino component of the neutralino.[5] This can be seen by recognising the different dependencies of squark mixing matrices $R^{\tilde{q}}_{i1}$ and $R^{\tilde{q}}_{i2}$ in the Lagrangians of the two interactions. The gluino, as a gaugino, connects the left-chiral mixing matrix $R^{\tilde{q}}_{i1}$ with the right-chiral parity operator P_R, see (C.8). Hence, the coupling quark needs to be right-chiral. In the neutralino-squark-quark interaction Lagrangian (C.2) we now immediately see that we need to differentiate between gaugino and higgsino components. In the gaugino part of the coupling matrices $a^{\tilde{q}}_{ij}$ and $b^{\tilde{q}}_{ij}$ the combination of squark mixing

4 Including t- and u-channel already, see Figure 4.1.

5 Recall that the neutralino $\tilde{\chi}^0$ is a mixing state of gauginos $\tilde{W}^0$ and $\tilde{B}$ and higgsinos $\tilde{H}^0_u$ and $\tilde{H}^0_d$.

matrices with chirality operators corresponds to the gluino one. But the neutralino parts have the exact opposite composition. Therefore, we need to include two more possible permutations of helicity states from neutralino and quark for every existing one. Resulting, we get eight amplitudes.

The coupling matrices corresponding to a gaugino- or higgsino-like transformation are denoted with upper g or h, respectively. It follows that

$$a_{ij}^{\tilde{q}} = a_{ij}^{g} + a_{ij}^{h} \quad \text{and} \quad b_{ij}^{\tilde{q}} = b_{ij}^{g} + b_{ij}^{h}. \tag{5.1}$$

Last, we have to note that the two vertices can be different chiral-coupled. In referring to our computing aid, to let the squark carry chirality, this means that we need to consider chirality mixing states of the squark. With this in mind, the number of amplitudes doubles and we now get 16 amplitudes, as we mentioned before.

Following these considerations we begin by setting the four first Feynman graphs for the squark coupling to the gaugino component of the neutralino. Here we do not consider $\tilde{q}_L$-$\tilde{q}_R$ mixing. With the two-component Feynman rules from Appendix C we get Figure 5.1. We then can build the corresponding invariant amplitudes corresponding

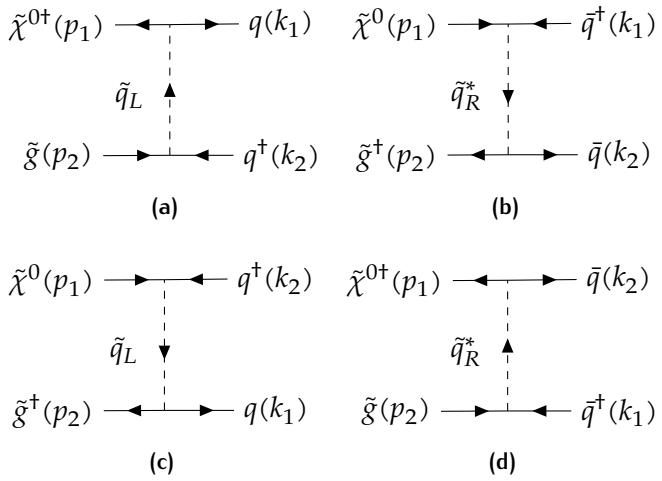

Figure 5.1: Feynman diagrams for gaugino coupling without $\tilde{q}_{L,R}$ mixing.

to the four diagrams. Here we recall the convention to differentiate the amplitudes by the squark's chirality. Using only the gaugino parts of the vertex terms constructed in (C.6), (C.7), (C.9), and (C.10) we get

$$iM_{t,g}^{\tilde{g}_L} = (-) - \Omega_{t,i} T_{st}^a b_{ij}^g R_{i1} (y_{\tilde{\chi}}^\dagger x_{q_1}^\dagger)(x_{\tilde{g}} y_{q_2}) \tag{5.2}$$

$$iM_{t,g}^{\tilde{g}_R} = (-)\Omega_{t,i} T_{st}^a a_{ij}^g R_{i2} (x_{\tilde{\chi}} y_{q_1})(y_{\tilde{g}}^\dagger x_{q_2}^\dagger) \tag{5.3}$$

$$iM_{u,g}^{\tilde{g}_L} = -\Omega_{u,i} T_{st}^a b_{ij}^g R_{i1} (x_{\tilde{\chi}} y_{q_2})(y_{\tilde{g}}^\dagger x_{q_1}^\dagger) \tag{5.4}$$

$$iM_{u,g}^{\tilde{g}_R} = \Omega_{u,i} T_{st}^a a_{ij}^g R_{i2} (y_{\tilde{\chi}}^\dagger x_{q_2}^\dagger)(x_{\tilde{g}} y_{q_1}), \tag{5.5}$$

where, the $(-)$ originates from the rule from Appendix C that one needs to impose a relative minus sign for odd, relative permutations of the spinors. E.g. in (5.2) and in (5.3) we have one permutation in comparison to our arbitrary chosen fixed order of external particles $(\tilde{\chi}, \tilde{g}, q_1, q_2)$. Further, for the sake of clarity, we defined

$$\Omega_{(t,u),i} \equiv \frac{i\sqrt{2} g_s}{(t,u) - m_{\tilde{q}_i}^2}. \tag{5.6}$$

As a next step we do the same but for the squark coupling to the higgsino component. Here we only need to change the helicities from the upper vertex compared to Figure 5.1. Except for this and the different constants one gets, the graphs are similar. The Feynman diagrams can be seen in Figure 5.2. Taking now the higgsino components of the vertex

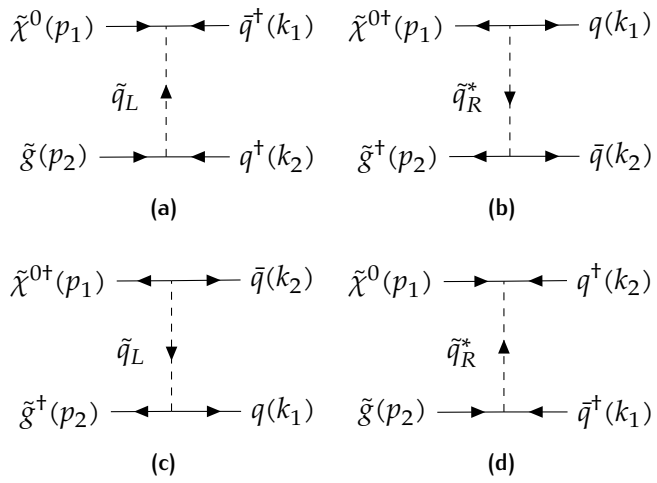

Figure 5.2: Feynman diagrams for higgsino coupling without $\tilde{q}_{L,R}$ mixing.

terms in (C.6)-(C.10) the resulting amplitudes, thence, are

$$iM_{t,h}^{\tilde{g}_L} = (-) - \Omega_{t,i} T_{st}^a a_{ij}^h R_{i1} (x_{\tilde{\chi}} y_{q_1})(x_{\tilde{g}} y_{q_2}) \tag{5.7}$$

$$iM_{t,h}^{\tilde{g}_R} = (-)\Omega_{t,i} T_{st}^a b_{ij}^h R_{i2} (y_{\tilde{\chi}}^\dagger x_{q_1}^\dagger)(y_{\tilde{g}}^\dagger x_{q_2}^\dagger) \tag{5.8}$$

$$iM_{u,h}^{\tilde{g}_L} = -\Omega_{u,i} T_{st}^a a_{ij}^h R_{i1} (y_{\tilde{\chi}}^\dagger x_{q_2}^\dagger)(y_{\tilde{g}}^\dagger x_{q_1}^\dagger) \tag{5.9}$$

$$iM_{u,h}^{\tilde{g}_R} = \Omega_{u,i} T_{st}^a b_{ij}^h R_{i2} (x_{\tilde{\chi}} y_{q_2})(x_{\tilde{g}} y_{q_1}). \tag{5.10}$$

Halfway done, we regard the $\tilde{q}_L$-$\tilde{q}_R$ mixing permutations in the following.

With the same coupling from squark to gaugino part, we can take the same graphs as in Figure 5.1 and just need to change the combination of left- and right-chiral couplings from the vertices. The resulting diagrams can be seen in Figure 5.3. And the corresponding

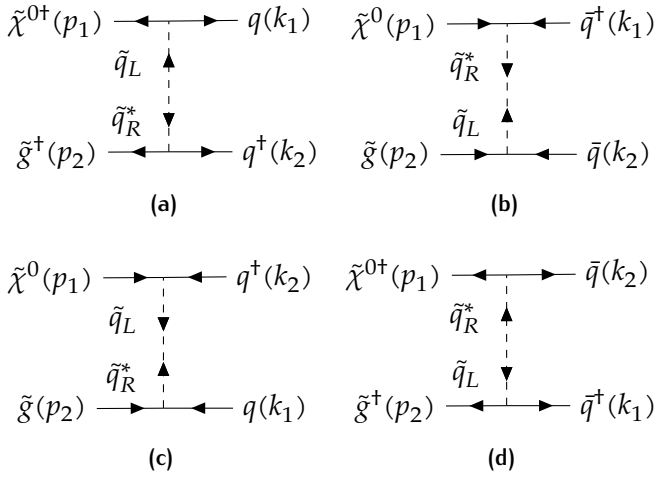

Figure 5.3: Feynman diagrams for gaugino coupling with $\tilde{q}_{L,R}$ mixing.

amplitudes are

$$iM_{t,g}^{\tilde{g}_{L,R}} = (-)\Omega_{t,i}T_{st}^{a}b_{ij}^{g}R_{i2}(y_{\tilde{\chi}}^{\dagger}x_{q_1}^{\dagger})(y_{\tilde{g}}^{\dagger}x_{q_2}^{\dagger}) \tag{5.11}$$

$$iM_{t,g}^{\tilde{g}_{R,L}} = (-) - \Omega_{t,i}T_{st}^{a}a_{ij}^{g}R_{i1}(x_{\tilde{\chi}}y_{q_1})(x_{\tilde{g}}y_{q_2}) \tag{5.12}$$

$$iM_{u,g}^{\tilde{g}_{L,R}} = \Omega_{u,i}T_{st}^{a}b_{ij}^{g}R_{i2}(x_{\tilde{\chi}}y_{q_2})(x_{\tilde{g}}y_{q_1}) \tag{5.13}$$

$$iM_{u,g}^{\tilde{g}_{R,L}} = -\Omega_{u,i}T_{st}^{a}a_{ij}^{g}R_{i1}(y_{\tilde{\chi}}^{\dagger}x_{q_2}^{\dagger})(y_{\tilde{g}}^{\dagger}x_{q_1}^{\dagger}). \tag{5.14}$$

Last, we need to construct the graphs for squark coupling to the higgsino part of $\tilde{\chi}^0$. From the Feynman diagrams in Figure 5.4 we build – the same way as before – the

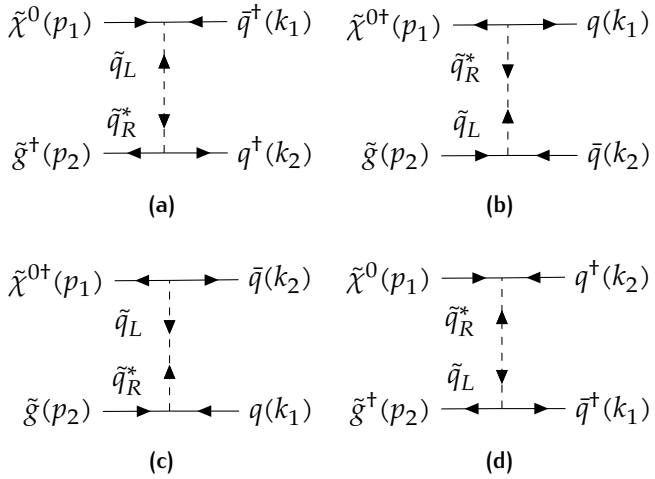

Figure 5.4: Feynman diagrams for higgsino coupling with $\tilde{q}_{L,R}$ mixing.

invariant amplitudes corresponding to the squark helicity mixing state

$$iM_{t,h}^{\tilde{g}_{L,R}} = (-)\Omega_{t,i}T_{st}^{a}a_{ij}^{h}R_{i2}(x_{\tilde{\chi}}y_{q_1})(y_{\tilde{g}}^{\dagger}x_{q_2}^{\dagger}) \tag{5.15}$$

$$iM_{t,h}^{\tilde{g}_{R,L}} = (-) - \Omega_{t,i}T_{st}^{a}b_{ij}^{h}R_{i1}(y_{\tilde{\chi}}^{\dagger}x_{q_1}^{\dagger})(x_{\tilde{g}}y_{q_2}) \tag{5.16}$$

$$iM_{u,h}^{\tilde{g}_{L,R}} = \Omega_{u,i}T_{st}^{a}a_{ij}^{h}R_{i2}(y_{\tilde{\chi}}^{\dagger}x_{q_2}^{\dagger})(x_{\tilde{g}}y_{q_1}) \tag{5.17}$$

$$iM_{u,h}^{\tilde{g}_{R,L}} = -\Omega_{u,i}T_{st}^{a}b_{ij}^{h}R_{i1}(x_{\tilde{\chi}}y_{q_2})(y_{\tilde{g}}^{\dagger}x_{q_1}^{\dagger}). \tag{5.18}$$

One can already see that, as promised, the amplitudes (5.2)-(5.18), that we get in two-component spinor calculation, are plainer than their Dirac counterparts. We do not have any matrices to consider and just need to evaluate the helicity sums of the external particle spinors. Although this simplification is pretty beautiful, the amount of amplitudes one needs to calculate is getting way bigger. The good thing is, as stated by [24], the summation of the amplitudes can be done fairly simply numerically. Here we will not do that. This is due to the fact that for comparison we only need the amplitudes corresponding to the ones we computed via Dirac calculation.

The total amplitude we need for the cross section is given by the composition

$$\overline{|M|}^2 = \overline{|M_t|}^2 + \overline{|M_u|}^2 + 2\,\mathrm{Re}\,\overline{M_t M_u^{\dagger}}, \tag{5.19}$$

equal to (4.16). In the following we will compute the total invariant amplitude by combining all the amplitudes we got to this point. This will be done in separate steps. Namely to calculate the averaged and summed amplitudes for t-channel and u-channel and their

interference individually, like in (5.19). The reason for this, next to simplicity, is the easier comparison to the amplitudes we calculated earlier, using standard four-component technique.

5.3 EVALUATION OF SQUARED AMPLITUDES

5.3.1 T-Channel

We begin by computing the pure t-channel squared amplitude $\overline{|M_t|}^2$ from (5.19). The total invariant amplitude for the t-channel is the sum of all t-channel helicity amplitudes from (5.2)-(5.18)

$$iM_t = iM_{t,g}^{\tilde{g}_L} + iM_{t,g}^{\tilde{g}_R} + iM_{t,h}^{\tilde{g}_L} + iM_{t,h}^{\tilde{g}_R} + iM_{t,g}^{\tilde{g}_{L,R}} + iM_{t,g}^{\tilde{g}_{R,L}} + iM_{t,h}^{\tilde{g}_{L,R}} + iM_{t,h}^{\tilde{g}_{R,L}}. \tag{5.20}$$

By averaging over helicity and colour

$$\overline{|M_t|}^2 = \overline{|M_{t,g}^{\tilde{q}_L}|}^2 + \overline{|M_{t,g}^{\tilde{q}_R}|}^2 + \cdots + 2\,\mathrm{Re}\left(\overline{M_{t,g}^{\tilde{q}} M_{t,g}^{\tilde{q}_R}}\right) + 2\,\mathrm{Re}\left(\overline{M_{t,g}^{\tilde{q}} M_{t,g}^{\tilde{q}_L}}\right) + \cdots \tag{5.21}$$

we obtain not only magnitude squares but interference terms as well.

There are 36 amplitudes in (5.21). The underlying techniques and calculations do not vary much, one only needs to take different helicity-sum relations[6] and trace theorems. As a conclusion, only one magnitude square and one interference term out of the 36 amplitudes are computed exemplary in the following.

First, the magnitude square example is calculated. Here we will take the amplitude $iM_{t,g}^{\tilde{q}_L}$, whose corresponding Feynman diagram is Figure 5.1a. Taking (5.2), multiplying it with its conjugate transpose[7] and the final averaging over spin and colour yields

$$\overline{|M_{t,g}^{\tilde{q}_L}|}^2 = -\frac{1}{2}\sum_{i,i'} \Omega_{t,i}\Omega_{t,i'} b_{ij}^{g} b_{i'j}^{g*} R_{i1} R_{i'1} \frac{1}{4} \sum_{s_1,s_3} (y_{\tilde{\chi}}^{\dagger} x_{q_1}^{\dagger})(x_{q_1} y_{\tilde{\chi}}) \sum_{s_2,s_4} (x_{\tilde{g}} y_{q_2})(y_{q_2}^{\dagger} x_{\tilde{g}}^{\dagger}). \tag{5.22}$$

Here we took advantage of the fact that the colour dependant term is the same as in the Dirac calculation and we can take the result directly from (4.21). Next to that, $\frac{1}{4}$ is – as before – the averaging factor we get from two initial spin 1/2 particles.

In (5.22) we already ordered the spinors according to their helicity in the corresponding helicity sums. This now simplifies the calculation by allowing us to compute the sums individually. Here we again show the explicit chirality indices in van der Waerden notation.[8] This will help us to identify the resulting traces. The first sum over helicities s_1 and s_3 from $\tilde{\chi}^0$ and q_1 simplifies under utilization of the "completeness relations for two-spinors", the helicity sum relations from [24], from Section D.2.2 to

$$\sum_{s_1,s_3} (y_{\tilde{\chi}\dot{\alpha}}^{\dagger} x_{q_1}^{\dagger\dot{\alpha}})(x_{q_1}^{\beta} y_{\tilde{\chi}\beta}) = (p_1 \cdot \sigma_{\beta\dot{\alpha}})(k_1 \cdot \bar{\sigma}^{\dot{\alpha}\beta}) \tag{5.23}$$

$$= {p_1}_{\mu} {k_1}_{\nu}\,\mathrm{Tr}\left[\sigma^{\mu}\bar{\sigma}^{\nu}\right] \tag{5.24}$$

$$= 2p_1 k_1, \tag{5.25}$$

6 As the counterpart to four-component completeness relations.

7 This will just complex conjugate the constants and invert the order of the helicity spinors x and y, next to taking their hermitian conjugate.

8 To not get confused with the colour index a and because [21] uses the same notation, we swap a, b – as used before – for greek indices starting from $\alpha, \beta, \cdots$.

where in the second step we see that with summation convention we calculate the trace of the sigma matrices. The final step is just solving the trace via trace theorem (D.24). The procedure for calculating the second helicity sum over s_2 and s_4 follows nearly equivalent. The only difference is that we have now other momenta and the indices are contracted the other way around. First the χ-like and then the ψ-like components of the sigma matrices. This does not change anything physical and so we get

$$\sum_{s_2,s_4} (x^{\alpha}_{\tilde{g}} y_{q_2\alpha})(y^{\dagger}_{q_2\dot{\beta}} x^{\dagger\dot{\beta}}_{\tilde{g}}) = (p_2 \cdot \bar{\sigma}^{\dot{\beta}\alpha})(k_2 \cdot \sigma_{\alpha\dot{\beta}}) \tag{5.26}$$

$$= {p_2}_{\mu} {k_2}_{\nu} \operatorname{Tr}\left[\bar{\sigma}^{\mu}\sigma^{\nu}\right] \tag{5.27}$$

$$= 2p_2k_2. \tag{5.28}$$

Combining (5.33) and (5.36) and substituting them into (5.22) yields

$$\overline{|M^{\tilde{q}_L}_{t,g}|}^2 = -\frac{1}{2} p_1 k_2 p_2 k_2 \sum_{i,i'} \Omega_{t,i}\Omega_{t,i'} b^{g}_{ij} b^{g*}_{i'j} R_{i1} R_{i'1} \tag{5.29}$$

as a result for the first computed invariant amplitude.

The second example calculation is one of the interference terms. We take the amplitudes $M^{\tilde{q}_L}_{t,g}$ and $M^{\tilde{q}_R}_{t,g}$ from (5.2) and (5.3), respectively. From their Feynman diagrams Figure 5.1a and Figure 5.1b we can immediately see that the spinor terms like $(y^{\dagger}_{\tilde{\chi}} x^{\dagger}_{q_1})$ now do not combine with their respective hermitian conjugate. By substituting the known results for the averaging factors and taking the sum over all squark generations we get

$$\operatorname{Re}\left(\overline{M^{\tilde{q}_L}_{t,g} M^{\tilde{q}_R\dagger}_{t,g}}\right) = \frac{-1}{2} \sum_{i,i'} \Omega_{t,i}\Omega_{t,i'} b^{g}_{ij} a^{g*}_{i'j} R_{i'2} R_{i1} \frac{1}{4} \sum_{s_1,s_3} (y^{\dagger}_{\tilde{\chi}} x^{\dagger}_{q_1})(y^{\dagger}_{q_1} x^{\dagger}_{\tilde{\chi}}) \sum_{s_2,s_4} (x_{\tilde{g}} y_{q_2})(x_{q_2} y_{\tilde{g}}), \tag{5.30}$$

with the averaging factors already embedded. Again, we now can separate by helicities and calculate the corresponding parts in the van der Waerden notation. The sum over helicities from $\tilde{\chi}^0$ and q_1 yields

$$\sum_{s_1,s_3} (y^{\dagger}_{\tilde{\chi}\dot{\alpha}} x^{\dagger\dot{\alpha}}_{q_1})(y^{\dagger}_{q_1\dot{\beta}} x^{\dagger\dot{\beta}}_{\tilde{\chi}}) = (-m_1 \delta^{\dot{\beta}}_{\dot{\alpha}})(-m'_1 \delta^{\dot{\alpha}}_{\dot{\beta}}) \tag{5.31}$$

$$= m_1 m'_1 \operatorname{Tr}\left[\mathrm{I}_2\right] \tag{5.32}$$

$$= 2 m_1 m'_1, \tag{5.33}$$

where we used the – by now well known – completeness relation for Weyl-spinors in (5.31). In the next step we identified, with Einstein's summation convention, a trace of the $2D$-unit-matrix.

The remaining helicity-sum can be derived nearly equivalently

$$\sum_{s_2,s_4} (x^{\alpha}_{\tilde{g}} y_{q_2\alpha})(x^{\beta}_{q_2} y_{\tilde{g}\beta}) = (-m_2 \delta^{\alpha}_{\beta})(-m'_2 \delta^{\beta}_{\alpha}) \tag{5.34}$$

$$= m_2 m'_2 \operatorname{Tr}\left[\mathrm{I}_2\right] \tag{5.35}$$

$$= 2 m_2 m'_2. \tag{5.36}$$

Taking the results from (5.33) and (5.36) and substituting them into (5.30) we get the invariant amplitude

$$\operatorname{Re}\left(\overline{M^{\tilde{q}_L}_{t,g} M^{\tilde{q}_R\dagger}_{t,g}}\right) = -\frac{1}{2} m_1 m'_1 m_2 m'_2 \sum_{i,i'} \Omega_{t,i}\Omega_{t,i'} b^{g}_{ij} a^{g*}_{i'j} R_{i'2} R_{i1}. \tag{5.37}$$

These two example calculations have shown the general procedure in calculating amplitudes for the t-channel of the process. The omitted amplitudes, which are not explicitly stated here, can be derived very closely to those calculated above.

With all 36 amplitudes, squared- and interference-terms, we can, by adding them as in (5.21), construct the total t-channel amplitude [9]

$$\begin{aligned}\overline{|M_t|}^2 = \frac{g_s^2}{N}\sum_{i,i'}\frac{1}{(t-m^2_{\tilde{q}_i})(t-m^2_{\tilde{q}_{i'}})}\\ \times\Big[p_1k_1(a^g_{ij}a^{g*}_{i'j}+2a^g_{ij}a^{h*}_{i'j}+a^h_{ij}a^{h*}_{i'j}+b^g_{ij}b^{g*}_{i'j}+2b^g_{ij}b^{h*}_{i'j}+b^h_{ij}b^{h*}_{i'j})\\ +m_1m_1'(2a^g_{ij}b^{g*}_{i'j}+2a^g_{ij}b^{h*}_{i'j}+2a^h_{ij}b^{g*}_{i'j}+2a^h_{ij}b^{h*}_{i'j})\Big]\\ \times\Big[p_2k_2(R_{1i}R_{1i'}+R_{2i}R_{2i'})-m_2m_2'(R_{1i}R_2i'+R_{2i}R_{1i'})\Big].\end{aligned}\tag{5.38}$$

5.3.2 U-Channel

Next the u-channel amplitude $\overline{|M_t|}^2$ from (5.19) needs to be calculated. The total invariant amplitude for the u-channel is now the sum of the 36 u-channel helicity amplitudes in (5.2)-(5.18)

$$iM_u = iM^{\tilde{g}_L}_{u,g}+iM^{\tilde{g}_R}_{u,g}+iM^{\tilde{g}_L}_{u,h}+iM^{\tilde{g}_R}_{u,h}+iM^{\tilde{g}_{L,R}}_{u,g}+iM^{\tilde{g}_{R,L}}_{u,g}+iM^{\tilde{g}_{L,R}}_{u,h}+iM^{\tilde{g}_{R,L}}_{u,h}.\tag{5.39}$$

And we again get pure and interference terms by building the magnitude square

$$\overline{|M_u|}^2 = \overline{|M^{\tilde{q}_L}_{u,g}|}^2+\overline{|M^{\tilde{q}_R}_{u,g}|}^2+\cdots+2\,\mathrm{Re}\,(\overline{M^{\tilde{q}}_{u,g}M^{\tilde{q}_R\dagger}_{u,g}})+2\,\mathrm{Re}\,(\overline{M^{\tilde{q}}_{u,g}M^{\tilde{q}_L\dagger}_{u,g}})+\cdots.\tag{5.40}$$

The independant contributions in (5.40) can be constructed via the same techniques showed in the previous section. Only the constants and matrix elements differ. Therefore, we will not state their calculations but will just give the final result in form of the squared u-channel amplitude

$$\begin{aligned}\overline{|M_u|}^2 = \frac{g_s^2}{N}\sum_{i,i'}\frac{1}{(u-m^2_{\tilde{q}_i})(u-m^2_{\tilde{q}_{i'}})}\\ \times\Big[p_1k_2(a^g_{ij}a^{g*}_{i'j}+2a^g_{ij}a^{h*}_{i'j}+a^h_{ij}a^{h*}_{i'j}+b^g_{ij}b^{g*}_{i'j}+2b^g_{ij}b^{h*}_{i'j}+b^h_{ij}b^{h*}_{i'j})\\ +m_1m_2'(2a^g_{ij}b^{g*}_{i'j}+2a^g_{ij}b^{h*}_{i'j}+2a^h_{ij}b^{g*}_{i'j}+2a^h_{ij}b^{h*}_{i'j})\Big]\\ \times\Big[p_2k_1(R_{1i}R_{1i'}+R_{2i}R_{2i'})-m_1'm_2(R_{1i}R_2i'+R_{2i}R_{1i'})\Big].\end{aligned}\tag{5.41}$$

5.3.3 Interference

To build the complete amplitude for this scattering we now only need to compute the last remaining contribution from (5.19). Namely, all 64 interference terms of u- and t-channel in (5.2)-(5.18)

$$\mathrm{Re}\,(\overline{M_tM_u^\dagger}) = \mathrm{Re}\,(\overline{M^{\tilde{g}_L}_{t,g}M^{\tilde{g}_L\dagger}_{u,g}})+\mathrm{Re}\,(\overline{M^{\tilde{g}_L}_{t,g}M^{\tilde{g}_R\dagger}_{u,g}})+\cdots+\mathrm{Re}\,(\overline{M^{\tilde{g}_R}_{t,g}M^{\tilde{g}_L\dagger}_{u,g}})+\cdots.\tag{5.42}$$

9 Remember that we only need the invariant amplitude M to build the cross section following the procedure from Section 4.1.

Here we encounter some differences. First of all, we now get different combinations of helicity spinors, and because of only interfering amplitudes, we can no longer separate the helicity sum and we, therefore, need to sum all spinors together.

Here we will only explicitly show the calculation of two examples out of the 64. These two need different relations compared to the computation of (5.22) and (5.30).

The first one being the interference of graphs Figure 5.1a and Figure 5.1c with their respective amplitudes (5.2) and (5.4)

$$\mathrm{Re}\left(\overline{M^{\tilde{q}_L}_{t,g} M^{\tilde{q}_L\dagger}_{u,g}}\right) = -\frac{1}{2}\sum_{i,i'} \Omega_{t,i}\Omega_{u,i'} b^g_{ij} b^{g*}_{i'j} R_{i2} R_{i'2} \frac{1}{4} \sum_{\substack{s_1,s_2\\ s_3,s_4}} (y^\dagger_{\tilde{\chi}} x^\dagger_{q_1})(x_{\tilde{g}} y_{q_2})(y^\dagger_{q_2} x^\dagger_{\tilde{\chi}})(x_{q_1} y_{\tilde{g}}), \tag{5.43}$$

where again averaging factors are already calculated and the summation is over helicities s_n of all four particles. This sum can be derived as follows, again using the van der Waerden-notation,

$$\begin{aligned}
&\sum_{\substack{s_1,s_2\\ s_3,s_4}} (y^\dagger_{\tilde{\chi}\dot{\alpha}} x^{\dagger\dot{\alpha}}_{q_1})(x^\beta_{q_1} y_{\tilde{g}\beta})(x^\gamma_{\tilde{g}} y_{q_2\gamma})(y^\dagger_{q_2\dot{\delta}} x^{\dagger\dot{\delta}}_{\tilde{\chi}}) && (5.44)\\
&\quad = (-m_1 \delta^{\dot{\delta}}_{\dot{\alpha}})(k_1 \cdot \bar{\sigma}^{\dot{\alpha}\beta})(-m_2 \delta_\beta^{\ \gamma})(k_2 \cdot \sigma_{\gamma\dot{\delta}}) && (5.45)\\
&\quad = m_1 m_2 k_{1\mu} k_{2\nu} \,\mathrm{Tr}\left[\bar{\sigma}^\mu \sigma^\nu\right] && (5.46)\\
&\quad = 2 m_1 m_2 k_1 k_2. && (5.47)
\end{aligned}$$

Here we used the completeness relations for helicity spinors from Section D.2.2 in (5.44). Following the usual procedure we then identify a trace with diagonal elements $M^{\dot{\delta}}_{\ \dot{\delta}}$ with $M = \bar{\sigma}^\mu \sigma^\nu$. In the final step in (5.46) trace theorem (D.24) was used. With this result we can write (5.43) as

$$\mathrm{Re}\left(\overline{M^{\tilde{q}_L}_{t,g} M^{\tilde{q}_L\dagger}_{u,g}}\right) = -\frac{1}{4} m_1 m_2 k_1 k_2 \sum_{i,i'} \Omega_{t,i}\Omega_{u,i'} b^g_{ij} b^{g*}_{i'j} R_{i2} R_{i'2}. \tag{5.48}$$

The second example will provide an illustration of a trace theorem for four sigma matrices. For this we choose the interference of graphs Figure 5.2a and Figure 5.2d with amplitudes (5.7) and (5.10), respectively. Again, we construct the combined invariant amplitude with averaging factors

$$\mathrm{Re}\left(\overline{M^{\tilde{q}_L}_{t,h} M^{\tilde{q}_R\dagger}_{u,h}}\right) = \frac{1}{2}\sum_{i,i'} \Omega_{t,i}\Omega_{u,i'} a^h_{ij} b^{h*}_{i'j} R_{i1} R_{i'2} \frac{1}{4} \sum_{\substack{s_1,s_2\\ s_3,s_4}} (x_{\tilde{\chi}} y_{q_1})(x_{\tilde{g}} y_{q_2})(y^\dagger_{q_2} x^\dagger_{\tilde{\chi}})(y^\dagger_{q_1} x^\dagger_{\tilde{g}}). \tag{5.49}$$

To solve the helicity sum we (using the van der Waerden-notation) exploit the helicity completeness relations and get a trace of now four σ-matrices

$$\begin{aligned}
&\sum_{\substack{s_1,s_2\\ s_3,s_4}} (x^\alpha_{\tilde{\chi}} y_{q_1\alpha})(y^\dagger_{q_1\dot{\beta}} x^{\dagger\dot{\beta}}_{\tilde{g}})(x^\gamma_{\tilde{g}} y_{q_2\gamma})(y^\dagger_{q_2\dot{\delta}} x^{\dagger\dot{\delta}}_{\tilde{\chi}}) && (5.50)\\
&\quad = (p_1 \cdot \bar{\sigma}^{\dot{\delta}\alpha})(k_1 \cdot \sigma_{\alpha\dot{\beta}})(p_2 \cdot \bar{\sigma}^{\dot{\beta}\gamma})(k_2 \cdot \sigma_{\gamma\dot{\delta}}) && (5.51)\\
&\quad = p_{1\mu} k_{1\nu} p_{2\rho} k_{2\sigma} \,\mathrm{Tr}\left[\bar{\sigma}^\mu \sigma^\nu \bar{\sigma}^\rho \sigma^\sigma\right] && (5.52)\\
&\quad = 2(p_1 k_1 p_2 k_2 - p_1 p_2 k_1 k_2 + p_1 k_2 k_1 p_2 - i\varepsilon^{p_1 k_2 p_2 k_2}), && (5.53)
\end{aligned}$$

where in (5.52), we used the trace theorem (D.26) to solve the trace. This yields for (5.49)

$$\mathrm{Re}\,(\overline{M^{\tilde{q}_L}_{t,h} M^{\tilde{q}_R\dagger}_{u,h}}) = \frac{1}{4}(p_1k_1p_2k_2 - p_1p_2k_1k_2 + p_1k_2k_1p_2) \sum_{i,i'} \Omega_{t,i}\Omega_{u,i'} a^h_{ij} b^{h*}_{i'j} R_{i1}R_{i'2}. \tag{5.54}$$

With calculating all 64 corresponding to the scheme and technique demonstrated on the two example calculations (5.43) and (5.49) we get, as a final result for the magnitude square of the interference of u- and t-channel graphs,

$$\begin{aligned}
\mathrm{Re}\,(\overline{M_t M_u^\dagger}) =& \frac{g_s^2}{2} \sum_{i,i'} \frac{1}{(t - m^2_{\tilde{q}_i})(u - m^2_{\tilde{q}_{i'}})} \Big\{ \\
&\times \Big[(b^g_{ij} a^{g*}_{i'j} + b^g_{ij} a^{h*}_{i'j} + b^h_{ij} a^{g*}_{i'j} + b^h_{ij} a^{h*}_{i'j}) R_{i1}R_{i'2} \\
&\quad + (a^g_{ij} b^{g*}_{i'j} + a^g_{ij} b^{h*}_{i'j} + a^h_{ij} b^{g*}_{i'j} + a^h_{ij} b^{h*}_{i'j}) R_{i2}R_{i'1} \Big] \\
&\times [k_1p_1k_2p_2 - k_1k_2p_1p_2 + k_1p_2p_1k_2] \\
&+ m_1 m_1' k_2p_2 \Big[(b^g_{ij} b^{g*}_{i'j} + b^g_{ij} b^{h*}_{i'j} + b^h_{ij} b^{g*}_{i'j} + b^h_{ij} b^{h*}_{i'j}) R_{i2}R_{i'1} \\
&\qquad + (a^{g*}_{i'j} a^g_{ij} + a^{g*}_{i'j} a^h_{ij} + a^{h*}_{i'j} a^g_{ij} + a^{h*}_{i'j} a^h_{ij}) R_{i1}R_{i'2} \Big] \\
&+ m_1' m_2' p_1p_2 \Big[(b^g_{ij} a^{g*}_{i'j} + b^g_{ij} a^{h*}_{i'j} + b^h_{ij} a^{g*}_{i'j} + b^h_{ij} a^{h*}_{i'j}) R_{i2}R_{i'1} \\
&\qquad + (a^g_{ij} b^{g*}_{i'j} + a^g_{ij} b^{h*}_{i'j} + a^h_{ij} b^{g*}_{i'j} + a^h_{ij} b^{h*}_{i'j}) R_{i1}R_{i'2} \Big] \\
&- m_2 m_1' k_2p_1 \Big[(b^g_{ij} a^{g*}_{i'j} + b^g_{ij} a^{h*}_{i'j} + b^h_{ij} a^{g*}_{i'j} + b^h_{ij} a^{h*}_{i'j}) R_{i'1}R_{i1} \\
&\qquad + (a^g_{ij} b^{g*}_{i'j} + a^g_{ij} b^{h*}_{i'j} + a^h_{ij} b^{g*}_{i'j} + a^h_{ij} b^{h*}_{i'j}) R_{i2}R_{i'2} \Big] \\
&+ m_1 m_2' k_1p_2 \Big[(b^g_{ij} b^{g*}_{i'j} + b^g_{ij} b^{h*}_{i'j} + b^h_{ij} b^{g*}_{i'j} + b^h_{ij} b^{h*}_{i'j}) R_{i1}R_{i'2} \\
&\qquad + (a^{g*}_{i'j} a^g_{ij} + a^{g*}_{i'j} a^h_{ij} + a^{h*}_{i'j} a^g_{ij} + a^{h*}_{i'j} a^h_{ij}) R_{i2}R_{i'1} \Big] \\
&- m_1 m_2 k_1k_2 \Big[(b^g_{ij} b^{g*}_{i'j} + b^g_{ij} b^{h*}_{i'j} + b^h_{ij} b^{g*}_{i'j} + b^h_{ij} b^{h*}_{i'j}) R_{i2}R_{i'2} \\
&\qquad + (a^{g*}_{i'j} a^g_{ij} + a^{g*}_{i'j} a^h_{ij} + a^{h*}_{i'j} a^g_{ij} + a^{h*}_{i'j} a^h_{ij}) R_{i'1}R_{i1} \Big] \\
&- m_2 m_2' k_1p_1 \Big[(b^g_{ij} a^{g*}_{i'j} + b^g_{ij} a^{h*}_{i'j} + b^h_{ij} a^{g*}_{i'j} + b^h_{ij} a^{h*}_{i'j}) R_{i2}R_{i'2} \\
&\qquad + (a^g_{ij} b^{g*}_{i'j} + a^g_{ij} b^{h*}_{i'j} + a^h_{ij} b^{g*}_{i'j} + a^h_{ij} b^{h*}_{i'j}) R_{i'1}R_{i1} \Big] \\
&- m_1 m_1' m_2 m_2' \Big[(b^g_{ij} b^{g*}_{i'j} + b^g_{ij} b^{h*}_{i'j} + b^h_{ij} b^{g*}_{i'j} + b^h_{ij} b^{h*}_{i'j}) R_{i'1}R_{i1} \\
&\qquad + (a^{g*}_{i'j} a^g_{ij} + a^{g*}_{i'j} a^h_{ij} + a^{h*}_{i'j} a^g_{ij} + a^{h*}_{i'j} a^h_{ij}) R_{i2}R_{i'2} \Big] \Big\}.
\end{aligned} \tag{5.55}$$

5.3.4 Comparison to Four-Component

In the following we will compare the results we achieved via the two-component calculation with their counterparts from the Dirac calculation. For this to work we need to do some preliminary work. First of all we see that, using (5.1),

$$\begin{aligned}
a^{\tilde{q}}_{ij} a^{\tilde{q}*}_{i'j} &= a^g_{ij} a^{g*}_{i'j} + a^g_{ij} a^{h*}_{i'j} + a^h_{ij} a^{g*}_{i'j} + a^h_{ij} a^{h*}_{i'j} && (5.56)\\
&= a^g_{ij} a^{g*}_{i'j} + 2a^g_{ij} a^{h*}_{i'j} + a^h_{ij} a^{h*}_{i'j}, && (5.57)
\end{aligned}$$

$$b^{\tilde{q}}_{ij} b^{\tilde{q}*}_{i'j} = b^{g}_{ij} b^{g*}_{i'j} + b^{g}_{ij} b^{h*}_{i'j} + b^{h}_{ij} b^{g*}_{i'j} + b^{h}_{ij} b^{h*}_{i'j} \tag{5.58}$$

$$= b^{g}_{ij} b^{g*}_{i'j} + 2 b^{g}_{ij} b^{h*}_{i'j} + b^{h}_{ij} b^{h*}_{i'j}, \tag{5.59}$$

$$a^{\tilde{q}}_{ij} b^{\tilde{q}*}_{i'j} = a^{g}_{ij} b^{g*}_{i'j} + a^{g}_{ij} b^{h*}_{i'j} + a^{h}_{ij} b^{g*}_{i'j} + a^{h}_{ij} b^{h*}_{i'j} \quad , \tag{5.60}$$

$$a^{\tilde{q}*}_{i'j} b^{\tilde{q}}_{ij} = a^{g*}_{i'j} b^{g}_{ij} + a^{g*}_{i'j} b^{h}_{ij} + a^{h*}_{i'j} b^{g}_{ij} + a^{h*}_{i'j} b^{h}_{ij}, \tag{5.61}$$

where in (5.57) and (5.59) we simplified by using the fact that $a^{\tilde{q}}_{ij} = a^{\tilde{q}*}_{i'j} \; \forall i = i'$ and, thence, $a^{g}_{ij} = a^{g*}_{i'j}$ and $a^{h}_{ij} = a^{h*}_{i'j} \; \forall i = i'$ and equivalently for $b^{\tilde{q}}_{ij}$ because the coupling matrices are real. By using the relations above in the results for t- u- and interference-term (5.38), (5.41) and (5.55) the expressions simplify and we can see that they are identical to the results from the preceding four-component calculation in (4.31), (4.46) and (4.66).

TO SUM UP: In this chapter, we presented an alternate way to calculate Feynman graphs and showed the physical equivalence to the usual four-component technique by computing this thesis' coannihilation in both ways. We have seen the advantage in hindsight to processes where one has to take into account the particles chiralities. The disadvantage, as stated in the beginning, would be the huge amount of amplitudes one has to compute, but with a suited numerical programme this can be bypassed and, because of simpler calculations and numerical summation of these, the error-proneness would be reduced significantly.

After this more technical chapter, we will finally implement the obtained results for the invariant amplitudes from this and the last chapter, into `DM@NLO` in the next chapter.

6 NUMERICAL ANALYSIS

Finally, we can now implement (4.31), (4.46) and (4.66) – the invariant amplitudes for u- and t-channel and their interference of the neutralino-gluino coannihilation – into DM@NLO. There, as described in Appendix B, the corresponding cross-section will be calculated and given to MicrOMEGAs, where the neutralino relic density will be computed.

The implementation with the most important results regarding the relic density and some SUSY masses will be described at first. Then, in the following section, we will give the numerical results of the calculated cross-sections in the implemented scenario. There, we also discuss the optional coannihilation of a chargino (the linear combination of the charged wino and the charged higgsino) with a gluino. Finally, we discuss the numerical results and their physical meaning via consideration of experimental and theoretical bounds.

6.1 IMPLEMENTATION

In order to get numerical results we need to define one specific pMSSM scenario via the 19 parameters from Table 3.3.

We have to add four new parameters, namely the three SM Yukawa couplings y_t, y_b and y_τ and the *SUSY soft breaking scale* Q_{SUSY}, which depicts the scale where we have to define the other parameters. The Yukawa couplings are needed for a slight adjustment compared to the SM values to get more sophisticated results. The chosen values for the now 24 parameters, we need to describe our model, are selected with hindsight on giving the most contribution possible to the neutralino relic density $\Omega_{\tilde{\chi}_1^0}$ but to still remain in a plausible range of the results from the Planck collaboration in (2.1) and so that the resulting masses of the SUSY particles will be in a range not excluded by collider experiments. Next to that, we need to get gluino and neutralino to have very similar masses (Δm = small), so that the coannihilation process really is contributing to the total relic density (see the explanation in Section 2.3.1).

$\tan\beta$	M_1	M_2	M_3	A_t	A_b	A_τ	μ
45.27	1005.54	1088.51	868	−2795.76	2160.9	−2445.45	−2290.38
m_{H^3}	$m_{\tilde{e}_L}$	$m_{\tilde{\tau}_L}$	$m_{\tilde{e}_R}$	$m_{\tilde{\tau}_R}$	$m_{\tilde{q}_{L1}}$	$m_{\tilde{q}_{L3}}$	$m_{\tilde{u}_R}$
3781.1	1883.29	3327.81	2905.44	3400.69	2657.91	3401.05	2326.09
$m_{\tilde{t}_R}$	$m_{\tilde{d}_R}$	$m_{\tilde{b}_R}$	y_t	y_b	y_τ	Q_{SUSY}	
1108.72	2808.38	3661.15	0.819286779	0.616429865	0.438025671	3146.951	

Table 6.1: The 23 DM@NLO-parameters and their values for the scenario used. Dimensionful quantities are given in GeV.

These restrictions in combination with the goal to get a high contribution from this process yield the scenario parameter values stated in Table 6.1. Immediately we can state

two interesting facts emerging from the chosen parameters. First of all, the neutralino is a mostly bino and wino mixed state, but less higgsino like, which can be seen via the relation $|M_1| \simeq |M_2| \ll |\mu|$. Secondly, $\mu \gg m_Z$, which again leads to a necessary fine-tuning. These will be further discussed in Section 6.3 and the so-called "little" hierarchy problem in Section 6.3.3.

The parameters are then given to `SPheno`, which calculates the SUSY mass spectrum and mixing matrices. We will only state the most important masses here. The Higgs sector masses are

$$m_{h^0} = 123.33\,\text{GeV}, \quad m_{H^0} = 3781.10\,\text{GeV} \quad \text{and} \quad m_{H^+} = 3782.08\,\text{GeV}. \tag{6.1}$$

The lightest quark is important for bounds set by collider searches. In our scenario this is the scalar top quark or stop $\tilde{t}$ with

$$m_{\tilde{t}} = 1173.4\,\text{GeV}. \tag{6.2}$$

The masses for neutralino, chargino and gluino are

$$m_{\tilde{\chi}_1^0} = 994.5\,\text{GeV}, \quad m_{\tilde{\chi}_1^\pm} = 1133.8\,\text{GeV} \quad \text{and} \quad m_{\tilde{g}} = 1071.4\,\text{GeV}. \tag{6.3}$$

As it should be, the neutralino is the LSP and the gluino's mass is similar to the neutralino's and is, therefore, the *next-to-lightest supersymmetry particle* (NLSP). Especially $m_{\tilde{\chi}_1^0}$ will be the main point for discussing the validity of this scenario and SUSY in general.[1] Then `MicrOMEGAs` takes the values from `SPheno` and cross-sections from `DM@NLO` and `CalcHEP` (see Appendix B) and calculates the relic density for the neutralino. In our scenario the relic density evaluates to

$$\Omega_{\tilde{\chi}_1^0} h^2 = 0.125. \tag{6.4}$$

One can see that this value is not in the confidence interval of the Planck result (2.1). However, the chosen scenario corresponds only to a single point in the mass spectrum and should be, as it is, near to the measured dark matter relic density. For further research one can then investigate the area around that point with slight adjustments to the parameters from Table 6.1. Secondly, the stated uncertainty is merely dependant on the integrated measurement techniques and should not be taken for absolute. And finally, some not yet in `DM@NLO` included cross-sections could decrease $\Omega_{\tilde{\chi}_1^0}$.

With that in mind, we can further compute the processes contributing to (6.4). These are listed in Table 6.2. We can see that one of this thesis' processes – with the final state quarks being top and anti-top – contributes to the total relic density with 0.2 %.

6.2 CROSS-SECTIONS

Let us now present this thesis' results in form of the cross-section from the neutralino-gluino coannihilation. The cross-section is calculated in `DM@NLO` by integrating the differential cross-section set by the invariant amplitude we derived and the initial particle flux (see Appendix B). In `DM@NLO` (and in our specific scenario set by Table 6.1) we can then specify the final state products, which we deliberately set to a general quark and anti-quark throughout this thesis, as two specific quarks and state a specific centre-of-mass (CM) momentum p_{cm}. With this, all possible quark final states can be computed. These are depicted in Figure 6.1.

1 This too will be (briefly) done in Section 6.3.

CONTR.	INITIAL	FINAL
60.7 %	$\tilde{g}, \tilde{g}$	g, g
8.4 %	$\tilde{g}, \tilde{g}$	$b, \bar{b}$
6.6 %	$\tilde{g}, \tilde{g}$	$d, \bar{d}$
6.6 %	$\tilde{g}, \tilde{g}$	$s, \bar{s}$
5.8 %	$\tilde{g}, \tilde{g}$	$u, \bar{u}$
5.8 %	$\tilde{g}, \tilde{g}$	$c, \bar{c}$
4.2 %	$\tilde{g}, \tilde{g}$	$t, \bar{t}$
1.2 %	$\tilde{g}, \tilde{t}$	g, t
0.2 %	$\tilde{\chi}_1^0, \tilde{g}$	$t, \bar{t}$
0.1 %	$\tilde{\chi}_1^0, \tilde{\chi}_1^0$	$t, \bar{t}$

Table 6.2: Contributions of (co)annihilation processes to the neutralino relic density $\Omega_{\tilde{\chi}_1^0}$.

We can see that, as seen in Table 6.2, the top t and antitop $\bar{t}$ final state possibility contributes the most. Especially at low p_{cm} this scattering makes up nearly 100 % of the total cross-section. The up/antiup $u\bar{u}$ and charm/anticharm $c\bar{c}$ final state sectors carry some significance at higher p_{cm} but are smaller than 0.1 % even then. The other final state sectors can be omitted without doubt. For $t\bar{t}$ being most significant, let us calculate the cross-sections for the three channels of this specific process separately (via each calculated invariant ampliudes (4.31), (4.46) and (4.66)).

The three-channel cross-sections, as in Figure 6.2, yield the interesting fact that t- and u-channel are – at least to numerical precision – exactly equal. Furthermore, one can see that both the interference term and the t- and u-channel cross-sections are up to two orders higher than the total cross-section σ_{tot}. That is, they cancel each other out, except for the small amount σ_{tot}. But this cancellation decreases drastically with higher p_{cm}. We see that all three amplitudes are significant for the total cross-section and one needs to consider all of them. Interestingly, σ_{tot} declines rather rapidly and does not show signs of why this behaviour would change. Furthermore, *leading-order* calculation (loop interactions) could reign significant change for the cross-section at low p_{cm} via the high susceptibility of the channels due to the cancellation of the individual cross-sections.But, because of the equal t- and u-channel cross-sections and because of their high order cancellation with the interference term, we suspect an unphysical symmetry originating in the calculation procedure. This symmetry could be feasible at higher orders too so that even then, the cancellation holds, and σ_{tot} would not experience a significant change.

It is to note that the computed cross-sections by `DM@NLO` deliver results deviating around 3 % compared to the same particle tree-level cross-sections from `CalcHEP`. This small deviation can originate in constants set by the programmes which differ slightly. Therefore, we will interpret this variance in such a way that our results can be assessed with a high degree of certainty.

6.2.1 Chargino-Gluino Coannihilation

We can, as an interludum, analyse the coannihilation of chargino and gluino. This will only change the constants and matrix elements and restrict the final state quarks colour

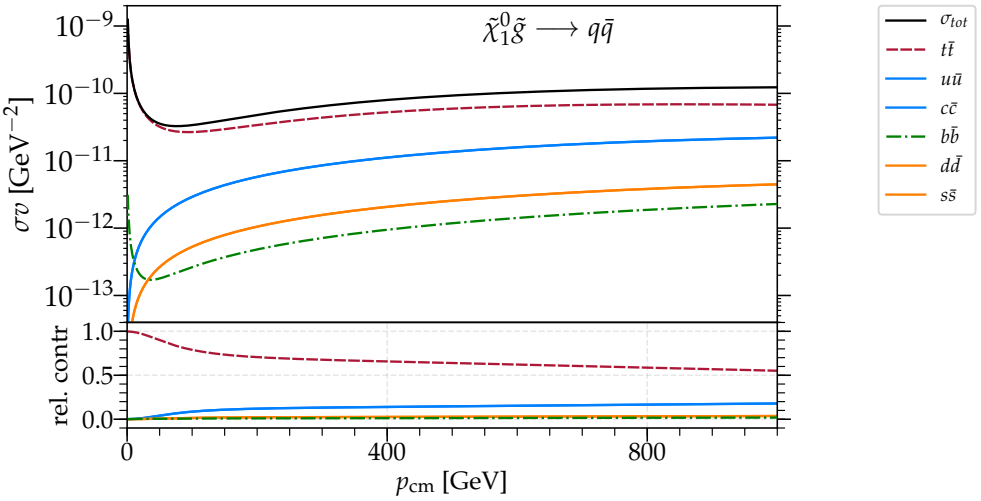

Figure 6.1: Cross-sections for all possible neutralino-gluino scatterings with quark final states. The solid, coloured lines state multiple cross-sections with exactly the same or at least not distinguishable courses. The subordinate figure gives the relative contribution (rel. contr) of specific final state to the total cross-section σ_{tot}.

by the chargino interacting strongly and, hence, changing the colour charge of the upper final state quark. The initial and final states, the propagator and the overall structure of the invariant amplitudes and, therefore, the cross-section, will stay the same. This is because the chargino-squark-quark interaction Lagrangian has also the same structure as the neutralino one (which is fitting because chargino and neutralino only differ so much).

With the constants being swapped and the regulations for the final state colours having changed, we can integrate the same three invariant amplitudes as before in `DM@NLO`. The resulting cross-sections – for all final state possibilities – can be seen in Figure 6.3.

As before one can identify that there is one most significant final state colour permutation, namely bottom b and stop $\tilde{t}$. Second to that, we see that the chargino cross-section is higher to one or two orders of magnitude compared to the neutralino one.

This process is, as it is, not relevant to our dark matter problem. However, it shows the simple transfer to be able to do only one calculation – for either chargino or neutralino – and get both. [2]

6.3 DISCUSSION

First of all, we can discuss the low contribution of the neutralino-gluino coannihilation to the relic density of the neutralino. From Table 6.2 we can see that especially gluino pair annihilations are the most dominant processes.

This was investigated by [41]. There, Profumo and Yaguna showed that for a bino like neutralino [3] with a quasi-degenerate gluino indeed the three main contributing processes are gluino-gluino, neutralino-gluino and neutralino-neutralino (co)annihilations. As

2 As a last note, we can state that the chargino gains importance in specific scenarios either being the NLSP for the neutralino LSP or for a gravitino LSP, as it was done in e.g. [36].

3 This mainly holds for wino and higgsino too. More precisely, the transition zone between gluino and neutralino pair annihilation dominance in Figure 6.4 would shift to smaller Δm.

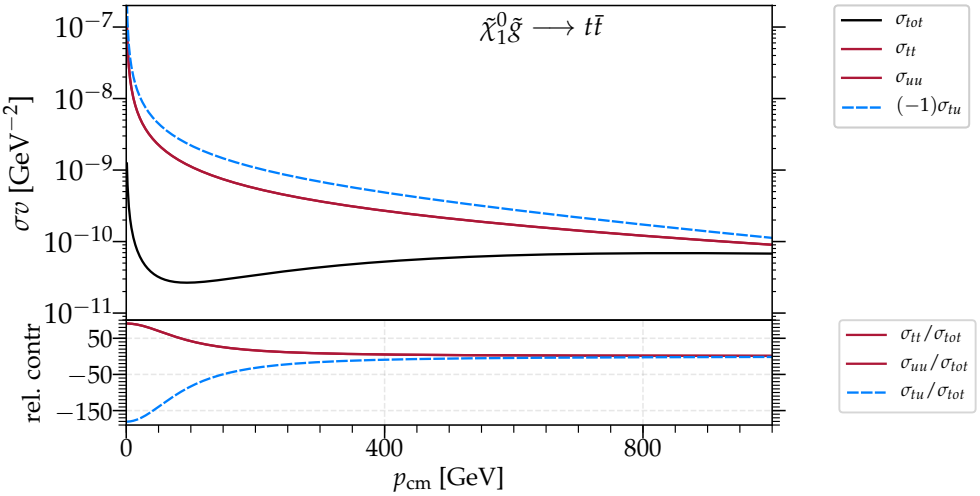

Figure 6.2: Relative channel-contributions for the significant $t\bar{t}$-process. The solid, coloured line states multiple channel cross-sections with exactly the same or at least not distinguishable courses.

depicted in Figure 6.4, for neutralino-gluino mass splittings $\Delta m \simeq 10\,\%$, the distribution of the contribution of the three processes is very similar to what we computed. So even at higher Δm we should not be expecting a more significant contribution of the neutralino-gluino coannihilation. This, in fact, is a unique property of gluino coannihilations. Other coannihilation partners would always make up the dominant process in the transition zone between both pair annihilations, at around $\Delta m \sim$ (10-20)%. In comparison to [41], we have a very light stop quark which is contributing too – in form of coannihilation with the gluino (see Table 6.2).

Furthermore, we see here and from Figure 6.1 that the top-antitop final state is the most relevant one. This is to be explained via the large top Yukawa coupling y_t.

Next to that, it is to be mentioned that the gluino pair annihilation would be dominant for all $\tan\beta$, for the gluinos interacting strong and, therefore, not depending on $\tan\beta$. The dominance of this annihilation is interesting because it suppresses the relic density. As shown in [41], this is especially the case for bino dark matter.

6.3.1 Neutralino Composition

We can now shortly discuss the bino-wino like nature of the neutralino in our pMSSM scenario.[4] We saw in Table 6.2 that the bino-wino like neutralino pair annihilation seems to be small. This is true and in fact leads – like all bino dark matter – to an over-abundance in the relic density. In our scenario, we suppressed the over-abundant relic density via two factors. First, we have M_2 not much bigger than M_1 and the wino part of our neutralino results in more reactive interactions and a greater cross-section. Secondly, we deliberately created an NLSP – in form of the gluino having near neutralino mass – and, therefore, we

4 Actually we only have a "mostly" bino-wino mixed state. Because of μ not much greater than 1-2 TeV, higgsino couplings are possible. These so-called *funnels* yield additional annihilation channels via a propagator. This propagator could, in our case, be one of the heavier MSSM Higgs bosons.

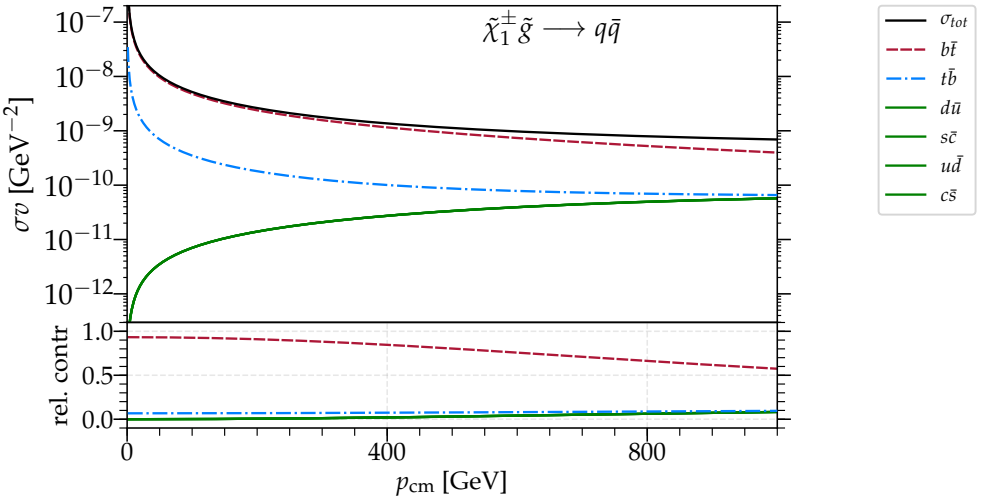

Figure 6.3: Cross-sections for all possible chargino-gluino scatterings with quark final states. The solid, coloured line states multiple cross-sections with exactly the same or at least not distinguishable courses. The subordinate figure gives the relative contribution (rel. contr) of specific final state to the total cross-section σ_{tot}.

allowed coannihilations of the LSP with the NLSP, which too suppresses the abundance of relic neutralinos.[5]

However, this means that we have to restrict our available parameter space significantly. We need to have very specific masses and couplings to get the abundance right to fit experimental data.[6] This too is shown in e.g. [23], where one solution to this problem is given as well. Their ansatz is to investigate an early matter-dominated universe as a cosmological scenario that widens the available MSSM parameter space.

We saw that (pure) bino dark matter is not the best candidate, but we needed to fine-tune the parameter space narrowly in combination with a mixed wino-bino to achieve the required relic density. Let us shortly – for the sake of completeness – state some thoughts about wino and higgsino. We will follow a review on higgsino dark matter, namely [35]. The wino like neutralino is the only dark matter candidate SU(2) triplet (whereas bino and higgsino are singlet and doublet, respectively), which emerges after EWSB if $|M_2| \ll |M_1|, |\mu|$. Wino, as higgsino, dark matter often carries an under-abundance. Adding to this, many annihilation channels of the wino have been excluded by experiment by now, further reducing the density, and, when including the Sommerfeld enhancement, the wino like neutralino is only able to saturate the relic density if $m_{\tilde{\chi}_0^1} \gtrsim 2.7\,\mathrm{TeV}$. The higgsino like neutralino, on the other hand, is a very promising candidate. It can be shown that, if $m_{\tilde{\chi}_0^1} \simeq 1.1\,\mathrm{TeV}$, the correct relic density would be achieved. Furthermore, a higgsino with this mass often yields a large Q_{SUSY}, and corresponding models are, thence, not very constrained by experiment.

So, to conclude the discussion about the composition of the neutralino, we can say that our chosen scenario – bino-wino dark matter – provides just the right relic density with a high enough SUSY breaking-scale so that this model should be phenomenological viable. Next to that, we should have a wider parameter space by the inclusion of wino mixture and *funnels* via higgsino couplings. For we have computed only one not significant cross-

5 In addition, as mentioned above, the stop also has low mass and can serve as an additional coannihilation partner.

6 Because of this fine-tuning we again have a problem of naturalness.

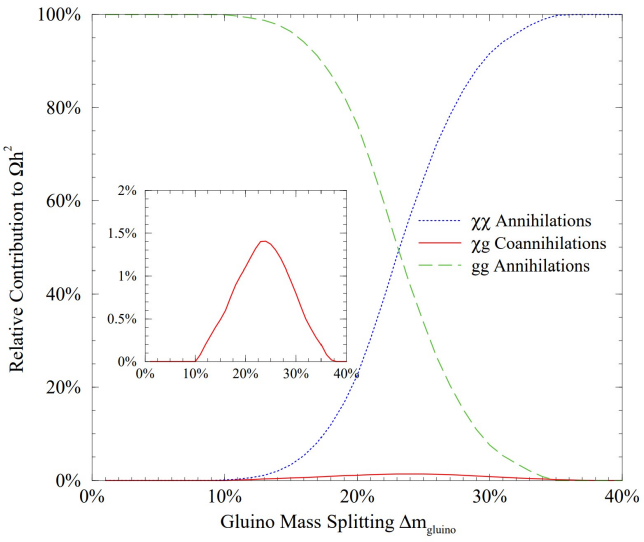

Figure 6.4: Relative contributions to $\Omega_{\tilde{\chi}_1^0}$ by $\tilde{\chi}\tilde{\chi}$, $\tilde{\chi}\tilde{g}$ and $\tilde{g}\tilde{g}$ (co)annihilations as a function of Δm.[41]

section, we are not able to plot meaningful or representative parameter spaces. Here it must suffice to have a look upon bounds for the parameters by theory and experiment, and assess them qualitatively.

6.3.2 Experimental Mass Bounds

Let us now discuss some experimental restrictions to the SUSY parameter space from the CERN experiments ATLAS [19] and CMS [20]. For these experiments presenting their SUSY searches in so-called *simplified models*, we will shortly describe them here. Simplified models often are like a pMSSM, but assume only some – for the experiment necessary – production or decay processes. This can be achieved by defining parameter space only for the relevant particles. Other particles, assumed to have no impact, are, therefore, not restricted in parameter space but should in the subordinate model be e.g. too heavy to be produced. This yields the advantage of only having to define a limited amount of parameters and gain more generality, wherein models with way more parameters one could easily change physical results by changing some parameters that can not be restricted with current knowledge or experiment. The disadvantage, of course, is that search limits tend to be overly strict because of the too strong branch ratios of SUSY decays in simplified models.

We will have a look at bounds for the gluino mass and squark masses in dependency on the neutralino mass. In Figure 6.5 the gluino-neutralino parameter space is shown, as restricted by the $\sqrt{s} = 13\,\text{TeV}$ CMS run.[7] The corresponding simplified models are depicted by the process listed there. As we can see, the area corresponding to our chosen scenario at ca. $m_{\tilde{\chi}_0^1} \simeq 1000\,\text{GeV}$ and $m_{\tilde{g}} \simeq 1000\,\text{GeV}$ (see (6.3)) is close to the limit but not excluded. Further, interesting to state is that gluino masses beyond $\sim 2.3\,\text{TeV}$ are excluded and for neutrinos above $\sim 1.5\,\text{TeV}$ the gluino mass is unrestricted.

Next to the gluino mass bounds, we can discuss limits given to squark and particular the stau quark in a $\sqrt{s} = 13\,\text{TeV}$ run by ATLAS and CMS, respectively. The resulting limits in neutralino parameter space are depicted in Figure 6.6. In the ATLAS run, left

7 ATLAS provides the same limits, see [51]

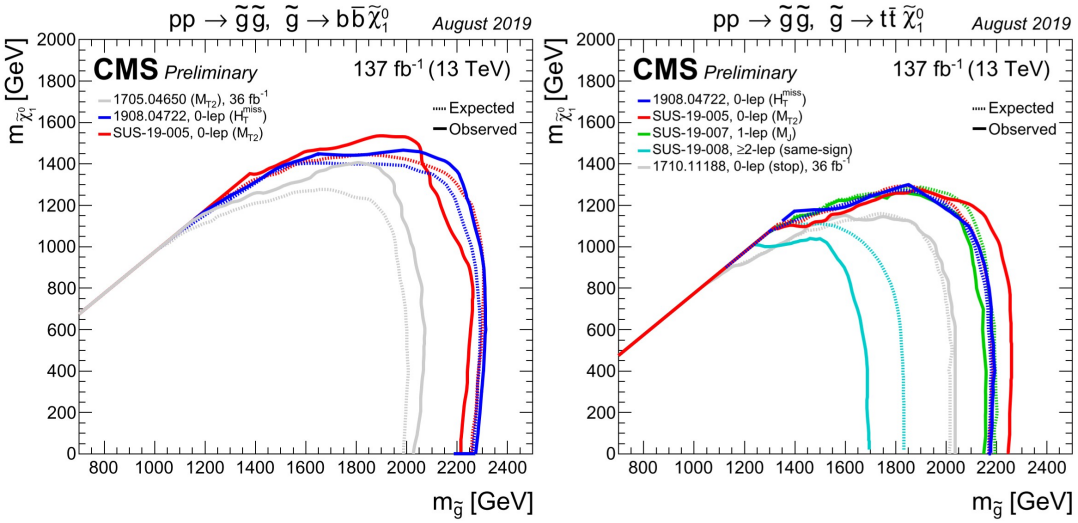

Figure 6.5: Lower mass limits, at 95% C.L., on gluino pair production for various decay chains in the framework of simplified models. Left: $\tilde{g} \to b\bar{b}\tilde{\chi}_1^0$. Right: $\tilde{g} \to t\bar{t}\tilde{\chi}_1^0$. Results of the CMS collaboration.[51]

in Figure 6.6, it is assumed that the $\tilde{u}$, $\tilde{d}$, $\tilde{s}$ and $\tilde{c}$ squarks are degenerate in mass. This is somewhat fitting for our scenario since their masses are arranged very sharply around about 3300 GeV and could, via slight parameter tuning, be adjusted to become truly degenerate. Next to that, a second assumption is that the gluino should be very heavy so one is able to neglect t-channel contributions to squark pair production. As this is not the case for the gluino mass we set to a low value at around 1 TeV, we, therefore, must not give too much credence to the limits set by this experiment. Nevertheless, with $m_{\tilde{\chi}_0^1} \simeq 1000\,\text{GeV}$ and $m_{\tilde{q}} \simeq 3300\,\text{GeV}$ we are well above the bounds as given by ATLAS, even for some significant parameter shifts and, presumably, also for a too low gluino mass. The CMS experiment in the right panel only probed the stau's mass $m_{\tilde{t}}$ in hindsight on the neutralino's. As we can see, our scenario is again far beyond the set limits (see (6.2)).

Concluding, we can say that the exemplary experimental bounds provided by ATLAS and CMS at CERN, do not give strong indications that our chosen pMSSM scenario is excluded or (yet) unphysically. Even so, our scenario point in parameter space lies rather close to the bounds given by Figure 6.5, we assume the simplified models used are too strict. Additionally, we can adjust masses slightly to once again concur with the experiment if newer limits arise – atleast to some extent.

6.3.3 The "little" Hierarchy Problem

As a last step, we will briefly discuss one theoretical "bound" or restriction, which directly loops back to one of our motivations for SUSY, namely the solution to the fine-tuning or hierarchy problem.

In comparison to the *"big" hierarchy problem*, which we discussed in Section 3.1.1, a new need to fine-tune occurs for high μ. We can visualize this in the following way:

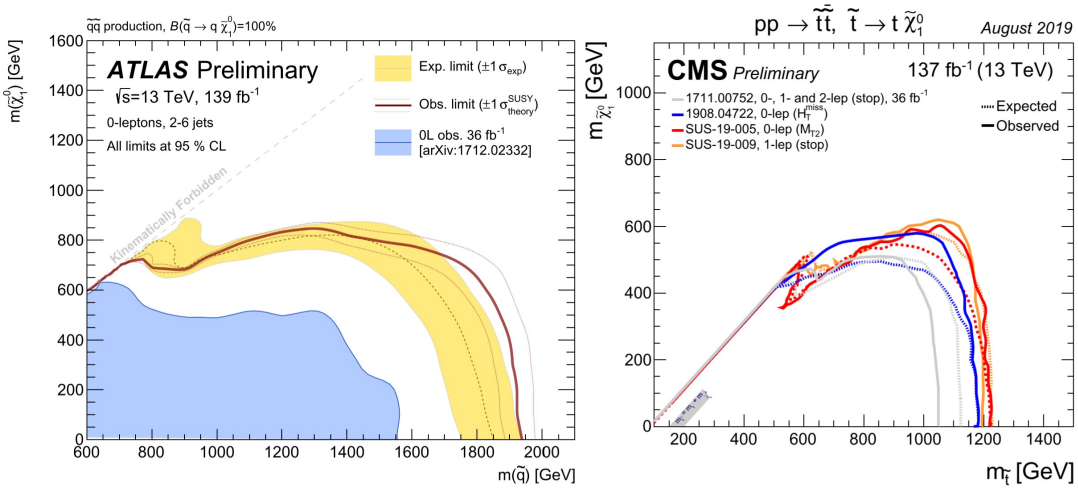

Figure 6.6: Left: 95% C.L. exclusion contours in the squark-neutralino mass plane defined in the framework of simplified models assuming a single decay chain of $\tilde{q} \to q\tilde{\chi}_1^0$, obtained by ATLAS. Right: the 95% C.L. exclusion contours in the stop-neutralino mass plane defined in the framework of a simplified model assuming a single decay chain of $\tilde{t} \to t\tilde{\chi}_1^0$ as obtained by CMS.[51]

Via the minimization conditions on the Higgs potential one can get an expression for the Z boson mass, namely [8]

$$\frac{1}{2}m_Z^2 = \frac{m_{H_d}^2 + \sum_d^d - (m_{H_u}^2 + \sum_u^u)\tan^2\beta}{\tan^2\beta - 1} - \mu^2, \tag{6.5}$$

where $\sum_d^d$ and $\sum_u^u$ represent the 1-loop corrections for the Higgs doublet masses. If then, for simplicity, we neglect loop corrections and consider, as in our case, large $\tan\beta$, (6.5) becomes

$$\frac{1}{2}m_Z^2 = -\mu^2 - m_{H_u}^2. \tag{6.6}$$

We can see that if $\mu^2 \gg m_Z^2, m_{H_u}$ needs to fine-tune μ to a degree, where the experimental measured Z boson mass is achieved. Because the Z mass is small at around 90 GeV, one could argue that $|\mu| \simeq 2290$ GeV, as in our scenario, yields again unnaturalness for the model. Even without the above simplifications, in (6.5) one still needs large cancellations between μ and one or several of the other contributing terms.

So is the SUSY a viable solution to the (big) hierarchy problem of the SM at all? Even so, we need to fine-tune, the magnitude of the degree of fine-tuning is many orders smaller than in the SM if the superpartner masses only go up to a few TeV because scalar masses do not carry quadratic sensitivity at high scale if SUSY is broken.[12] The motivation is, therefore, still viable, if not as strong of an argument as before.

8 Taken from [12].

7 CONCLUSION

To summarize, we showed that the SM can not explain dark matter and, therefore, introduced SUSY as the most general natural extension. In the minimal-parameter SUSY, which was adjusted to be in concordance with experimental evidence (the pMSSM), we saw that the WIMP neutralino as the LSP fulfils all requirements of being a valid and promising dark matter candidate.

The main goal of this thesis was, after introducing the theories behind dark matter and SUSY, to calculate one specific – to the neutralino relic density $\Omega_{\tilde{\chi}_1^0}$ contributing – coannihilation process with the NLSP gluino. This was done analytically in four- and two-component technique. The resulting invariant amplitudes then were implemented in the programme `DM@NLO`, where – via connected dark matter software `MicrOMEGAs`, `SPheno` and `CalcHEP` – we integrated the cross-section and the corresponding neutralino Boltzmann equation numerically. The final outcome was the relic density $\Omega_{\tilde{\chi}_1^0}$ for our chosen pMSSM scenario.

For calculating the Feynman graphs we had to establish fermion number violating Feynman rules for the Majorana particles neutralino and gluino. Interestingly all resulting fermion flow permutations proofed to be invariant in the case of couplings only involving γ^5 matrices in combination with a scalar propagator.

It was shown that the Weyl two-component calculation yields – next to a more elemental nature, some attractive advantages over the usual Dirac four-component one. This led us to conclude that in theoretical models including distinctions regarding the chirality of spinors (e.g. SUSY), we would prefer this technique over the standard Dirac calculation.

The computed relic density and the scenario-associated SUSY parameter masses were discussed, and we conclude that this specific MSSM scenario agrees with at least recent ATLAS and CMS experimental data. Furthermore, even under future-coming restrictions, our scenario provides enough room to adjust to new limits. This originates from the high SUSY soft-breaking scale Q_{SUSY}. But, the discussed little hierarchy problem would be affected when Q_{SUSY} and, therefore, μ would grow larger. With the current scenario, this is, however, only a small inconvenience compared to the way more "unnatural" big hierarchy problem of the SM.

Although the chosen scenario, and, hence, SUSY, seems to be physically feasible, the coannihilation process yields – with only 0.2 % – no overly significant contribution to the thermal relic density. However, more precise calculations are required along with more precise experimental results. In that regard and the fact that possible QCD 1-loop interactions could yield – as discussed – relevant adjustments to the cross-section, we still see some importance in the here calculated process. But, since now no loop corrections have been made, the mostly only benefit from this calculation is the first implementation in `DM@NLO`, so that fewer `CalcHEP` results are needed. This is of importance because, as we saw, `DM@NLO` and `CalcHEP` differ by some margin so that it will yield less uncertainty when calculating all processes in the same environment with the same initial conditions and techniques. Furthermore, the coannihilation specific code is implemented and future 1-loop corrections can be added quite easily.

7.1 OUTLOOK

As indicated, the next obvious step would be to calculate and implement into DM@NLO the 1-loop QCD corrections for the neutralino-gluino coannihilation. Although this could change the cross-section, presumably it would be more beneficial to first implement some of the not yet included but more significantly contributing (co)annihilation processes, which are right now only given by CalcHEP.

Next to that, we only discussed fairly few bounds by experiment and theory. So, another future step might be to first compute all cross-sections important for the neutralino relic density of one scenario and then to examine the contributions from all relevant mass parameters. After that, one could analyze the mass spectra in combination with including more experimental data and theoretical considerations.

The most far-reaching task that can be done in the future is the modernisation and rewriting into a stand-alone application of DM@NLO. In particular, the implementation of linearisation and scaling will be of great interest, so that computations can be run faster and non-ideal parameter spaces can be calculated without implementing corresponding processes.

A AUXILIARY CALCULATION

A.1 DIRAC CALCULATION

A.1.1 Hermitian Conjugate of Gauge Vertices

Two calculate the Hermitian conjugate of a general gauge vertex with chirality operator one can do the following steps (note the validity under $u \leftrightarrow v$ exchange)

$$(\bar{u}(p)P_{L,R}u(k))^\dagger = \frac{1}{2}u(k)^\dagger(1 \mp \gamma^5)^\dagger(u(p)^\dagger\gamma^0)^\dagger \tag{A.1}$$

$$= \frac{1}{2}u(k)^\dagger(1 \mp \gamma^5)\gamma^0 u(p) \tag{A.2}$$

$$= \frac{1}{2}u(k)^\dagger\gamma^0(1 \pm \gamma^5)u(p) \tag{A.3}$$

$$= \frac{1}{2}\bar{u}(k)(1 \pm \gamma^5)u(p) \tag{A.4}$$

$$= \bar{u}(k)P_{R,L}u(p), \tag{A.5}$$

where in each of (A.1) and (A.4) we made use of the definition $\bar{u} = u^\dagger\gamma^0$. Next to that we took advantage of the very useful anticommutation relation of γ^μ and γ^5-matrices (D.5).

A.1.2 Trace Calculation I

The first of the two often reoccurring traces gives

$$\mathrm{Tr}\left[(aP_L + bP_R)(cP_R + dP_L)\right] = \mathrm{Tr}\left[adP_L + bcP_R\right] \tag{A.6}$$

$$= \frac{1}{2}\mathrm{Tr}\left[ad + bc\right] \tag{A.7}$$

$$= 2(ad + bc), \tag{A.8}$$

where a, b, c, d are real arbitrary constants. In (A.6) we exploited the commutation relations of the chirality operator and, as a next step, replaced the chirality operators with their corresponding γ-matrix definition (see Section D.1.1). Then we can take advantage of trace theorem (D.14), which tells us that the single γ^5-terms will be zero, drag the constants out of the trace and use $\mathrm{Tr}\, I_4 = 4$.

A.1.3 Trace Calculation II

The second needed trace-calculation equals the first one except of the occurrence of two impulses $\not{p}$ and $\not{k}$ in the trace. The trace then results in

$$\begin{aligned}
\mathrm{Tr}\left[\not{p}(aP_L + bP_R)\not{k}(cP_R + dP_L)\right] &= \mathrm{Tr}\left[\not{p}\not{k}(aP_R + bP_L)(cP_R + dP_L)\right] && \text{(A.9)}\\
&= \mathrm{Tr}\left[\not{p}\not{k}(acP_R + bdP_L)\right] && \text{(A.10)}\\
&= \frac{1}{2}\,\mathrm{Tr}\left[\not{p}\not{k}(ac + bd)\right] && \text{(A.11)}\\
&= 2pk(ac + bd). && \text{(A.12)}
\end{aligned}$$

To calculate this trace we made use of the same techniques applied before, but with two changes: first, in (A.9), we dragged $\not{k}$ in front of the first two chirality operators and exploited the anticommutation relation between the γ^5 from the slashed impulses and the γ-matrix we get from the chirality operators. Second, as the last step in (A.11), we needed to determine the trace of the two impulses, instead of the unit matrix, with trace theorem (D.12).

A.1.4 Omitted Trace Calculations

$$\begin{aligned}
&\mathrm{Tr}\left[V^{\tilde{\chi}}_{ij}V^{\tilde{\chi}}_{i'j}\not{k}_2 V^{\tilde{g}}_{i}\not{p}_2 V^{\tilde{g}}_{i'}\right] && \text{(A.13)}\\
&\quad= \mathrm{Tr}\left[\not{k}_2\not{p}_2(b^{\tilde{q}}_{ij}P_L + a^{\tilde{q}}_{ij}P_R)(b^{\tilde{q}*}_{i'j}P_R + a^{\tilde{q}*}_{i'j}P_L)(R_{i2}P_L - R_{i1}P_R)(R_{i'2}P_L - R_{i'1}P_R)\right] && \text{(A.14)}\\
&\quad= \frac{1}{2}\,\mathrm{Tr}\left[\not{k}_2\not{p}_2(b^{\tilde{q}}_{ij}a^{\tilde{q}*}_{i'j}R_{i2}R_{i'2} + a^{\tilde{q}}_{ij}b^{\tilde{q}*}_{i'j}R_{i1}R_{i'1})\right] && \text{(A.15)}\\
&\quad= 2(b^{\tilde{q}}_{ij}a^{\tilde{q}*}_{i'j}R_{i2}R_{i'2} + a^{\tilde{q}}_{ij}b^{\tilde{q}*}_{i'j}R_{i1}R_{i'1})k_2p_2 && \text{(A.16)}
\end{aligned}$$

$$\begin{aligned}
&\mathrm{Tr}\left[V^{\tilde{\chi}}_{ij}\not{p}_1 V^{\tilde{\chi}}_{i'j}V^{\tilde{g}}_{i}\not{p}_2 V^{\tilde{g}}_{i'}\right] && \text{(A.17)}\\
&\quad= \mathrm{Tr}\left[\not{p}_1\not{p}_2(b^{\tilde{q}}_{ij}P_L + a^{\tilde{q}}_{ij}P_R)(a^{\tilde{q}*}_{i'j}P_R + b^{\tilde{q}*}_{i'j}P_L)(R_{i2}P_R - R_{i1}P_L)(R_{i'2}P_L - R_{i'1}P_R)\right] && \text{(A.18)}\\
&\quad= \frac{1}{2}(b^{\tilde{q}}_{ij}b^{\tilde{q}*}_{i'j}R_{i2}R_{i'2} + a^{\tilde{q}}_{ij}a^{\tilde{q}*}_{i'j}R_{i1}R_{i'1})\,\mathrm{Tr}\left[\not{p}_1\not{p}_2\right] && \text{(A.19)}\\
&\quad= 2(b^{\tilde{q}}_{ij}b^{\tilde{q}*}_{i'j}R_{i2}R_{i'2} + a^{\tilde{q}}_{ij}a^{\tilde{q}*}_{i'j}R_{i1}R_{i'1})p_1p_2 && \text{(A.20)}
\end{aligned}$$

$$\begin{aligned}
&\mathrm{Tr}\left[V^{\tilde{\chi}}_{ij}\not{p}_1 V^{\tilde{\chi}}_{i'j}\not{k}_2 V^{\tilde{g}}_{i}V^{\tilde{g}}_{i'}\right] && \text{(A.21)}\\
&\quad= \mathrm{Tr}\left[\not{p}_1\not{k}_2(b^{\tilde{q}}_{ij}P_L + a^{\tilde{q}}_{ij}P_R)(a^{\tilde{q}*}_{i'j}P_R + b^{\tilde{q}*}_{i'j}P_L)(R_{i2}P_R - R_{i1}P_L)(R_{i'2}P_L - R_{i'1}P_R)\right] && \text{(A.22)}\\
&\quad= -\frac{1}{2}(b^{\tilde{q}}_{ij}b^{\tilde{q}*}_{i'j}R_{i1}R_{i'2} + a^{\tilde{q}}_{ij}a^{\tilde{q}*}_{i'j}R_{i2}R_{i'1})\,\mathrm{Tr}\left[\not{p}_1\not{k}_2\right] && \text{(A.23)}\\
&\quad= -2(b^{\tilde{q}}_{ij}b^{\tilde{q}*}_{i'j}R_{i1}R_{i'2} + a^{\tilde{q}}_{ij}a^{\tilde{q}*}_{i'j}R_{i2}R_{i'1})p_1k_2 && \text{(A.24)}
\end{aligned}$$

$$\mathrm{Tr}\left[\not{k}_1 V^{\tilde{\chi}}_{ij} V^{\tilde{\chi}}_{i'j} V^{\tilde{g}}_{i} \not{p}_2 V^{\tilde{g}}_{i'}\right] \tag{A.25}$$

$$= \mathrm{Tr}\left[\not{k}_1 \not{p}_2 (b^{\tilde{q}}_{ij} P_R + a^{\tilde{q}}_{ij} P_L)(a^{\tilde{q}*}_{i'j} P_R + b^{\tilde{q}*}_{i'j} P_L)(R_{i2} P_L - R_{i1} P_R)(R_{i'2} P_L - R_{i'1} P_R)\right] \tag{A.26}$$

$$= \frac{1}{2}(b^{\tilde{q}}_{ij} a^{\tilde{q}*}_{i'j} R_{i1} R_{i'1} + a^{\tilde{q}}_{ij} b^{\tilde{q}*}_{i'j} R_{i2} R_{i'2}) \,\mathrm{Tr}\left[\not{k}_1 \not{p}_2\right] \tag{A.27}$$

$$= 2(b^{\tilde{q}}_{ij} a^{\tilde{q}*}_{i'j} R_{i1} R_{i'1} + a^{\tilde{q}}_{ij} b^{\tilde{q}*}_{i'j} R_{i2} R_{i'2}) k_1 p_2 \tag{A.28}$$

$$\mathrm{Tr}\left[\not{k}_1 V^{\tilde{\chi}}_{ij} V^{\tilde{\chi}}_{i'j} \not{k}_2 V^{\tilde{g}}_{i} V^{\tilde{g}}_{i'}\right] \tag{A.29}$$

$$= \mathrm{Tr}\left[\not{k}_1 \not{k}_2 (b^{\tilde{q}}_{ij} P_R + a^{\tilde{q}}_{ij} P_L)(a^{\tilde{q}*}_{i'j} P_L + b^{\tilde{q}*}_{i'j} P_R)(R_{i2} P_L - R_{i1} P_R)(R_{i'2} P_L - R_{i'1} P_R)\right] \tag{A.30}$$

$$= -\frac{1}{2}(b^{\tilde{q}}_{ij} a^{\tilde{q}*}_{i'j} R_{i2} R_{i'1} + a^{\tilde{q}}_{ij} b^{\tilde{q}*}_{i'j} R_{i1} R_{i'2}) \,\mathrm{Tr}\left[\not{k}_1 \not{k}_2\right] \tag{A.31}$$

$$= -2(b^{\tilde{q}}_{ij} a^{\tilde{q}*}_{i'j} R_{i2} R_{i'1} + a^{\tilde{q}}_{ij} b^{\tilde{q}*}_{i'j} R_{i1} R_{i'2}) k_1 k_2 \tag{A.32}$$

B DM@NLO

DM@NLO [30], standing for *dark matter at next-to-leading order*, is a programme that provides SUSY-QCD corrections on 1-loop level for (co)annihilation cross-sections, which are of importance for the determination of the thermal relic density of the neutralino as the LSP in the MSSM. In DM@NLO implemented amplitudes are integrated numerically and the programme yields an easy access and modifiability of the resulting cross-sections.

DM@NLO is integrated in a software bundle including the dark matter tool MicrOMEGAs [16] as its core component. The complete software chain is sketched in Figure B.1. Input given

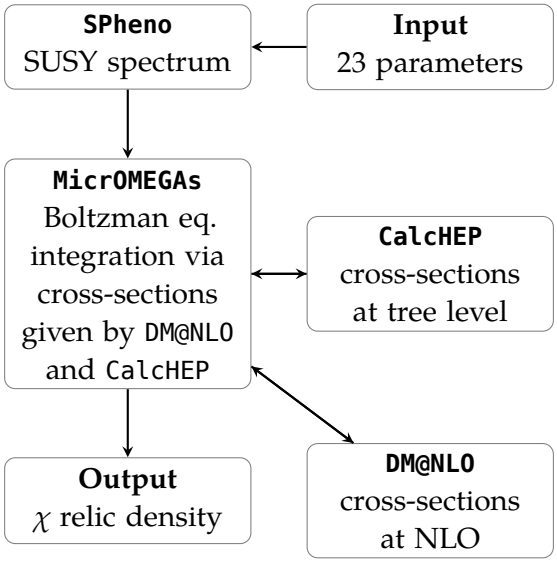

Figure B.1: Software chain with DM@NLO for calculation of the neutralino relic density Ω_{χ^0}.

to the programme are the parameters describing a specific MSSM model according to the convention set by the *Supersymmetry Les Houches Accord* [9]. The spectrum calculator SPheno [40] then calculates the masses of SUSY particles, mixing matrices and observables. These are given to MicrOMEGAs, where the Boltzmann equation for the neutralino will be integrated on the basis of the contributing annihilation and coannihilation cross-sections. The cross-sections are delivered – on tree-level – by CalcHEP [42], but for each cross-setion it is checked if the cross-section is already implemented in DM@NLO. If so, the cross-section computed by DM@NLO supercedes the CalcHEP cross-section. Output is then the relic density.

Concluding, DM@NLO provides QCD loop graphs for the calculation of neutralino relic density and is constructed including radiative corrections and is specifically build for this task, so that a more precise computation, reducing some uncertainties, can be done.

C FEYNMAN RULES

C.1 FOUR-COMPONENT

C.1.1 Particle Lines

External spin 1/2 particles are to be set as four component spinor wave functions u and v following the rules from Figure C.1.

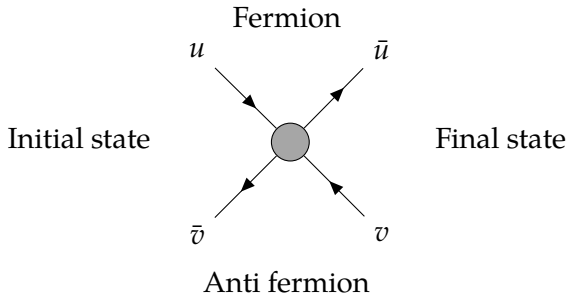

Figure C.1: External wave function spinors.

The Squark propagator term is

$$a \xrightarrow{p} b = \frac{i}{p^2 - m^2_{\tilde{q}_i}} \cdot \delta_{ba}. \tag{C.1}$$

C.1.2 Vertices

The Neutralino-Squark-Quark interaction Lagrangian, taken from [43], is

$$\mathcal{L}_{\tilde{\chi}\tilde{q}q} = \bar{q}(a^{\tilde{q}}_{ij} P_R + b^{\tilde{q}}_{ij} P_L)\tilde{\chi}^0_j \tilde{q}_i + \bar{\tilde{\chi}}^0_j (a^{\tilde{q}}_{ij} P_L + b^{\tilde{q}}_{ij} P_R) q \tilde{q}^*_i, \tag{C.2}$$

with the coupling matrices

$$a^{\tilde{q}}_{ij} = h_f Z_{jx} R^{\tilde{q}}_{i2} + g_s f^q_{Lj} R^{\tilde{q}}_{i1} \qquad \text{where} \quad f^q_{Lj} = \sqrt{2}[(e_q - I^{3l}_q)\tan\theta_W Z_{j1} + I^{3l}_q Z_{j2}], \tag{C.3}$$

$$b^{\tilde{q}}_{ij} = h_f Z_{jx} R^{\tilde{q}}_{i1} + g_s f^q_{Rj} R^{\tilde{q}}_{i2} \qquad \text{where} \quad f^q_{Rj} = -\sqrt{2} e_q \tan\theta_W Z_{j1}, \tag{C.4}$$

where x is standing for {down, up}-type case and can take the values of {3,4}, respectively. The Squark mixing matrix with mixing angle $\theta_{\tilde{q}}$ is

$$R = (R_{i1}, R_{i2}) = \begin{pmatrix} \cos\theta_{\tilde{q}} & \sin\theta_{\tilde{q}} \\ -\sin\theta_{\tilde{q}} & \cos\theta_{\tilde{q}} \end{pmatrix}. \tag{C.5}$$

Coming from the Lagrangian in (C.2) we can construct the vertices

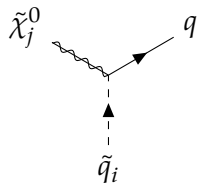

$$= -i(b_{ij}^{\tilde{q}} P_L + a_{ij}^{\tilde{q}} P_R) \tag{C.6}$$

and

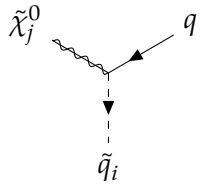

$$= -i(a_{ij}^{\tilde{q}} P_L + b_{ij}^{\tilde{q}} P_R). \tag{C.7}$$

The second vertex from the Gluino-Squark-Quark coupling yields the Lagrangian [43]

$$\mathcal{L}_{\tilde{g}\tilde{q}q} = -\sqrt{2} g_s T_{st}^a \Big[\bar{q}_s (R_{i1}^{\tilde{q}} P_R - R_{i2}^{\tilde{q}} P_L) \tilde{g}^a \tilde{q}_{i,t} + \bar{\tilde{g}}^a (R_{i1}^{\tilde{q}} P_L - R_{i2}^{\tilde{q}} P_R) q_s \tilde{q}_{i,t}^* \Big], \tag{C.8}$$

note that in between the left and right handed terms there is a relative minus sign. This is due to the fact that the SU(N) anti-colour generator is $-T^{a\dagger}$.

Again, from the Lagrangian (C.8), the coupling terms for the two fermion flow possibilities

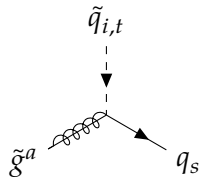

$$= -i\sqrt{2} g_s T_{st}^a (R_{i1}^{\tilde{q}} P_R - R_{i2}^{\tilde{q}} P_L) \tag{C.9}$$

and

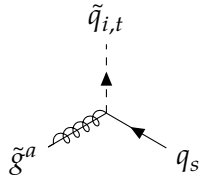

$$= -i\sqrt{2} g_s T_{st}^a (R_{i1}^{\tilde{q}} P_L - R_{i2}^{\tilde{q}} P_R) \tag{C.10}$$

can be achieved.

C.1.3 Fermion Number Violation

Taken from [21] in the following stated are the three, for this thesis relevant, rules for Majorana fermion interactions:

- Take for each external line the appropiate expression from (C.11) to (C.14) to match the corresponding fermion flow.
- Scalar particles are not changed via fermion flow invertion.
- For fermion flow antiparallel to flow of fermion number take the coupling Γ' instead of Γ.

Feynman rules for external fermions with momentum p going from left to right

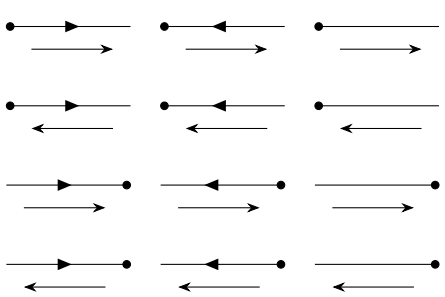

$$= \bar{u}(p,s) \tag{C.11}$$

$$= v(p,s) \tag{C.12}$$

$$= u(p,s) \tag{C.13}$$

$$= \bar{v}(p,s) \tag{C.14}$$

C.2 TWO-COMPONENT

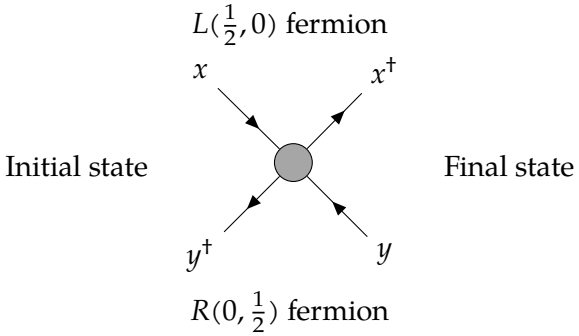

Figure C.2: External wave function spinors.

- For every odd permutation of external state spinors between terms that contribute to the same amplitude one has to impose a relative minus sign.[24]

D RELATIONS AND FORMULAE

D.1 FOUR-COMPONENT

D.1.1 γ-Matrices

$$\{\gamma^\mu, \gamma^\nu\} = 2g^{\mu\nu} \tag{D.1}$$
$$(\gamma^0)^2 = I_4 \tag{D.2}$$
$$\gamma^{0\dagger} = \gamma^0 \tag{D.3}$$
$$\gamma^{\mu\dagger} = \gamma^0\gamma^\mu\gamma^0 \tag{D.4}$$
$$\{\gamma^\mu, \gamma^5\} = 0 \tag{D.5}$$

D.1.2 Chirality Operator

$$P_L \equiv \frac{1}{2}(1-\gamma^5), \qquad P_R \equiv \frac{1}{2}(1+\gamma^5) \tag{D.6}$$

$$P_L^2 = P_L, \qquad P_R^2 = P_R \tag{D.7}$$
$$P_L P_R = P_R P_L = 0 \tag{D.8}$$

D.1.3 Completeness Relations

$$\sum_s u^{(s)}(p,m)\bar{u}^{(s)}(p,m) = \not{p} + m, \qquad \sum_s v^{(s)}(p)\bar{v}^{(s)}(p) = \not{p} - m \tag{D.9}$$

D.1.4 Trace Theorems

Trace of an odd number of γ^μ is zero. (D.10)

Trace of γ^5 times an odd number of γ^μ is still zero. (D.11)

$$\mathrm{Tr}\left[\gamma^\mu\gamma^\nu\right] = 4\eta^{\mu\nu} \tag{D.12}$$
$$\mathrm{Tr}\left[\gamma^\mu\gamma^\nu\gamma^\rho\gamma^\sigma\right] = 4(\eta^{\mu\nu}\eta^{\rho\sigma} - \eta^{\mu\rho}\eta^{\nu\sigma} + \eta^{\mu\sigma}\eta^{\nu\rho}) \tag{D.13}$$
$$\mathrm{Tr}\left[\gamma^5\right] = \mathrm{Tr}\left[\gamma^\mu\gamma^\nu\gamma^5\right] = 0 \tag{D.14}$$
$$\mathrm{Tr}\left[\gamma^\mu\gamma^\nu\gamma^\rho\gamma^\sigma\gamma^5\right] = 4i\varepsilon^{\mu\nu\rho\sigma} \tag{D.15}$$
$$\mathrm{Tr}\left[\gamma^{\mu_1}\ldots\gamma^{\mu_n}\right] = \mathrm{Tr}\left[\gamma^{\mu_n}\ldots\gamma^{\mu_1}\right] \tag{D.16}$$

D.2 TWO-COMPONENT

D.2.1 σ-Matrices

$$\sigma^{\mu}_{\alpha\dot{\alpha}}\bar{\sigma}_{\mu}^{\dot{\beta}\beta} = 2\delta_{\alpha}^{\ \beta}\delta^{\dot{\beta}}_{\ \dot{\alpha}} \tag{D.17}$$
$$\sigma^{\mu}_{\alpha\dot{\alpha}}\sigma_{\mu\beta\dot{\beta}} = 2\epsilon_{\alpha\beta}\epsilon_{\dot{\alpha}\dot{\beta}} \tag{D.18}$$
$$\bar{\sigma}^{\mu\dot{\alpha}\alpha}\bar{\sigma}_{\mu}^{\dot{\beta}\beta} = 2\epsilon^{\alpha\beta}\epsilon^{\dot{\alpha}\dot{\beta}} \tag{D.19}$$

D.2.2 Spin and Helicity Sums

$$\sum_s x_\alpha(\vec{p},s)x^\dagger_{\dot{\beta}}(\vec{p},s) = p\cdot\sigma_{\alpha\dot{\beta}}, \qquad \sum_s x^{\dot{\alpha}\dagger}(\vec{p},s)x^{\beta}(\vec{p},s) = p\cdot\bar{\sigma}^{\dot{\alpha}\beta} \tag{D.20}$$
$$\sum_s y^{\dot{\alpha}\dagger}(\vec{p},s)y^{\beta}(\vec{p},s) = p\cdot\bar{\sigma}^{\dot{\alpha}\beta}, \qquad \sum_s y_\alpha(\vec{p},s)y^\dagger_{\dot{\beta}}(\vec{p},s) = p\cdot\sigma_{\alpha\dot{\beta}} \tag{D.21}$$
$$\sum_s x_\alpha(\vec{p},s)y^{\beta}(\vec{p},s) = m\delta_{\alpha}^{\ \beta}, \qquad \sum_s y_\alpha(\vec{p},s)x^{\beta}(\vec{p},s) = -m\delta_{\alpha}^{\ \beta} \tag{D.22}$$
$$\sum_s y^{\dot{\alpha}\dagger}(\vec{p},s)x^\dagger_{\dot{\beta}}(\vec{p},s) = m\delta^{\dot{\alpha}}_{\ \dot{\beta}}, \qquad \sum_s x^{\dot{\alpha}\dagger}(\vec{p},s)y^\dagger_{\dot{\beta}}(\vec{p},s) = -m\delta^{\dot{\alpha}}_{\ \dot{\beta}} \tag{D.23}$$

D.2.3 Trace Theorems

$$\mathrm{Tr}\left[\sigma^\mu\bar{\sigma}^\nu\right] = \mathrm{Tr}\left[\bar{\sigma}^\mu\sigma^\nu\right] = 2\eta^{\mu\nu} \tag{D.24}$$
$$\mathrm{Tr}\left[\sigma^\mu\bar{\sigma}^\nu\sigma^\rho\bar{\sigma}^\sigma\right] = 2(g^{\mu\nu}g^{\rho\sigma} - g\mu\rho g^{\nu\sigma} + g^{\mu\sigma}g^{\nu\rho} + i\varepsilon^{\mu\nu\rho\sigma}) \tag{D.25}$$
$$\mathrm{Tr}\left[\bar{\sigma}^\mu\sigma^\nu\bar{\sigma}^\rho\sigma^\sigma\right] = 2(g^{\mu\nu}g^{\rho\sigma} - g\mu\rho g^{\nu\sigma} + g^{\mu\sigma}g^{\nu\rho} - i\varepsilon^{\mu\nu\rho\sigma}) \tag{D.26}$$

D.3 SU(N)

$$(T^a_F)_{ij} = (T^a)_{ij} = \frac{\lambda^a_{ij}}{2} \tag{D.27}$$

$$\mathrm{Tr}\left[T^a_F T^b_F\right] = T_F\delta^{ab} \quad \text{with } T_F = \frac{1}{2} \tag{D.28}$$

$$\sum_{a,k}(T^a_F)_{ik}(T^a_F)_{kj} = C_F\delta_{ij}, \qquad C_F = T_F\frac{N^2-1}{N} \tag{D.29}$$

BIBLIOGRAPHY

[1] G. Aad et al. "Observation of a new particle in the search for the Standard Model Higgs boson with the ATLAS detector at the LHC". In: *Physics Letters B* 716.1 (Sept. 2012), pp. 1–29. ISSN: 0370-2693. DOI: 10.1016/j.physletb.2012.08.020. URL: http://dx.doi.org/10.1016/j.physletb.2012.08.020.

[2] M.G. Aartsen et al. "The IceCube Neutrino Observatory: instrumentation and online systems". In: *Journal of Instrumentation* 12.03 (Mar. 2017), P03012–P03012. ISSN: 1748-0221. DOI: 10.1088/1748-0221/12/03/p03012. URL: http://dx.doi.org/10.1088/1748-0221/12/03/P03012.

[3] S. Abachi et al. "Observation of the Top Quark". In: *Physical Review Letters* 74.14 (Apr. 1995), pp. 2632–2637. ISSN: 1079-7114. DOI: 10.1103/physrevlett.74.2632. URL: http://dx.doi.org/10.1103/PhysRevLett.74.2632.

[4] F. Abe et al. "Observation of Top Quark Production in $p\bar{p}$ Collisions with the Collider Detector at Fermilab". In: *Physical Review Letters* 74.14 (Apr. 1995), pp. 2626–2631. ISSN: 1079-7114. DOI: 10.1103/physrevlett.74.2626. URL: http://dx.doi.org/10.1103/PhysRevLett.74.2626.

[5] B. Abi et al. "Measurement of the Positive Muon Anomalous Magnetic Moment to 0.46 ppm". In: *Phys. Rev. Lett.* 126 (14 Apr. 2021), p. 141801. DOI: 10.1103/PhysRevLett.126.141801. URL: https://link.aps.org/doi/10.1103/PhysRevLett.126.141801.

[6] National Aeronautics and Space Administration. *Wilkinson Microwave Anisotropy Probe*. URL: https://map.gsfc.nasa.gov/.

[7] N. Aghanim et al. "Planck 2018 results". In: *Astronomy & Astrophysics* 641 (Sept. 2020), A6. ISSN: 1432-0746. DOI: 10.1051/0004-6361/201833910. URL: http://dx.doi.org/10.1051/0004-6361/201833910.

[8] Ian Aitchison. *Supersymmetry in particle physics: an elementary introduction*. Cambridge University Press, 2007.

[9] B.C. Allanach et al. "SUSY Les Houches Accord 2". In: *Computer Physics Communications* 180.1 (Jan. 2009), pp. 8–25. ISSN: 0010-4655. DOI: 10.1016/j.cpc.2008.08.004. URL: http://dx.doi.org/10.1016/j.cpc.2008.08.004.

[10] E. Aprile et al. "The XENON1T dark matter experiment". In: *The European Physical Journal C* 77.12 (Dec. 2017). ISSN: 1434-6052. DOI: 10.1140/epjc/s10052-017-5326-3. URL: http://dx.doi.org/10.1140/epjc/s10052-017-5326-3.

[11] Q. Arnaud et al. "First Germanium-Based Constraints on Sub-MeV Dark Matter with the EDELWEISS Experiment". In: *Physical Review Letters* 125.14 (Oct. 2020). ISSN: 1079-7114. DOI: 10.1103/physrevlett.125.141301. URL: http://dx.doi.org/10.1103/PhysRevLett.125.141301.

[12] Howard Baer et al. "Natural SUSY with a bino- or wino-like LSP". In: *Physical Review D* 91.7 (Apr. 2015). ISSN: 1550-2368. DOI: 10.1103/physrevd.91.075005. URL: http://dx.doi.org/10.1103/PhysRevD.91.075005.

[13] Neta A. Bahcall and Xiaohui Fan. "The Most Massive Distant Clusters: Determining Ω and σ". In: *The Astrophysical Journal* 504.1 (Sept. 1998), pp. 1–6. DOI: 10.1086/306088. URL: https://doi.org/10.1086/306088.

[14] Michael J. Baker et al. "The coannihilation codex". In: *Journal of High Energy Physics* 2015.12 (Dec. 2015), pp. 1–86. ISSN: 1029-8479. DOI: 10.1007/jhep12(2015)120. URL: http://dx.doi.org/10.1007/JHEP12(2015)120.

[15] K. G. Begeman, A. H. Broeils, and R. H. Sanders. "Extended rotation curves of spiral galaxies: dark haloes and modified dynamics." In: *Monthly Notices of the Royal Astronomical Society* 249 (1991), p. 523. DOI: 10.1093/mnras/249.3.523.

[16] Geneviève Bélanger et al. *MicrOMEGAs*. URL: https://lapth.cnrs.fr/micromegas/.

[17] Gianfranco Bertone, Dan Hooper, and Joseph Silk. "Particle dark matter: evidence, candidates and constraints". In: *Physics Reports* 405.5-6 (Jan. 2005), pp. 279–390. ISSN: 0370-1573. DOI: 10.1016/j.physrep.2004.08.031. URL: http://dx.doi.org/10.1016/j.physrep.2004.08.031.

[18] Adel Bilal. "Introduction to Supersymmetry". In: (Jan. 2001). arXiv: hep-th/0101055.

[19] CERN. *ATLAS Experiment*. URL: https://atlas.cern/.

[20] CERN. *CMS Detector*. URL: https://home.cern/science/experiments/cms.

[21] A. Denner et al. "Feynman rules for fermion-number-violating interactions". In: *Nuclear Physics B* 387.2 (1992), pp. 467–481. ISSN: 0550-3213. DOI: https://doi.org/10.1016/0550-3213(92)90169-C. URL: https://www.sciencedirect.com/science/article/pii/055032139290169C.

[22] Lance J. Dixon. "A brief introduction to modern amplitude methods". In: *Journeys Through the Precision Frontier: Amplitudes for Colliders: TASI 2014 Proceedings of the 2014 Theoretical Advanced Study Institute in Elementary Particle Physics*. World Scientific, 2016, pp. 39–97.

[23] Manuel Drees and Fazlollah Hajkarim. "Neutralino dark matter in scenarios with early matter domination". In: *Journal of High Energy Physics* 2018.12 (Dec. 2018). ISSN: 1029-8479. DOI: 10.1007/jhep12(2018)042. URL: http://dx.doi.org/10.1007/JHEP12(2018)042.

[24] Herbi K. Dreiner, Howard E. Haber, and Stephen P. Martin. "Two-component spinor techniques and Feynman rules for quantum field theory and supersymmetry". In: *Physics Reports* 494.1 (2010), pp. 1–196. ISSN: 0370-1573. DOI: https://doi.org/10.1016/j.physrep.2010.05.002. URL: https://www.sciencedirect.com/science/article/pii/S0370157310001171.

[25] Sonja Esch. "Dark matter, neutrino masses and lepton flavor violation in radiative see-saw models". PhD thesis. University of Münster, 2018.

[26] L.D. Faddeev and V.N. Popov. "Feynman diagrams for the Yang-Mills field". In: *Physics Letters B* 25.1 (1967), pp. 29–30. ISSN: 0370-2693. DOI: https://doi.org/10.1016/0370-2693(67)90067-6. URL: https://www.sciencedirect.com/science/article/pii/0370269367900676.

[27] Jonathan L. Feng. "Dark Matter Candidates from Particle Physics and Methods of Detection". In: *Annual Review of Astronomy and Astrophysics* 48.1 (2010), pp. 495–545. DOI: 10.1146/annurev-astro-082708-101659. eprint: https://doi.org/10.1146/annurev-astro-082708-101659. URL: https://doi.org/10.1146/annurev-astro-082708-101659.

[28] K. Griest and D. Seckel. "Three exceptions in the calculation of relic abundances". In: *Physical Review D* 43.10 (1991), pp. 3191–3203. DOI: 10.1103/PhysRevD.43.3191. URL: https://www.scopus.com/inward/record.uri?eid=2-s2.0-0000633545&doi=10.1103%2fPhysRevD.43.3191&partnerID=40&md5=f3d30c12b19c447a3bb75d848ef0c1aa.

[29] Francis Halzen and Alan D Martin. *Quark & Leptons: An Introductory Course In Modern Particle Physics*. John Wiley & Sons, 1984.

[30] B. Herrmann et al. *DM@NLO*. URL: https://dmnlo.hepforge.org/.

[31] Hugh F. Jones. *Groups, representations and physics*. 2. Taylor & Francis Group, 1998.

[32] Gerard Jungman, Marc Kamionkowski, and Kim Griest. "Supersymmetric dark matter". In: *Physics Reports* 267.5 (1996), pp. 195–373. ISSN: 0370-1573. DOI: https://doi.org/10.1016/0370-1573(95)00058-5. URL: https://www.sciencedirect.com/science/article/pii/0370157395000585.

[33] K. Kodama et al. "Observation of tau neutrino interactions". In: *Physics Letters B* 504.3 (Apr. 2001), pp. 218–224. ISSN: 0370-2693. DOI: 10.1016/s0370-2693(01)00307-0. URL: http://dx.doi.org/10.1016/S0370-2693(01)00307-0.

[34] Edward W. Kolb and Michael S. Turner. *The Early Universe*. Vol. 69. 1990. ISBN: 978-0-201-62674-2.

[35] Kamila Kowalska and Enrico Maria Sessolo. "The Discreet Charm of Higgsino Dark Matter: A Pocket Review". In: *Advances in High Energy Physics* 2018 (July 2018), pp. 1–15. ISSN: 1687-7365. DOI: 10.1155/2018/6828560. URL: http://dx.doi.org/10.1155/2018/6828560.

[36] Graham D Kribs, Adam Martin, and Tuhin S Roy. "Supersymmetry with a chargino NLSP and gravitino LSP". In: *Journal of High Energy Physics* 2009.01 (Jan. 2009), pp. 023–023. ISSN: 1029-8479. DOI: 10.1088/1126-6708/2009/01/023. URL: http://dx.doi.org/10.1088/1126-6708/2009/01/023.

[37] Sven Krippendorf, Fernando Quevedo, and Oliver Schlotterer. *Cambridge Lectures on Supersymmetry and Extra Dimensions*. 2010. arXiv: 1011.1491 [hep-th].

[38] Moritz Meinecke. "SUSY-QCD Corrections to the (Co) Annihilation of Neutralino Dark Matter within the MSSM". PhD thesis. University of Münster, 2015.

[39] R. Mertig, M. Böhm, and A. Denner. "Feyn Calc - Computer-algebraic calculation of Feynman amplitudes". In: *Computer Physics Communications* 64.3 (1991), pp. 345–359. ISSN: 0010-4655. DOI: https://doi.org/10.1016/0010-4655(91)90130-D. URL: https://www.sciencedirect.com/science/article/pii/001046559190130D.

[40] W. Porod and F. Staub. *SPheno*. URL: https://spheno.hepforge.org/.

[41] S. Profumo and C. E. Yaguna. "Gluino coannihilations and heavy bino dark matter". In: *Phys. Rev. D* 69 (2004), p. 115009. DOI: 10.1103/PhysRevD.69.115009. arXiv: hep-ph/0402208.

[42] Alexander Pukhov, Alexander Belyaev, and Neil Christensen. *CalcHEP*. URL: https://theory.sinp.msu.ru/~pukhov/calchep.html.

[43] Janusz Rosiek. "Complete set of Feynman rules for the minimal supersymmetric extension of the standard model". In: *Physical Review D* 41.11 (June 1990), pp. 3464–3501. ISSN: 0556-2821. DOI: 10.1103/physrevd.41.3464. URL: http://dx.doi.org/10.1103/PhysRevD.41.3464.

[44] Matthew D. Schwartz. *Quantum field theory and the standard model*. Cambridge University Press, 2014.

[45] Jakob Schwichtenberg. *Physics from Symmetry*. 3. Undergraduate Lecture Notes in Physics. Springer, 2018.

[46] Bernd Thaller. *The Dirac equation*. Springer Science & Business Media, 2013.

[47] BL van der Waerden. "Nachrichten Akad. Wiss. Göttingen, Math". In: *Physik. Kl* 100 (1929), p. 21.

[48] Christopher W. Walter. "The Super-Kamiokande Experiment". In: *Neutrino Oscillations* (Mar. 2008), pp. 19–43. DOI: 10.1142/9789812771971_0002. URL: http://dx.doi.org/10.1142/9789812771971_0002.

[49] Hermann Weyl. "Quantenmechanik und gruppentheorie". In: *Zeitschrift für Physik* 46.1-2 (1927), pp. 1–46.

[50] F. Zwicky. "Die Rotverschiebung von extragalaktischen Nebeln". In: *Helvetica Physica Acta* 6 (1933), pp. 110–127.

[51] P.A. Zyla et al. "Review of Particle Physics". In: *PTEP* 2020.8 (2020), p. 083C01. DOI: 10.1093/ptep/ptaa104.

DECLARATION OF ACADEMIC INTEGRITY

I hereby confirm that this thesis on *Neutralino-Gluino coannihilation in the MSSM* is solely my own work and that I have used no sources or aids other than the ones stated. All passages in my thesis for which other sources, including electronic media, have been used, be it direct quotes or content references, have been acknowledged as such and the sources cited.

Münster, 21 September 2021

Jorin Overwiening

I agree to have my thesis checked in order to rule out potential similarities with other works and to have my thesis stored in a database for this purpose.

Münster, 21 September 2021

Jorin Overwiening

COLOPHON

This document was typeset using the typographical look-and-feel `classicthesis` developed by André Miede. The style was inspired by Robert Bringhurst's seminal book on typography "*The Elements of Typographic Style*". `classicthesis` is available for both LaTeX and LyX:

https://bitbucket.org/amiede/classicthesis/